SYSTEM INTERACTIONS AND DESIGN CONSIDERATIONS FOR DISTRIBUTED POWER SYSTEMS

by

Steven E. Schulz

Thesis submitted to the Faculty of the

Virginia Polytechnic Institute and State University

in partial fulfillment of the requirements for the degree of

Master of Science

in

Electrical Engineering

APPROVED:

Bo H. Cho
B. H. Cho, Co-chairman

Fred C. Lee
F. C. Lee, Co-chairman

Dan Y. Chen
D. Y. Chen

January 21, 1991

Blacksburg, Virginia

SYSTEM INTERACTIONS AND DESIGN CONSIDERATIONS FOR DISTRIBUTED POWER SYSTEMS

by

Steven E. Schulz

B. H. Cho, Co-chairman

F. C. Lee, Co-chairman

Electrical Engineering

(ABSTRACT)

Methods of analysis and important design considerations for distributed power systems (DPS) are addressed. A generalized analysis of subsystem interaction is presented. Emphasis is placed on absolute stability and eigenvalue location of the integrated system. Terminal properties of the decoupled subsystems are used in determining the stability criteria. Either analytical models or empirical data may be used in the interaction analysis.

Design of EMI filters for a two-stage DPS is comprehensively discussed. A detailed analysis of the effects of input filters on current-mode controlled single-module regulators is given. It is shown that the criteria used to minimize filter interaction for voltage-mode and current-mode controlled regulators are identical. The results of the single-module regulator input filter interaction analysis are extended to the multi-module DPS case. Both line input filters and intermediate bus filters are designed for stability and to minimize interaction with the regulator modules. Implications of non-minimal dimensional subsystems are discussed. The eigenvalues due to parallel interaction are described, and it is shown how appropriate damping can be used to insure their stability. Straight-forward design guidelines are provided for the filters.

Interaction of a non-ideal generator source with the DPS is described. This provides a useful application of the general subsystem interaction analysis. Stability is determined from differ-

ent points in the system, and subsystem impedances are used to qualitatively describe the integrated system eigenvalue location.

Acknowledgements

I would first like to express my gratitude to my advisors Dr. Bo H. Cho and Dr. Fred C. Lee. Their support and encouragement, along with experienced guidance, have made a large contribution leading to the completion of this thesis.

I would also like to thank Dr. Dan Y. Chen for the interest he has shown in my research, and for serving on my advisory committee.

Special thanks go to Dr. Vatche Vorperian and Byung C. Choi for answering my questions and providing helpful comments. I must also acknowledge all of my fellow students and the staff members at VPEC, who not only provided a fertile environment for technical interaction, but created a pleasant social environment as well.

Finally, I would like to thank my mother, my late father, and my friends for all they have done for me.

Table of Contents

List of Illustrations

List of Tables

Chapter 1

INTRODUCTION

In recent years, many applications for the distributed power system (DPS) have been proposed. The DPS is often required in situations where the limitations imposed by centralized power supplies prove to be unacceptable. Centralized power supplies use a single regulator module to convert an unregulated input voltage to the regulated output voltage required by the load. In a DPS, the power is processed by cascaded stages of parallel switching regulators. Typically, one stage of regulators, called the line conditioners, takes an unregulated input voltage and converts it to a regulated intermediate bus voltage. This intermediate bus is then used to distribute power throughout the system. A second stage of regulators, called the load converters, takes the intermediate bus voltage and generates the appropriate output voltage required by the load. The load converters are usually located in close proximity to the load. In some instances where the load consists of logic boards, the load converters can be mounted on the logic boards themselves.

Cascading stages of regulators can offer many benefits over the single-stage, centralized conversion process. In conventional centralized power supplies, the regulator is often placed some distance from the actual load. For low voltage applications, significant conduction

losses can occur in the power distribution. Also, centralized power supplies may have difficulty in maintaining regulation at the point of load. However, with the DPS, the intermediate bus may use a relatively high voltage to distribute power throughout the system, thus reducing the conduction losses. Also, the proximity of the load converters to the load enhances the ability to regulate the load voltage precisely. Finally, cascading regulators can greatly increase the isolation afforded between source and load.

Paralleling regulator modules also offers several advantages over the single module centralized supply. With parallel regulators, each module carries only a fraction of the total load current, thus allowing low-power, high frequency designs to be utilized. Phase shifting of the parallel modules can result in a significant decrease in the output voltage ripple and input current harmonics drawn by the regulator stage. Modularity of the DPS allows reconfiguration for almost any power level by adding or removing parallel modules. Lastly, the system's reliability can be controlled by the addition of redundant parallel modules.

Much of the current research found in the literature is focused on the design of regulator modules to be used in the DPS environment. Since these modules will not be operating independently, but will be incorporated into a large-scale system, it is important to understand the potential interaction problems involved with a DPS. Implementation of the regulator technologies will require the interfacing of regulators and filters to meet certain specifications while avoiding unwanted interactions.

This thesis addresses aspects of integrating subsystems to form a high performance distributed power system. Methods of analyzing the various interactions present in a DPS are presented. Design guidelines for system components are provided, and design examples are shown.

For the examples presented in this thesis, a two-stage DPS was used. Figure 1 shows a block diagram of the system configuration. The line conditioner stage (Stage 1) takes an unregu-

lated DC bus voltage (125 to 475V as defined by MIL-STD 704D) and steps it down to a regulated 48V intermediate bus. The line conditioners are connected in parallel at both their input and output terminals. The line conditioners use a 600W buck-derived topology operating at 250kHz. The load converters (Stage 2) are supplied by the 48V bus, and step this voltage down to the required 5V output. The load converters are also connected in parallel at both their input and output terminals. The load converters use a 200W buck-derived topology operating at 500kHz. All regulators use two-loop current-mode control. The system is designed for a power level of 2.4kW. Therefore, four line conditioners and twelve load converters are required to supply the full output power. An additional line conditioner and load converter module are added for redundancy. It is assumed that the regulator modules have been previously designed to provide stable, high performance operation.

Chapter 2 of this thesis presents a discussion of the general subsystem interaction analysis. The analysis makes use of the terminal properties of subsystems to determine the stability and performance of an integrated system. The techniques described are found to be extremely useful in analyzing the complex interactions which occur in a large-scale DPS.

Chapter 3 addresses the design of filters for the DPS. First, the design of input filters for current-mode controlled single module regulators is discussed. It is shown how a non-ideal source impedance presented to a regulator can effect the regulator's stability and performance. The analysis is then extended to the design of filters for parallel module regulators. It is shown that additional constraints are placed on the filter to avoid instabilities due to parallel interaction. Both intermediate bus and line input filters are designed for a two-stage conversion topology to minimize interaction and avoid performance degradation. Design guidelines are provided. Non-minimal dimensional systems are discussed, since a DPS may very likely be non-minimal due to parallel modules.

Chapter 4 presents the power source interaction analysis. The effects of a non-ideal generator source are determined using the techniques developed in Chapter 2. This example provides

a good demonstration of the subsystem integration analysis techniques which can be used in the design and analysis of a DPS.

Chapter 5 presents the conclusions of this thesis.

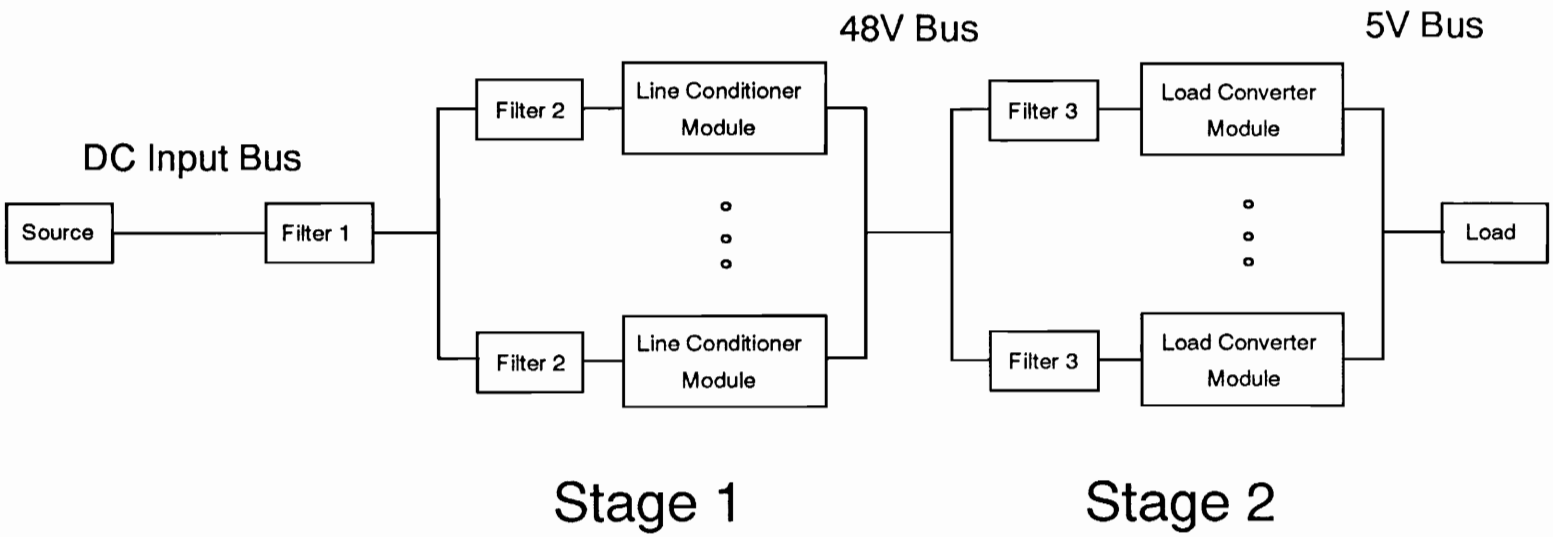

Figure 1. Block diagram of two-stage DPS

Chapter 2

GENERAL SUBSYSTEM INTERACTION ANALYSIS

2.1 Introduction

When designing large-scale systems, it is often impractical to analyze and design the system as a whole. If possible, it is desirable to divide the system into manageable subsystems which can then be designed independently. In this manner, known design techniques and analytical equations can be applied to the low-order subsystems. The subsystems may then be interconnected to form the complete integrated system. One of the major difficulties in large-scale system analysis involves the subsystem interaction problem. As a system becomes more complex, the interaction problems create a large degree of uncertainty in the system response even though each subsystem may be well understood and documented. It is known that the subsystem performance may degrade upon integration with the rest of the system. Thus, the

total integrated system analysis must include the interaction analysis that allows one to predict the system level response and to trouble-shoot the system. The interaction analysis also provides design information for a component or subsystem at the initial design phase and for future modification of the system.

In this chapter, the methodology of large-scale system interaction analysis is presented. The effects of integrating subsystems on the integrated system performance are determined. It is assumed that the subsystems have been previously designed to meet the required specifications. The approach presented in this chapter is general, and is applicable to any linear (or linearized) subsystems. These general methods are then applied to the DPS analysis, as shown in Chapters 3 and 4.

2.2 Series Integration of Two Subsystems

Consider the series integration of the two subsystems shown in Figure 2. The two subsystems are to be connected in series at the interface bus. No other point of interaction exists between the two subsystems. The characteristics of each subsystem operating independently are known and well behaved, and we would like to know how the integrated system behaves. The overall forward gain of the integrated system can be expressed as the product of the individual subsystem forward gains (F_1 and F_2) and a loading factor:

$$F_{12} = \frac{F_1 F_2}{1 + \frac{Z_s}{Z_i}} \tag{2.1}$$

Where:

F_{12} = Integrated system forward gain

F_1 = Forward gain of source subsystem without load

F_2 = Forward gain of load subsystem without source

Z_s = Output impedance of the source subsystem

Z_i = Input impedance of the load subsystem

$$\frac{1}{1+\frac{Z_s}{Z_i}} = \text{Loading (feedback) factor} \tag{2.2}$$

The minor loop gain has been defined as [1,2]:

$$T_m = \frac{Z_s}{Z_i} \tag{2.3}$$

Therefore, the integrated system forward gain is simply the product of the decoupled subsystem transfer functions times a loading factor. Both Z_s and F_1 are input-to-output transfer functions of the source subsystem and have common denominators (characteristic equation of the source subsystem). Also, Y_i (or $1/Z_i$) and F_2 are input-to-output transfer functions of the load subsystem and have common denominators (characteristic equation of the load subsystem). Since the denominator of F_1F_2 is cancelled by the denominator of the loading factor in Equation (2.2) (also the denominator of T_m), the integrated system characteristic equation is $1 + T_m = 0$. Hence, by using T_m, the integrated system stability and eigenvalue location can be determined. Also note that classical control theory may be utilized by treating T_m as the open-loop gain of a closed-loop system. For example, the Nyquist criterion could be applied to T_m to determine system stability. It should also be noted that the choice of source and load subsystems is not dependent on the direction of power flow. However, the source subsystem

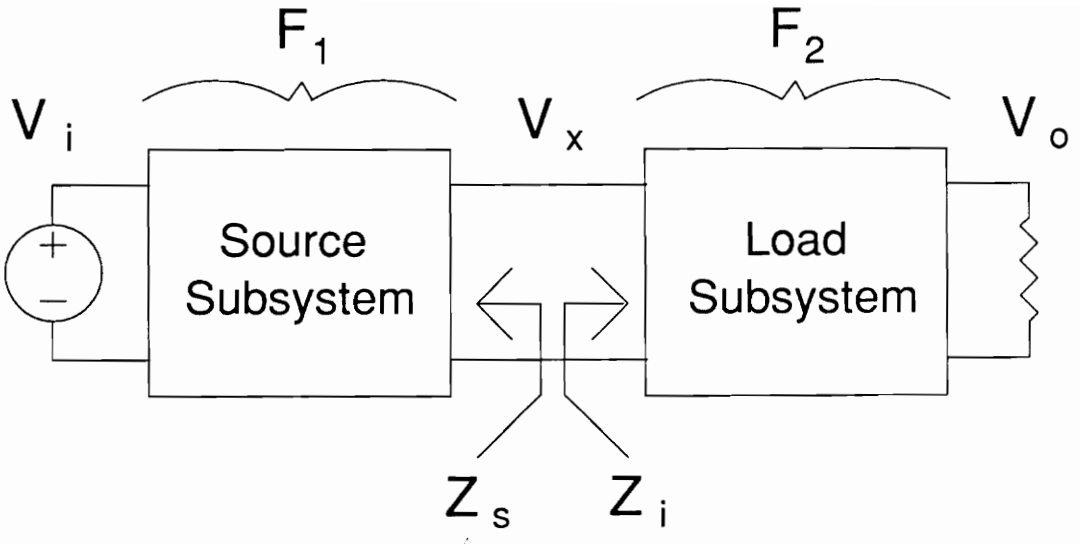

$$F_1 = \left.\frac{V_x}{V_i}\right|_{\text{w/o load}} \qquad F_2 = \left.\frac{V_o}{V_x}\right|_{\text{w/o source}}$$

$$F_{12} = \frac{V_o}{V_i} = \frac{F_1 F_2}{1 + \frac{Z_s}{Z_i}}$$

Figure 2. Series integration of two subsystems

must be chosen such that its output impedance at the interface bus is an input-to-output transfer function of the source subsystem. Similarly, the load subsystem must be chosen such that its input admittance at the interface bus is an input-to-output transfer function of the load subsystem.

Looking at Equation (2.1), two conditions are apparent:

$$F_{12} \simeq F_1 F_2 \quad \text{when } |T_m| << 1 \tag{2.4}$$

$$F_{12} \simeq \frac{F_1 F_2}{T_m} \quad \text{when } |T_m| >> 1 \tag{2.5}$$

First, in Section 2.2.1 we will study the system where the condition of Equation (2.4) holds for all frequencies. Then, in Section 2.2.2 we will consider the case where the condition of Equation (2.5) holds for some frequencies.

Before proceeding, it should be noted that in certain cases either of the subsystems may be non-minimal dimensional. That is, the subsystem may be unobservable or uncontrollable at the interface bus. It will be shown in Chapter 3 that the parallel module configuration typical in a DPS can result in a non-minimal system. Therefore, Section 3.4.3 will describe the non-minimal dimensional system, and address the case when either the source or load subsystem (or both) is unobservable and uncontrollable at the interface bus.

2.2.1 Decoupled (Minimal Interaction) Subsystems

Consider the case when two subsystems are to be integrated and the minor loop gain as defined in Equation (2.3) satisfies $|T_m| << 1$ for all frequencies. Under this condition, it can be seen that the loading factor Equation (2.2) is approximately equal to one. Hence, $F_{12} \simeq F_1 F_2$ and the two subsystems interconnected at the interface bus do not interact. Thus, if the charac-

teristics of the decoupled subsystems are known, then we also know the characteristics of the integrated system. This is obviously the simplest case of subsystem integration.

It is apparent that the load subsystem is not affected by source impedance, nor is the source subsystem affected by the load impedance (audio and response speed are unchanged). The system eigenvalue locations are easily determined by the position of the decoupled subsystem eigenvalue locations. That is, the integrated system eigenvalues lie at the poles of F_1 and F_2. The effect on the integrated system input and output impedance is described in [2] utilizing the hybrid g-parameter representation of the subsystems.

In this case, system design and analysis is simplified, since each subsystem can be designed independently, and integrated system performance predicted from the decoupled subsystem performance. The stability of the system is determined by that of each subsystem. Also, the system transient response (settling time) is determined by the dominant pole of either subsystem.

In this case the interface bus impedance becomes:

$$Z_B = Z_s \| Z_l \simeq Z_s \tag{2.6}$$

Knowledge of Z_B, or equivalently Z_s for this case, will tell us the bus quality (response to step disturbance at the bus) and a subset of the system eigenvalues (the eigenvalues of the source subsystem). Z_B provides no information on the load subsystem eigenvalues in this case, since the response at the bus is independent of the load subsystem. The smaller Z_s, the better the bus quality.

Notice that both Z_s and Z_l can be determined from either an analytical model or empirical data. The latter method can be very useful when an analytical model is not readily available but measurements on the subsystems can be made.

2.2.2 Interaction of Subsystems

We now consider the case when the loading factor Equation (2.2) is not equal to one. In this case, $|Z_s| > |Z_i|$ for some frequencies. The two subsystems, when connected, will interact. It is apparent from Equation (2.1) that the system characteristics will be changed, but it is not immediately known to what extent.

First, consider the location of the system eigenvalues. Examination of Equation (2.1) shows that the system eigenvalues will, in general, not lie in the same locations as in the decoupled subsystems. The characteristic equation for the source subsystem can be found in the denominator of F_1 or Z_s. The characteristic equation of the load subsystem can be found in the denominator of F_2 or Y_i. Therefore, the integrated system eigenvalues are determined by:

$$1 + T_m = 0 \tag{2.7}$$

The stability of the system can be determined by calculating the zeros of Equation (2.7), or by applying the Nyquist Criterion to T_m. The Nyquist plot can easily be determined from either analytical models or measurement data. Further insight can be gained by an examination of the source and load impedances seen by the bus.

Consider the system whose bus impedances appear as in Figure 3(a). The eigenvalues of the decoupled subsystems are boxed on the plots of Z_s and Z_i. The minor loop gain can be plotted as the ratio of the two impedances and is shown in Figure 3(b). Notice that this plot is a straight-line approximation and does not consider peaking at the transfer function singularities. The minor loop gain exceeds 0dB only in region where $|Z_s| > |Z_i|$. Now, the system eigenvalues may be determined by referring back to Equations (2.4) and (2.5).

In the range of frequencies defined by Equation (2.4), any pole of F_1F_2 (decoupled subsystem eigenvalue) will also appear as an integrated system eigenvalue. For these frequencies, the

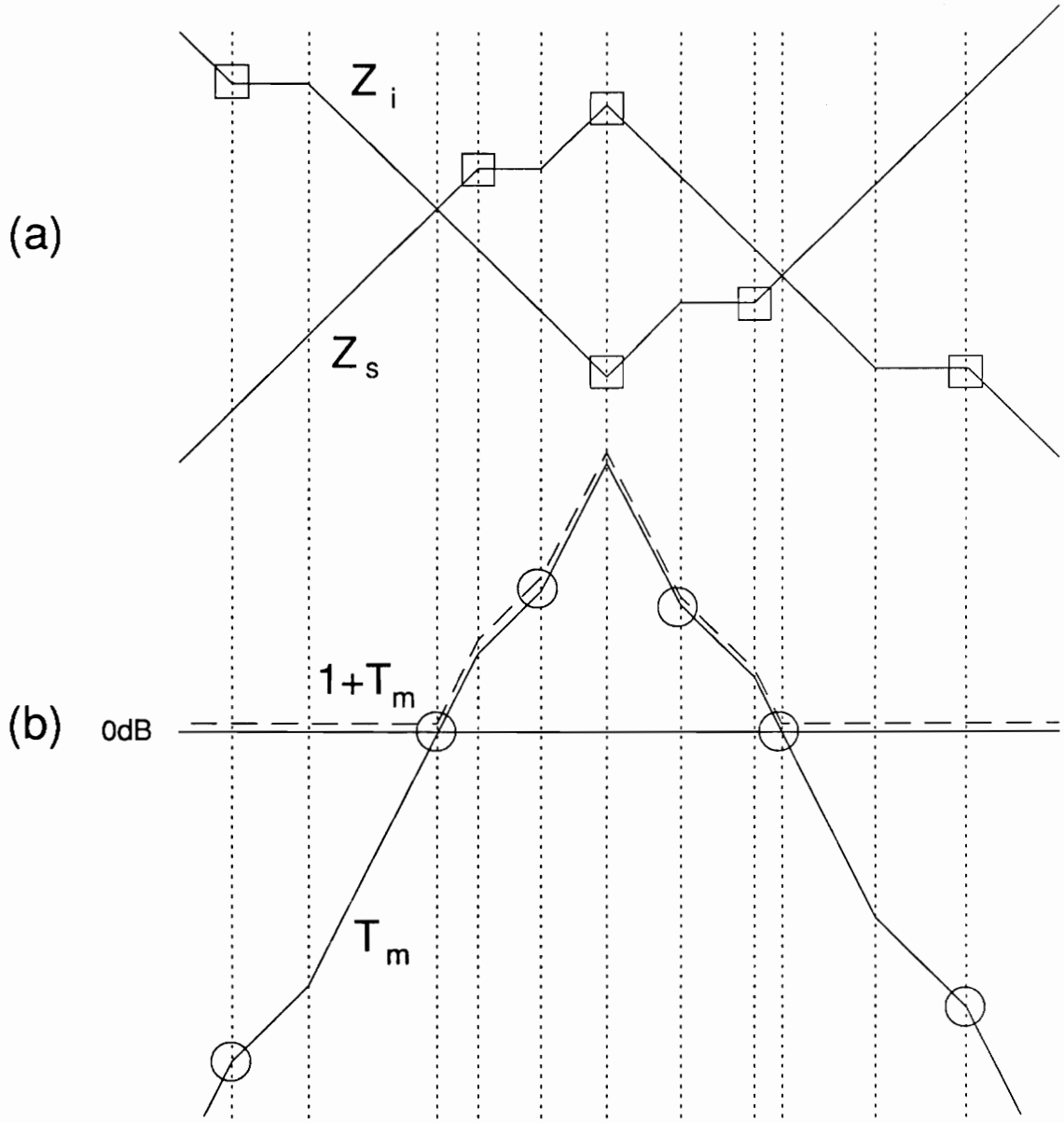

Figure 3. Interaction of subsystems: (a) source and load impedances seen at interface bus, (b) minor loop gain

two subsystems are essentially decoupled. For this particular example, integrated system eigenvalues in the range defined by Equation (2.4) are found at ω_1 and ω_{11} as defined in Figure 3.

In the range of frequencies defined by Equation (2.5), poles of F_1F_2 (at frequencies ω_4, ω_6, and ω_8 for this example) will in general not appear as system eigenvalues. This is because the denominator of T_m cancels the denominator of F_1F_2. Interaction between the two subsystems causes any subsystem eigenvalue in this range to shift position upon integration. Thus, the region of interaction is defined as the range of frequencies where $|T_m| > 1$. In this region, the zeros of T_m become poles of the integrated system (ω_5 and ω_7). That is, a zero of Z_s or Y_i (pole of Z_i) in the region of interaction is also a system eigenvalue. Thus, zeros of the decoupled subsystems may become system poles upon integration.

The remaining system eigenvalues can be found by examining Figure 3. Notice there are zeros in $1 + T_m$ where $|Z_s| = |Z_i|$. These are integrated system eigenvalues not found in either subsystem. The type of zeros present at these points (real or complex, RHP or LHP) is determined by the characteristics of Z_s and Z_i at the points of intersection. Instability could therefore arise due to RHP system poles introduced at the point of impedance overlap, or due to RHP zeros in Z_s or Y_i in the region of interaction. The integrated system eigenvalues are circled on the plot of T_m.

To determine the stability of the integrated system poles introduced at the point of impedance overlap (ω_3 and ω_9 in Figure 3), the Bode plot of either $1 + T_m$ or T_m may be used. RHP zeros of $1 + T_m$ can be detected by observing the phase characteristics of $1 + T_m$. If the phase of $1 + T_m$ is decreasing at the point of impedance overlap, then $1 + T_m$ has RHP zeros and the system is unstable. Alternatively, RHP zeros of $1 + T_m$ at the point of impedance overlap can be predicted from the phase characteristics of T_m. To do this, phase margins of T_m must be defined as follows:

If T_m has a positive slope at the crossover, the phase of T_m should be less than $+180$ degrees.

$$PM_1 = 180 - \angle T_m \tag{2.8}$$

If T_m has a negative slope at the crossover, phase of T_m should be greater than -180 degrees.

$$PM_2 = 180 + \angle T_m \tag{2.9}$$

Figure 4 shows the graphical definition of the phase margins on both the Bode and polar plots of T_m. The phase margin definitions come about by applying the Nyquist Criterion to the polar plot in Figure 4(b). For the system to be stable, the polar plot must not encircle the (-1,0) point (recall that T_m has no RHP poles since the decoupled subsystems were assumed to be stable). In practical systems, the condition $|T_m| << 1$ will be satisfied at very low and very high frequencies. In the region where $|T_m| > 1$, the phase of T_m will tend to decrease since there will be more poles than zeros in T_m in this region. Therefore, to avoid encircling the (-1,0) point, the phase of T_m should be in the first or second quadrants at the positive slope crossover, and in the third or fourth quadrants at the negative slope crossover. PM_1 represents the amount of phase *lead* that would have to be introduced at the positive slope crossover to cause the polar plot to encircle the (-1,0) point. Similarly, PM_2 represents the amount of phase *lag* that would have to be introduced at the negative slope crossover to cause the polar plot to encircle the (-1,0) point. In certain cases, as will be shown in an example at the end of this section, one must be careful when using the definitions of phase margin. However, in these cases, the proper use of phase margins will become clear if one recalls the argument given above.

From the previous discussion, it is apparent that knowledge of Z_s and Z_i (or Y_i) can provide full information as to the location of the system eigenvalues. It can be helpful to think of T_m as the open-loop gain of a simple closed-loop system described by Equation (2.1). The shift in

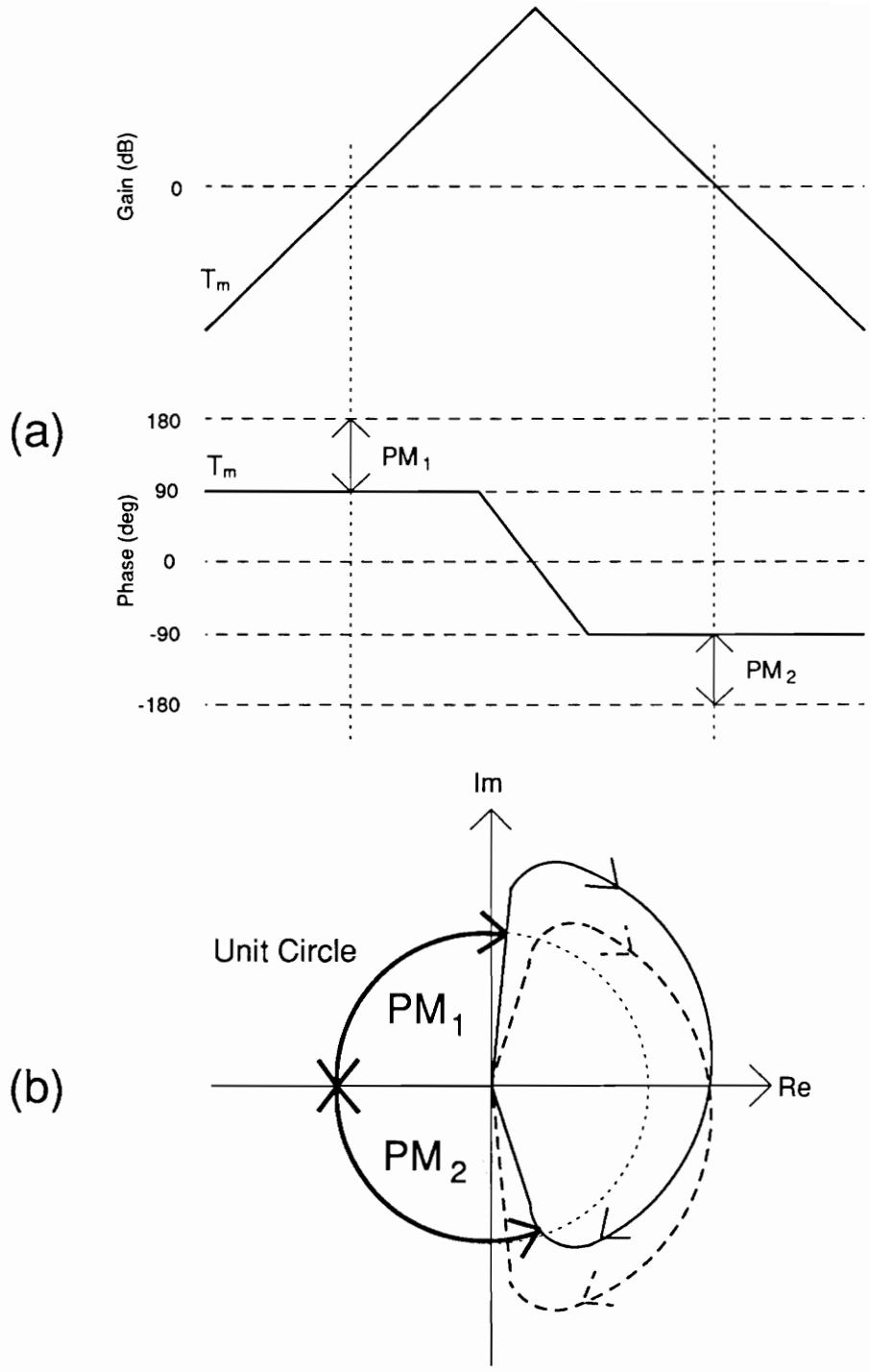

Figure 4. Definition of phase margins for minor loop gain: (a) Bode plot, (b) polar plot

eigenvalue location should then be easily understood. Only when the feedback effect is prominent (where $|T_m|$ is greater than 0dB) will the subsystem eigenvalues change location. It is important to remember that subsystem interaction only significantly affects eigenvalue location in the region of impedance overlap.

Three methods of determining system stability result. First, the roots of Equation (2.7) may be calculated directly. Second, the polar plot of T_m may be used in applying the Nyquist Criterion. Third, the Bode plots of Z_s, Z_i, T_m, and $1 + T_m$ can be used to graphically determine the eigenvalue location and phase margins. All of these techniques require either analytical models of the subsystems or empirical data.

For the case of interacting subsystems, the bus impedance is defined as:

$$Z_B = Z_s \| Z_i \tag{2.10}$$

It is desirable to maintain a low bus impedance, but peaking may occur in the bus impedance when Z_s and Z_i overlap. If Z_s and Z_i are close to 180° out of phase when $|Z_s| = |Z_i|$, then $|Z_B| \rightarrow \infty$. This condition would also indicate lightly damped system eigenvalues and small phase margin; a situation we would like to avoid. It should be noted that degradation occurs primarily at frequencies of impedance overlap. Also remember that interaction at a particular bus may not affect impedances at other buses in the system.

To conclude this section, an example is in order. Consider the integration of the two subsystems shown in Figure 5. The $-R_i$ load represents the dynamic input impedance of a regulator. The source subsystem represents an EMI filter. The source and load impedances at the interface bus are therefore:

$$Z_s(s) = R_f \frac{\left(1 + s\frac{L_f}{R_f}\right)}{s^2 L_f C_f + s C_f R_f + 1} \tag{2.11}$$

$$Z_i(s) = -R_i \tag{2.12}$$

These impedances are shown in Figure 5. Figure 6 shows the minor loop gain T_m in both Bode plot and polar plot forms. If the R_f/L_f zero is over one decade below the complex pole, then the peak in T_m occurs when the phase is at -180 degrees. Hence, if $|T_m| > 1$ at this frequency, the polar plot will encircle the (-1,0) point, and the system will be unstable. This can be seen in Figure 6(b), in which the polar plot encircles the (-1,0) point twice, indicating two RHP eigenvalues. Instability can also be predicted by the phase margins obtained from the Bode plot of T_m. At the lower point where $|T_m| = 1$, T_m has a positive slope and a phase greater than $+180$ degrees. This means $PM_1 < 0$ and the system is unstable. When determining the phase margin at the higher frequency crossover, care must be exercised. It would be incorrect to use $\angle T_m = 90°$ in Equation (2.9) to determine PM_2. Rather, we should use the value $\angle T_m = -270°$. This apparent anomaly can be explained by the fact that the phase of Z_i could be given as $+180$ degrees or -180 degrees with equal validity. The important point here is that the phase of T_m should lie in the third or fourth quadrants for stability. Therefore, the correct value of PM_2 is negative since T_m has a phase less than -180 degrees, indicating a RHP eigenvalue and instability. The analytic form of the characteristic equation is:

$$1 + T_m = \frac{s^2 L_f C_f + s\left(C_f R_f - \dfrac{L_f}{R_i}\right) + 1 - \dfrac{R_f}{R_i}}{s^2 L_f C_f + s C_f R_f + 1} \tag{2.13}$$

It can be seen that the zeros of $1 + T_m$ will be in the RHP if:

$$\frac{L_f}{R_i} > C_f R_f \quad \text{and} \quad R_f < R_i \tag{2.14}$$

This inequality could also be derived using the graphical technique, since the peak magnitude of T_m at the filter resonance (again assuming the R_f/L_f zero is over one decade below the

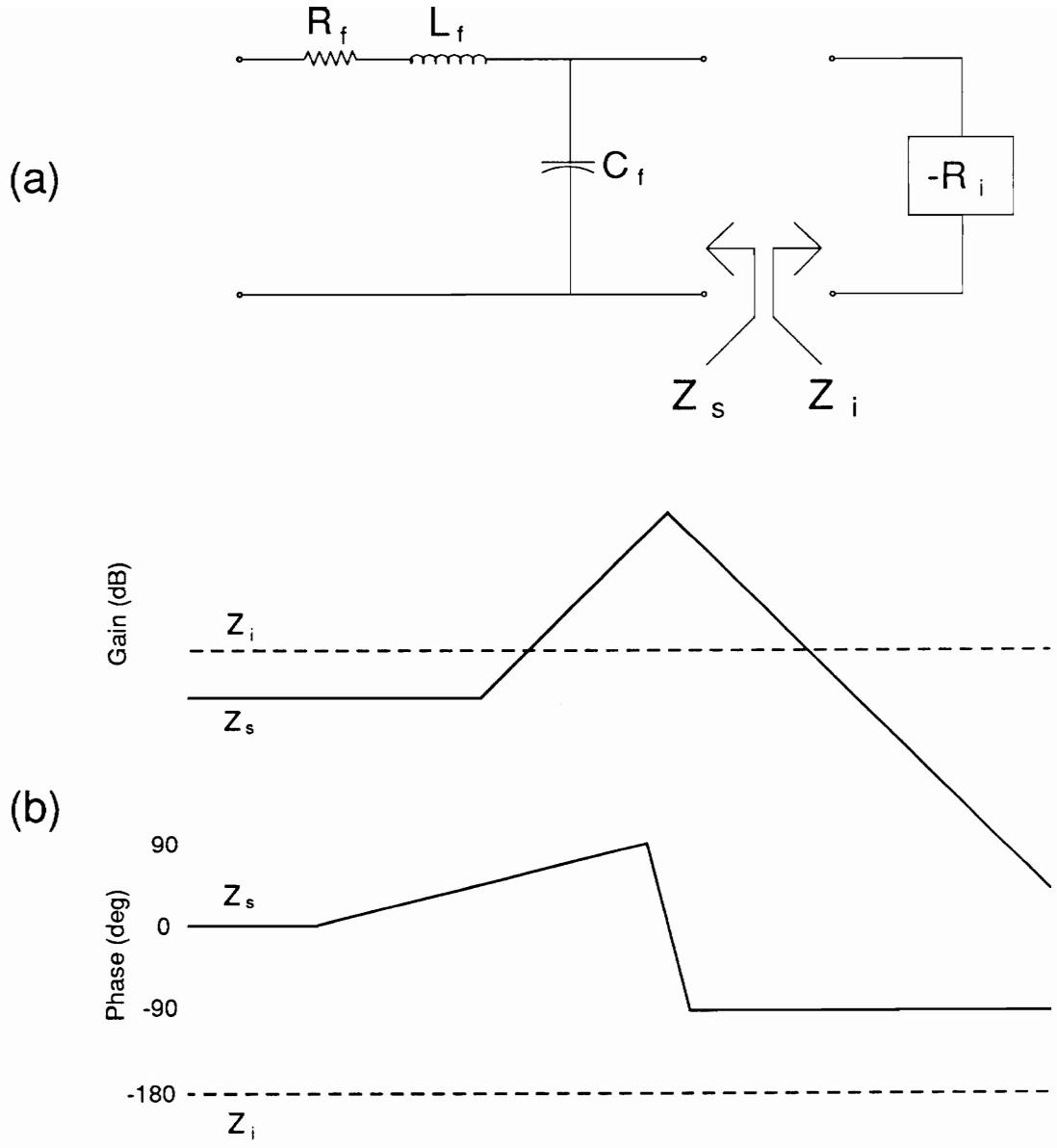

Figure 5. Example of subsystem integration: (a) subsystem circuit diagram, (b) impedances seen at interface bus

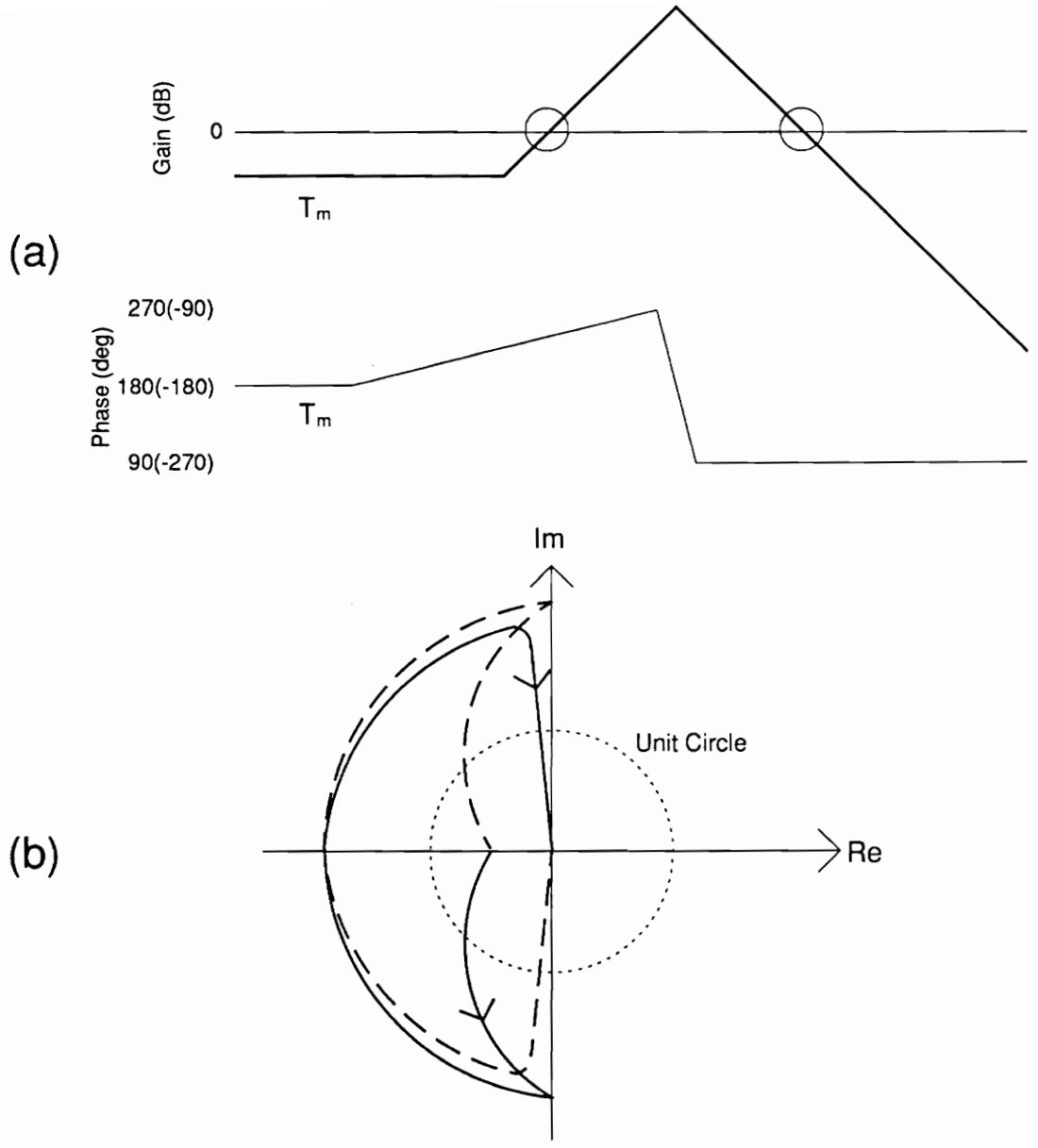

Figure 6. Example of subsystem integration: (a) Bode plot of minor loop gain, (b) polar plot of minor loop gain

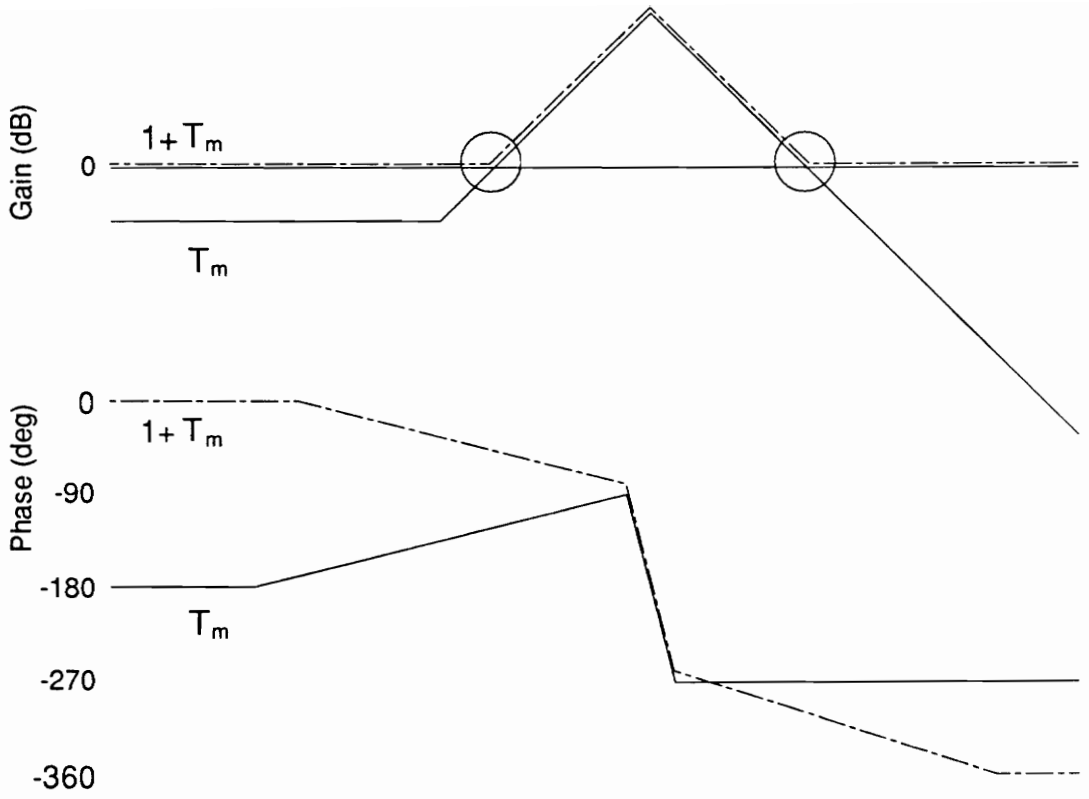

Figure 7. Bode plot of $1 + T_m$

complex pole) is $L_f/(R_fC_f)$. Hence, setting $|Z_s| > |Z_i|$ at resonance also yields the above inequality. When heavy interaction causes the system eigenvalues to become overdamped, then the characteristic equation is approximated by:

$$1 + T_m \simeq \frac{\left(1 - s\frac{L_f}{R_i}\right)(1 - sC_fR_i)}{s^2L_fC_f + sC_fR_f + 1} \tag{2.15}$$

The RHP zeros in $1 + T_m$ correspond to the points where $|Z_s| = |Z_i|$ in Figure 5. Shown in Figure 7 are the Bode plots of T_m and $1 + T_m$. The decreasing phase at the zeros of $1 + T_m$ indicates that these zeros lie in the RHP. Thus, the impedance analysis technique can provide qualitative information about stability and eigenvalue location of the integrated system. However, it is expected that in more complex systems, the information available from the impedance comparison will not be as easy to interpret.

2.3 Summary

In this chapter, the analysis of subsystem interaction was presented. The general case of series integration of two subsystems was addressed, and a complete explanation of the interaction phenomena was given. The important results were the development of techniques used for determining stability and eigenvalue location based on the terminal quantities of the subsystems.

In Section 2.2, it was shown that the output impedance of the source subsystem and the input impedance of the load subsystem contain all of the information necessary to determine the characteristics of the integrated system. The minor loop gain was defined in Equation (2.3)

and can be used to determine system stability. Two cases of subsystem integration were addressed. In Section 2.2.1, the case of minimal interaction was discussed. It was shown that a wide separation of source and load impedances seen at the interface bus was a sufficient condition to insure minimal interaction between the two subsystems. In this case, the integrated system performance can be predicted from the decoupled subsystem performance. In Section 2.2.2, the case of interacting subsystems was presented. It was shown that interaction occurs when the impedances seen at the interface bus overlap for some frequencies. A graphical approach was used to determine the location of the integrated system eigenvalues. Only the subsystem eigenvalues in the range of impedance overlap will shift position upon integration. Stability margins were defined for the phase of the minor loop gain in both the Bode plot and polar plot forms.

Chapter 3

FILTER DESIGN

3.1 Introduction

This chapter deals with the design of EMI filters for the DPS. It is well known that almost all power systems using switched-mode regulators require auxiliary filtering to meet certain EMI specifications. Filters may be required at the input or output of the regulator. Output filters are generally needed where boost or buck-boost type converters are used. These converters have a large output voltage ripple due to the large RMS current passing thru the power stage filter capacitor. Thus, a secondary EMI output filter may be required to smooth the output voltage to meet output ripple specifications. Input filters, on the other hand, are needed to attenuate the harmonic input currents drawn by switching regulators. Harmonic currents on the power line, when combined with a non-ideal source impedance, may cause noise prob-

lems at the source bus. The harmonic currents produce a noise voltage at the source, which may in turn interfere with other equipments fed by the source. For this reason, both military and commercial specifications exist which limit the amount of harmonic current which may be drawn from the power line. Input filters are usually needed with all switching regulators, but are especially important for the buck-derived type regulators due to the extremely high harmonic content of their pulsating input currents. Since all of the converters in the DPS under consideration are in the buck-derived family, only input filters will be considered in this chapter.

In designing an input filter, three tasks must be taken into consideration. First, the filter must provide the appropriate attenuation of the input currents to meet specifications. Secondly, absolute stability of the system must be maintained. Thirdly, the various performance indices of the regulator, such as audiosusceptibility and output impedance, must maintain acceptable levels. The design of input filters for single module regulators has already been widely discussed [1,4,5,6]. However, filtering for a DPS is more complicated due to the additional interactions at various points in the system.

Before discussing the design and interaction analysis of input filters for parallel modules, it is necessary to understand the design and interaction analysis for single module systems. By examining the simplified case of a single module system, much insight can be gained as to how the input filter affects the system, and how to minimize any degradation by proper filter design. With this goal in mind, Section 3.2 will address the design and interaction analysis methodology for current-mode controlled single module regulators fed by a non-ideal source. It will be shown how the non-ideal source impedance presented to the regulator due to the input filter affects the regulator's loop gain, audiosusceptibility, and output impedance.

In a DPS environment, many of the regulator modules do not see an ideal resistive load. For example, the line conditioner stage sees as its load the input impedance of the load converter stage. Also, the load converters see a largely capacitive load due to the decoupling

capacitances of the load logic boards. Therefore, the non-ideal load impedance seen by the regulator will also be taken into account in Section 3.2 when analyzing filter interaction.

In Section 3.3, design and interaction analysis for parallel module regulator systems will be discussed. A general input filter configuration will be assumed, making the analysis valid for any filter topology. The problem of parallel interaction is presented, and a simple method for determining system stability is presented. A single module model of the system is discussed, and its uses and limitations are outlined.

Section 3.4 deals with the design of the line input filter for the line conditioners. The selection of the filter topology is discussed, and a detailed explanation of the possible instability problem is given. It is shown how proper damping of the filter can eliminate instability, and a set of comprehensive design guidelines are established. An example is presented, and through this example the explanation of non-minimal dimensional systems is given. The implications of unobservable and uncontrollable modes on subsystem integration is discussed.

Finally, Section 3.5 will discuss the design of an intermediate bus filter. While the results of Section 3.3 are still valid for analyzing interaction with the load converters, it is shown that additional constraints must be placed on the filter input impedance to avoid interaction with the line conditioner stage. It will be shown that a practical compromise can be achieved between the desired low filter output impedance and high filter input impedance. A set of design guidelines are given for the intermediate bus filter.

Section 3.5 summarizes the results of this chapter.

3.2 Input Filters for Current-mode Controlled Single Module Regulators

This section will provide a methodology used to analyze input filter interaction with single module regulators. Many papers in the literature have addressed the problem of input filter interaction. The classic papers by Middlebrook [1,4], set the standard for most other papers to follow. While his papers only addressed voltage-mode controlled regulators directly, it will be shown that his results may be extended without modification to the current-mode controlled case as well. The same criteria presented in Middlebrook's paper to assure minimal degradation of performance indices for voltage-mode control are exactly the same as those which can be applied to current-mode regulators.

When assessing the effect of a non-ideal source on a closed-loop regulator, one typically determines the effect of the source impedance on the various small-signal transfer functions of the power stage. It will be assumed that the regulator module has been designed assuming an ideal voltage source. The object of this section is to determine the impact of a non-ideal source impedance, due to an input filter, on the regulator system.

Consider the case of a current-mode controlled buck converter fed by an arbitrary low-pass input filter as shown in Figure 8. The small-signal model of such a system is shown in Figure 9. In the figure, the input filter has been replaced by its Thevenin equivalent circuit. Therefore, the input filter is fully characterized by its output impedance $Z_s(s)$, and its unloaded forward voltage gain $H_s(s)$. The power stage is modeled using the PWM switch technique [7], and the load is represented by its dynamic load impedance $Z_{oc}(s)$.

$H_s(s)$ = Unloaded forward voltage gain of input filter

$Z_s(s)$ = Output impedance of input filter

$Z_{ac}(s)$ = Dynamic load impedance seen by regulator

$H_e(s)$ = Forward voltage gain of power stage output filter

$Z_{ie}(s)$ = Open-loop input impedance of power stage output filter

$$R_L = \frac{V_o}{I_o}$$

Notice that V_o and I_o are DC, steady-state values, and therefore R_L is not necessarily related to the dynamic load impedance $Z_{ac}(s)$. From Figure 9 the following power stage transfer functions can be found:

$$F'_{vd} = \frac{\hat{v}_o}{\hat{d}} = V_g H_e \left[\frac{1 - D^2 \frac{Z_s}{R_L}}{1 + D^2 \frac{Z_s}{Z_{ie}}} \right] = F_{vd} G_f \tag{3.1}$$

$$F'_{id} = \frac{\hat{i}_L}{\hat{d}} = \frac{V_g}{Z_{ie}} \left[\frac{1 - D^2 \frac{Z_s}{R_L}}{1 + D^2 \frac{Z_s}{Z_{ie}}} \right] = F_{id} G_f \tag{3.2}$$

$$F'_{vg} = \frac{\hat{v}_o}{\hat{v}_g} = D H_e \left[\frac{H_s}{1 + D^2 \frac{Z_s}{Z_{ie}}} \right] = F_{vg} G_x \tag{3.3}$$

$$F'_{ig} = \frac{\hat{i}_L}{\hat{v}_g} = \frac{D}{Z_{ie}} \left[\frac{H_s}{1 + D^2 \frac{Z_s}{Z_{ie}}} \right] = F_{ig} G_x \tag{3.4}$$

$$Z'_o = \frac{\hat{v}_o}{\hat{i}_o} = \frac{1}{sC + \frac{1}{Z_{ac}} + \frac{1}{sL + D^2 Z_s}} \tag{3.5}$$

$$F'_{io} = \frac{\hat{i}_L}{\hat{i}_o} = -\frac{Z'_o}{sL + D^2 Z_s} \tag{3.6}$$

All transfer functions denoted with a prime are those found in the presence of an input filter. Notice that $Z_{ac}(s)$ appears explicitly only in Equation (3.5). It does affect other transfer functions, though, through the terms $Z_{ie}(s)$ and $H_e(s)$ which are functions of $Z_{ac}(s)$. F_{vd} and F_{id} are the control-to-output transfer functions in the absence of any input filter. The control-to-output correction factor can then be defined as:

$$G_f(s) = \frac{1 - D^2 \frac{Z_s}{R_L}}{1 + D^2 \frac{Z_s}{Z_{ie}}} \tag{3.7}$$

Similarly, F_{vg} and F_{ig} are the input-to-output transfer functions in the absence of any input filter. We may therefore define the input-to-output correction factor as:

$$G_x(s) = \frac{H_s}{1 + D^2 \frac{Z_s}{Z_{ie}}} \tag{3.8}$$

The open-loop output impedance of the regulator with input filter is given by Equation (3.5). This expression differs from that found in the absence of any input filter only by the D^2Z_s term in the denominator. Notice that the size of the reflected source impedance, D^2Z_s, relative to the output filter inductor impedance, sL, determines the effect of the filter on the open-loop output impedance. This is also true for the output current-to-inductor current transfer function, $F'_{io}(s)$.

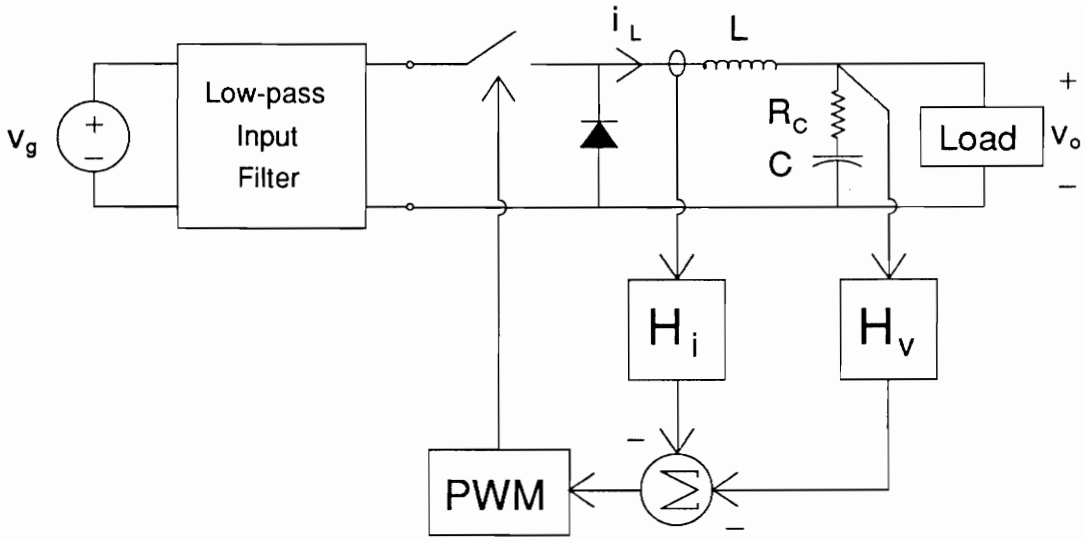

Figure 8. Current-mode controlled buck regulator with input filter

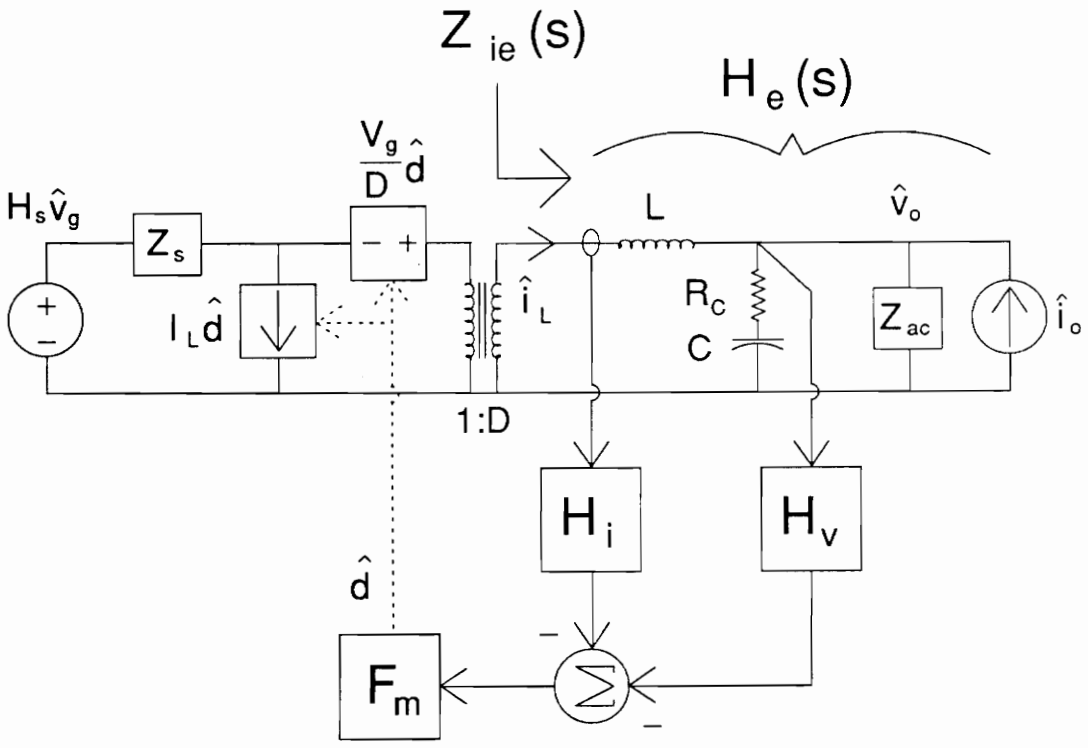

Figure 9. Small-signal model of system in Figure 8

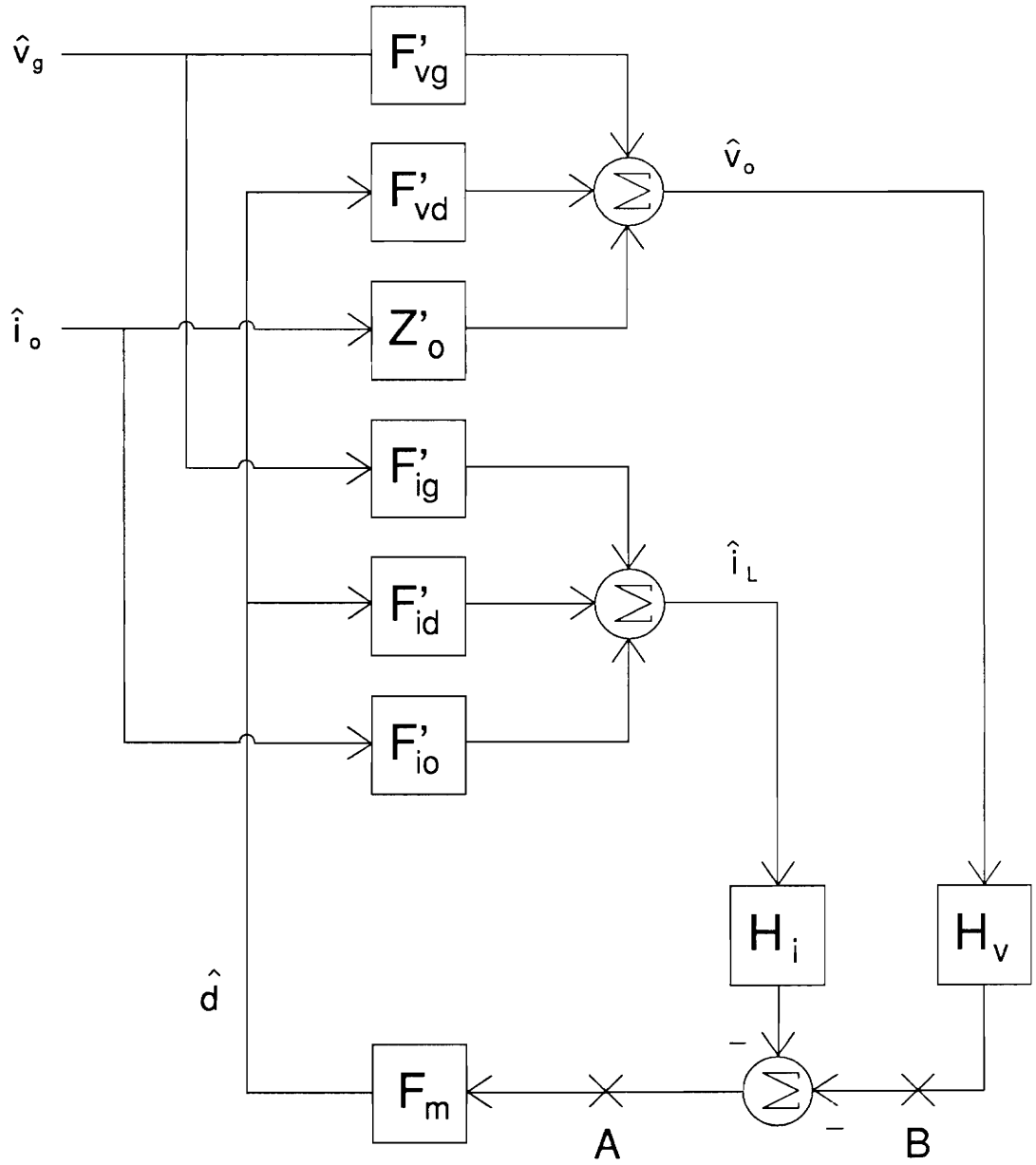

Figure 10. Block diagram of small-signal model in Figure 9

Figure 10 shows the small-signal block diagram of the system. Using this diagram, expressions for various transfer functions and loop gains of interest may be found. In the following sections, this diagram will be used to find expressions for the overall loop gain, outer loop gain, closed-loop audiosusceptibility, and the closed-loop output impedance.

3.2.1 Effect on Loop Gain

First we would like to determine the effect of the input filter on the regulator's overall loop gain. Notice that the two power stage transfer functions, F'_{vd} and F'_{id}, differ from those that would be found for the converter with no filter by the correction factor $G_f(s)$. In the absence of an input filter, the overall loop gain T_1 is defined as:

$$T_1 = F_m(H_i F_{id} + H_v F_{vd}) = T_i + T_v \tag{3.9}$$

This is the loop gain which would be measured by breaking the loop at point A in Figure 10. F_m is the gain of the pulse-width modulator. In the presence of the input filter, the overall loop gain T'_1 can be written as:

$$T'_1 = [T_i + T_v]G_f(s) = T_1 G_f(s) \tag{3.10}$$

Thus, the effect of the input filter on the overall loop gain is completely described by the correction factor $G_f(s)$. Examining the expression for $G_f(s)$ in Equation (3.7), one can easily determine the criteria which are sufficient to guarantee no degradation of the overall loop gain due to input filter interaction.

$$|Z_s(s)| << \left| \frac{R_L}{D^2} \right| \tag{3.11}$$

$$|Z_s(s)| << \left| \frac{Z_{ie}(s)}{D^2} \right| \tag{3.12}$$

If the conditions in Equations (3.11) and (3.12) are satisfied, then:

$$G_f(s) \simeq 1 \quad \text{and} \quad T'_1 \simeq T_1 \tag{3.13}$$

Thus, by tailoring the input filter output impedance to satisfy the above conditions, we may guarantee that the input filter will not degrade the regulator overall loop gain. Note that if interaction does occur and the two conditions are not satisfied, the interaction will be observed in the overall loop gain (or either of the loop gain components). Here it should be noted that the two conditions in Equations (3.11) and (3.12) are the same as those derived by Middlebrook for voltage-mode control. It should also be pointed out that in most cases R_L is the low frequency asymptote of the magnitude of $Z_{ie}(s)$, and thus the two conditions may be redundant at low frequencies. In this case, Equation (3.12) offers the more restrictive condition at frequencies above the R_LC corner but below the R_L/L corner.

It is also of interest to examine the effect of the input filter on the outer loop gain T_2, which could be measured by breaking the loop at point B in Figure 10. In the absence of an input filter, the outer loop gain T_2 is defined as:

$$T_2 = \frac{T_v}{1 + T_i} \tag{3.14}$$

In the presence of the input filter, the overall loop gain T'_2 can be written as:

$$T'_2 = \frac{T_v G_f(s)}{1 + T_i G_f(s)} = \frac{T'_v}{1 + T'_i} \tag{3.15}$$

Obviously, if Equations (3.11) and (3.12) are satisfied, then the input filter will not affect the outer loop gain. However, consider the case when the filter does interact with the regulator

for a certain range of frequencies. If the term $|T_i G_f(s)| >> 1$ at the frequencies of interaction (which is likely to occur at any frequency below the current loop crossover), then:

$$T'_2 \simeq \frac{T_v}{T_i} \quad \text{when} \quad |T_i G_f(s)| >> 1 \tag{3.16}$$

Under these conditions, the outer loop gain is independent of the input filter. It is therefore very likely that interaction with the input filter will not be observed in the outer loop gain if the interaction occurs below the current loop crossover. Thus, the outer loop gain is not a reliable measurement for determining the input filter interaction.

3.2.2 Effect on Audiosusceptibility

The audiosusceptibility (audio), or line rejection ratio, of a regulator is often given as a design specification. It is therefore of interest to determine the effect of an input filter on this quantity. For the buck regulator without an input filter, it is known that the closed-loop audio may be expressed as:

$$F_{CL} = \frac{F_{vg}}{1 + T_1} \tag{3.17}$$

Using the block diagram in Figure 10, the closed loop audio of the regulator with an input filter was found.

$$F'_{CL} = \frac{F'_{vg} + T'_i\left(F'_{vg} - \dfrac{F'_{ig}F'_{vd}}{F'_{id}}\right)}{1 + T'_1} \tag{3.18}$$

For the buck converter, this equation reduces to:

$$F'_{CL} = \frac{F'_{vg}}{1 + T'_1} \tag{3.19}$$

Both the open-loop transfer function in the numerator of Equation (3.19), and the loop gain in the denominator are affected by the input filter. Recall Equations (3.3) and (3.8). If Equation (3.12) is satisfied, then:

$$G_x(s) \simeq H_s \quad \text{and} \quad F'_{vg} \simeq H_s F_{vg} \tag{3.20}$$

Also, if Equation (3.11) is satisfied, then the overall loop gain will not be affected by the filter. In this case:

$$F'_{CL} \simeq \frac{H_s F_{vg}}{1 + T_1} = H_s F_{CL} \tag{3.21}$$

Therefore, if the two conditions in Equations (3.11) and (3.12) are satisfied by the filter design, then the overall audio of the system is simply the product of the forward gains of the unloaded input filter and the closed-loop regulator. As long as peaking in H_s is controlled, the audio of the system will not be degraded by the presence of the input filter.

Consider the frequencies where $|T'_1(s)| >> 1$. In this case, Equation (3.19) may be simplified as shown below:

$$F'_{CL} \simeq \frac{F_{vg} H_s}{T_1 \left(1 - D^2 \frac{Z_s}{R_L} \right)} \tag{3.22}$$

This equation shows that Equation (3.11) is sufficient to guarantee no degradation of the audio if interaction occurs below the overall loop gain crossover. The same result could be obtained by treating the closed-loop regulator as a black box. Recall the analysis of Section 2.4. If we

consider the input filter as the source subsystem, and the closed loop regulator as the load subsystem, then from Equation (2.1) we get:

$$F'_{CL} = \frac{H_s F_{CL}}{1 + \frac{Z_s}{Z_i}} \tag{3.23}$$

$Z_i(s)$ is the closed-loop input impedance of the regulator. When $|Z_s(s)| << |Z_i(s)|$ for all frequencies, then $F'_{CL} \simeq H_s F_{CL}$ by Equation (2.4). For typically designed regulators, $|Z_i| = |R_L/D^2|$ below the loop gain crossover. Thus, satisfying $|Z_s(s)| << |Z_i(s)|$ is the same as satisfying Equation (3.11). These results indicate that examination of the audio may not reveal degradation of the loop gain in cases when Equation (3.11) is satisfied but Equation (3.12) is not.

3.2.3 Effect on Output Impedance

Another performance index very important to voltage regulators is the output impedance. In this section, we will determine the effect of the input filter on the output impedance. In the absence of an input filter, the closed-loop output impedance can be shown to be:

$$Z_{o_{CL}} = \frac{Z_o + T_i\left(Z_o - \frac{F_{io}F_{vd}}{F_{id}}\right)}{1 + T_1} \tag{3.24}$$

Where Z_o and F_{io} are the open-loop output impedance and output current-to-inductor current transfer functions, respectively, in the absence of an input filter. Notice the T_i term in the numerator. This term represents the effect of closing the current loop on the low frequency output impedance as described in [8]. Again, using Figure 10, we can find an expression for the closed loop output impedance in the presence of the input filter.

$$Z'_{o_{CL}} = \frac{Z'_o + T'_i\left(Z'_o - \frac{F'_{io}F'_{vd}}{F'_{id}}\right)}{1 + T'_1} = \frac{Z'_o + T_iG_f(s)\left(Z'_o - \frac{F'_{io}F_{vd}}{F_{id}}\right)}{1 + T_1G_f(s)} \tag{3.25}$$

If Equations (3.11) and (3.12) are satisfied, then $G_f(s) \simeq 1$. Additionally, if:

$$\left|D^2Z_s(s)\right| << |sL| \tag{3.26}$$

Then:

$$Z'_o \simeq Z_o \quad \text{and} \quad F'_{io} \simeq F_{io} \tag{3.27}$$

Under these conditions:

$$Z'_{o_{CL}} \simeq Z_{o_{CL}} \tag{3.28}$$

It can be shown that examination of the closed-loop output impedance of the regulator may not reveal unwanted interaction under certain conditions. For example, when $|T'_i(s)| >> 1$, we may approximate the output impedance by:

$$Z'_{o_{CL}} \simeq \frac{Z'_o\left(1 + \frac{F_{vd}}{\left(sL + D^2Z_s\right)F_{id}}\right)}{1 + T_2} \tag{3.29}$$

If:

$$\left|\frac{F_{vd}}{\left(sL + D^2Z_s\right)F_{id}}\right| >> 1 \quad \text{and} \quad Z'_o \simeq sL + D^2Z_s \tag{3.30}$$

Then Equation (3.29) reduces to (3.28). Thus, even when the condition in Equation (3.26) is not satisfied, the output impedance may not be affected by the input filter. Under certain conditions, Equation (3.30) may be satisfied, while Equations (3.26) and (3.12) are not. In this case,

degradation of the loop gains will not be revealed by examination of the closed-loop output impedance. This may occur for frequencies below the power stage output filter *LC* resonance.

3.3 Input Filters for Parallel Module Regulators

The design of parallel module regulators supplied by an ideal source has already been published in [9,10,11]. However, in a real world situation, the parallel modules will not see an ideal source either due to the presence of an input filter or other equipments upstream. In this section, we will assume that a set of parallel module regulators has already been designed assuming an ideal source. The goal of this section is to determine the effect of a non-ideal source impedance on the parallel modules, and to determine design criteria for an input filter which will minimize interaction with the regulators.

Consider the system shown in Figure 11. This is a generalized representation of a stage of parallel modules supplied by a non-ideal source, and supplying a common load. For generality, the Filter 1 and 2 boxes may represent any source impedance presented to the regulators, but for simplicity, we shall consider them as discrete input filters. Since we are interested in the dynamic characteristics of the system, a small-signal model must be derived. From [7], it is known that the entire non-linearity of the power stage, due to the active switch and diode, may be replaced by the three terminal PWM switch. This may be done for each individual regulator module, resulting in the system small-signal model of Figure 12. The Filters 1 and 2 remain as black boxes for generality.

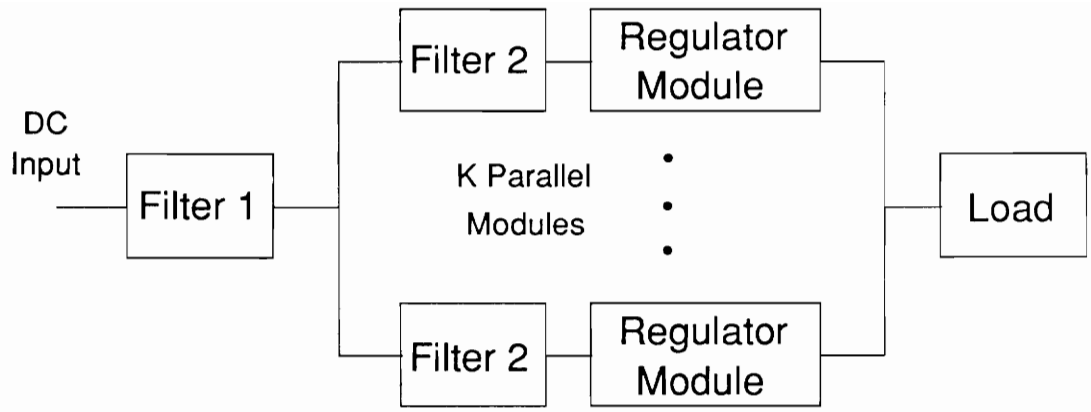

Figure 11. Block diagram of parallel module line conditioners with line input filter

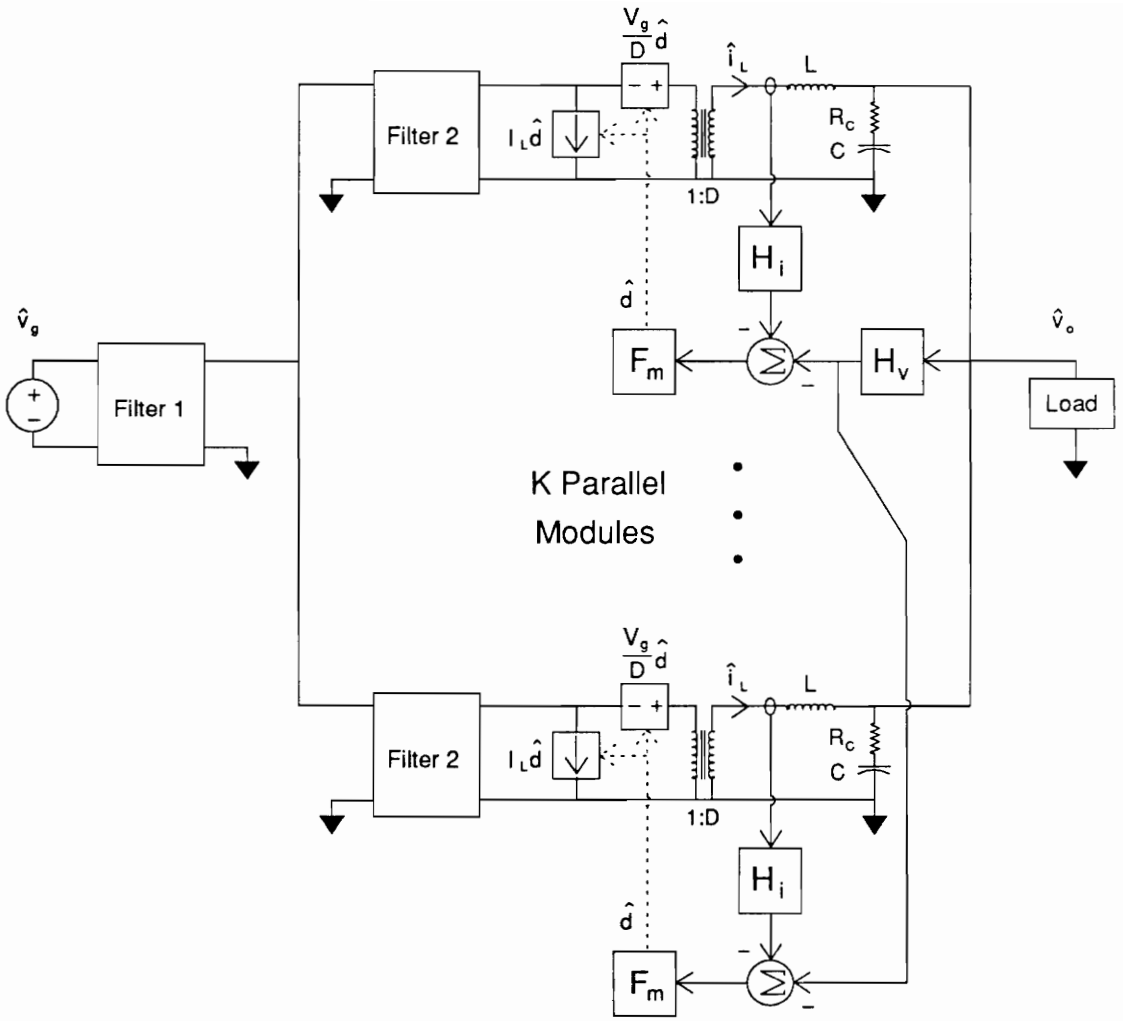

Figure 12. Small-signal model of the system in Figure 11

3.3.1 Stability Analysis/Eigenvalue Location

In this section, we are interested in determining the location of the eigenvalues of the model shown in Figure 12 to verify system stability. Examining Figure 12, the symmetry of the system is obvious. Due to the symmetry, one might be tempted to combine all of the parallel portions of the system to get one reduced "equivalent" network. For a stability analysis, this should be avoided because information on some of the system eigenvalues due to parallel interaction will be lost in the simplification process. The simple example which follows should clarify the previous statement.

Consider the system shown in Figure 13(a). This system has an obvious symmetry in the parallel filters. Also shown in the figure are the eigenvalues of the system. Now examine the simplified system model in Figure 13(b). From the eigenvalue listing, it is apparent that the simplified model does not account for all of the system dynamics. However, consider the model in Figure 13(c). Here, all but one of the parallel filters have been reduced. This model maintains all of the dynamics of the original system, including those due to parallel interaction. Looking at the eigenvalues in Figure 13(c), it is seen that this model has the same eigenvalues as the original system, but does not predict the same multiplicity. For a stability analysis, multiplicity is irrelevant, and the model in Figure 13(c) provides all the necessary information.

Keeping the previous example in mind, we may now formulate a simple method for determining stability of the system in Figure 12. One approach to finding the eigenvalues of the system would be to introduce a perturbation at a point where the system is observable (an ac current source across the output filter inductor of one regulator module, for example). Then we could write the state equations for the entire closed-loop system and solve the characteristic equation. This approach, however, would be tedious at best. Rather, we would like to find an easy method of determining system stability that can be carried out quickly.

(a)

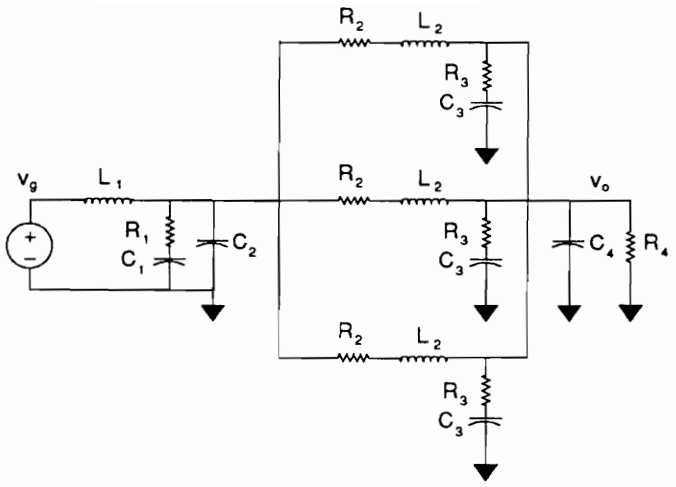

Eigenvalues	
Real	Imag
-1021	±4356
-20000	0
-20000	0
-24228	±41776
-24602	0
-666667	0
-666667	0
-4.8E6	0

(b)

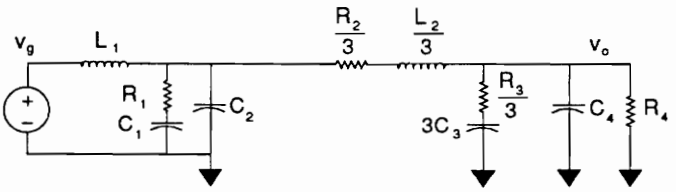

Eigenvalues	
Real	Imag
-1021	±4356
-24228	±41776
-24602	0
-4.8E6	0

(c)

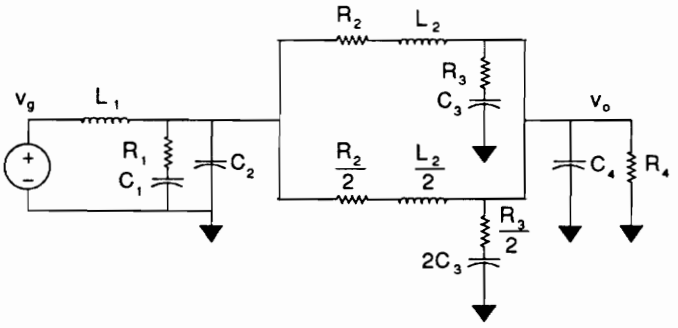

Eigenvalues	
Real	Imag
-1021	±4356
-20000	0
-24228	±41776
-24602	0
-666667	0
-4.8E6	0

Figure 13. Example of system with eigenvalues due to parallel interaction: (a) full system, (b) simplified model, (c) reduced model maintaining all dynamics

Therefore, we will now develop a simplified model of the system which will maintain the dynamics due to parallel interaction and provide all of the information necessary to determine stability.

It is known that the closed-loop input impedance of a regulator module may be approximated by a negative valued resistance for all but high frequencies. Therefore, we may replace the input ports of the parallel modules with simple negative resistances, as shown in Figure 14(a). Since we are only concerned with the location of the eigenvalues and not the multiplicity, we may simplify the model in Figure 14(a) as shown in Figure 14(b). This model is analogous to that in Figure 13(c), and will predict system instability caused by the addition of an input filter.

With the new input filter model shown in Figure 14(b), the Filters 1 and 2 may be designed such that the filter eigenvalues are well damped and in the LHP, insuring system stability. In Section 3.4, this model will be used in the design of the line input filter. It will be shown how the model can predict instability resulting from an incorrectly designed filter. In Section 3.5, the model will be used in the design of the intermediate bus filter.

3.3.2 Single Module Model

Again consider the system shown in Figure 12. If we are interested in determining the audiosusceptibility of this system, we could perturb the input, $\hat{v}_g$, and measure the response at the output $\hat{v}_o$. As we perturb the input, each line conditioner module will see the same perturbation in its inductor current, output voltage, and duty cycle. If we are only interested in the response at the output (ignoring the eigenvalues due to parallel interaction), we may combine the parallel modules to obtain the single module model shown in Figure 15. This single module model is analogous to the simplified model in Figure 13(b) for the example in

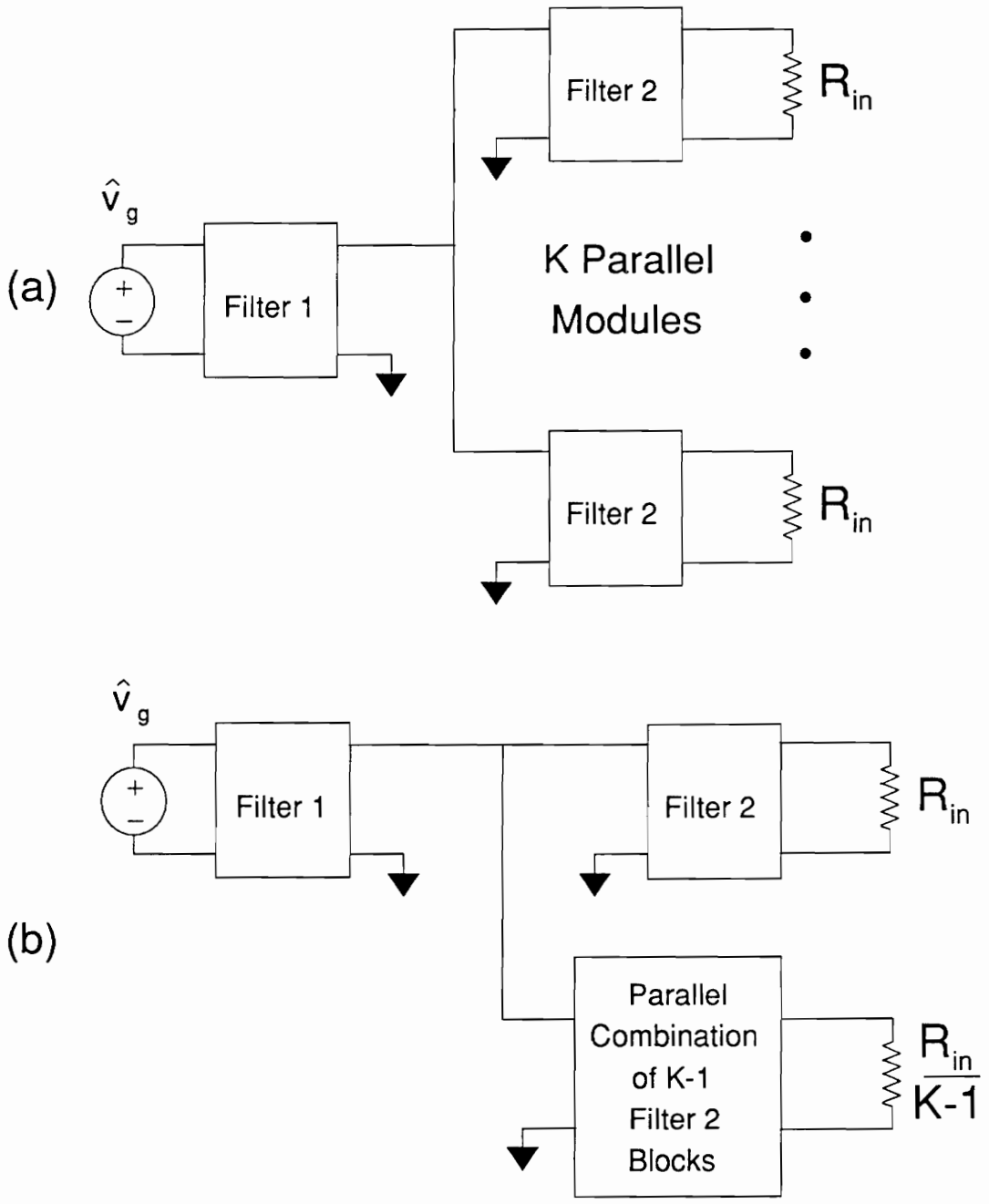

Figure 14. Source model used to predict input filter interaction: (a) full model, (b) reduced model maintaining all dynamics

the previous section. While this model does not predict all of the eigenvalues of the system, it will provide the same audiosusceptibility curve as would the actual system in Figure 12.

In a similar fashion, if we were interested in measuring the output impedance or outer loop gain of the system, the single module model would provide the same measurement as the system in Figure 12. An equivalent overall loop gain discussed in [9,10,11] may also be found using the single module, but it should be remembered that this loop gain cannot be measured in the actual circuit.

Before proceeding, some clarifications need to be made. First, it is obvious that the systems in Figure 12 and Figure 15 are not the same. They have a different number of states, and their characteristic equations must be different, as shown in the example in the previous section. However, the single module model will provide the same audio, output impedance, outer loop gain, and equivalent overall loop gain measurements as the system in Figure 12 since the eigenvalues due to parallel interaction are unobservable from these points. This can be explained by noting that for each of those transfer functions, the system in Figure 12 is non-minimal. None of these transfer functions can reveal the presence of parallel interaction. This could lead to in erroneous results when attempting to determine stability from the single module model. However, the single module model is still a useful tool if one keeps in mind its limitations. In Section 3.4.3, the definitions of non-minimal dimensional, observable, and controllable are given.

Here we will use the single module model to determine the effect of the input filter on the audio, output impedance, and loop gains. The single module model shown in Figure 15 is identical to a single module regulator being fed by a non-ideal source. Therefore, to determine the effect of the line input filter on the audio, output impedance, and loop gains of the system, we can use the single module model and apply the results of Section 3.2. In this manner we can design an input filter to avoid degradation of the regulator performance. The audiosusceptibility provided by the single module will correctly predict the response at the

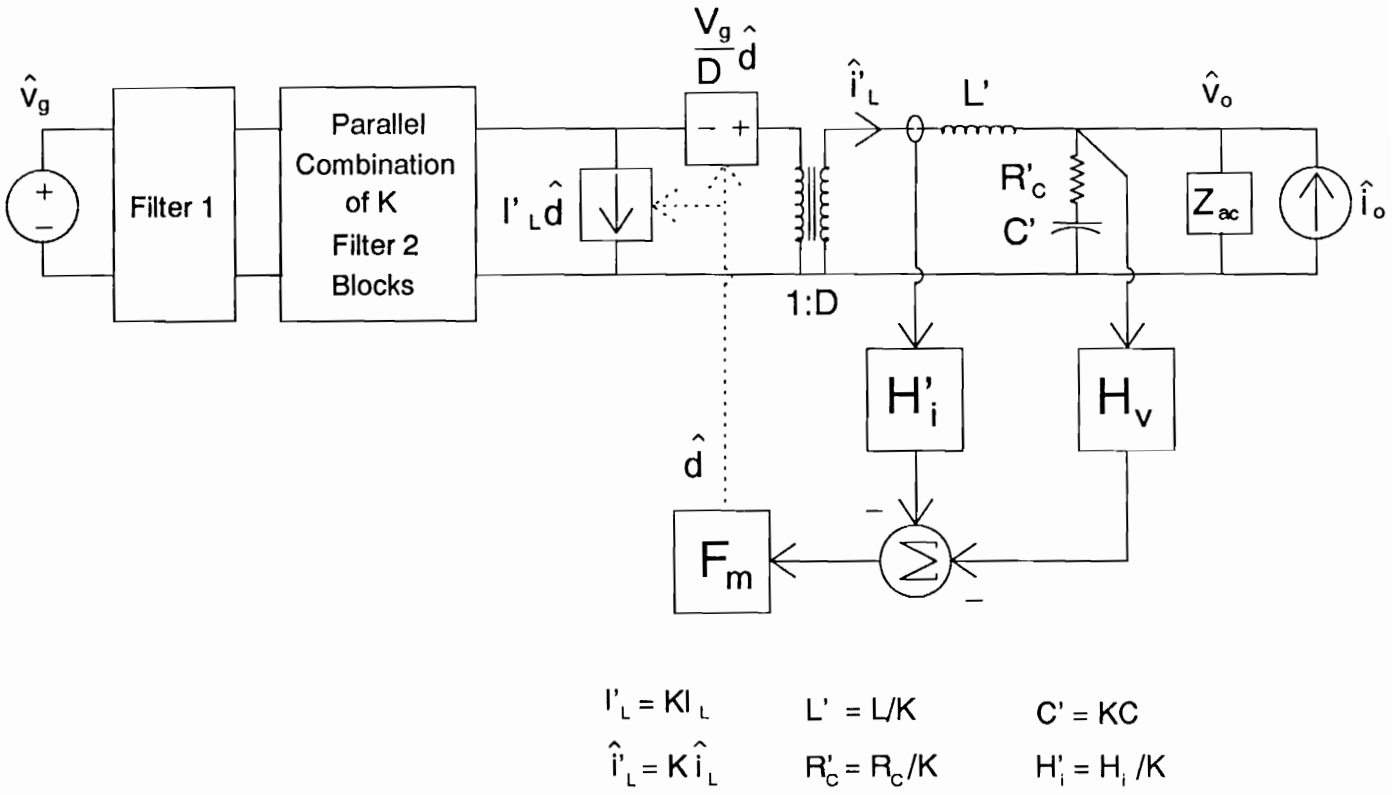

Figure 15. Single module model of system in Figure 12

system output to a perturbation at the input. Similarly, the output impedance provided by the single module will correctly predict the response at the output due to a perturbation in the load. However, one must be careful not to use the single module model to determine absolute stability. On the other hand, if stability of the eigenvalues due to parallel interaction has already been assured using the technique of Section 3.3.1, the equivalent single module may be used to determine relative stability of the remaining eigenvalues of the system.

The single module model will be used when designing both the line input filter in Section 3.4, and when designing the intermediate bus filter in Section 3.5.

3.4 Design of the Line Input Filter

As previously discussed, almost all power supplies need some type of filtering on the input to attenuate the harmonic currents generated by the regulator. For the DPS under consideration, the MIL-STD 461B CE03 conducted emissions specification needed to be met at the system input. This specification, issued by the U.S. Department of Defense, places a limit on the harmonic currents which may be seen on the power line between 15kHz and 50MHz. For Naval applications drawing less than 1*A* of load current from the line, the specification is given as the solid curve in Figure 16. This curve determines the maximum peak-to-peak current which may be drawn from the source at any frequency between 15kHz and 50MHz. For equipment drawing more than 1*A* load current, the specification may be relaxed between 15kHz and 2MHz as follows. Increase the 15kHz limit by 20log(load current). Draw a line from the relaxed limit at 15kHz to the 2MHz, 20dBμA point. This line is the new limit between 15kHz and 2MHz. Above 2MHz, the specification remains unchanged. The relaxed specification for the system under consideration is shown as the dashed line in Figure 18.

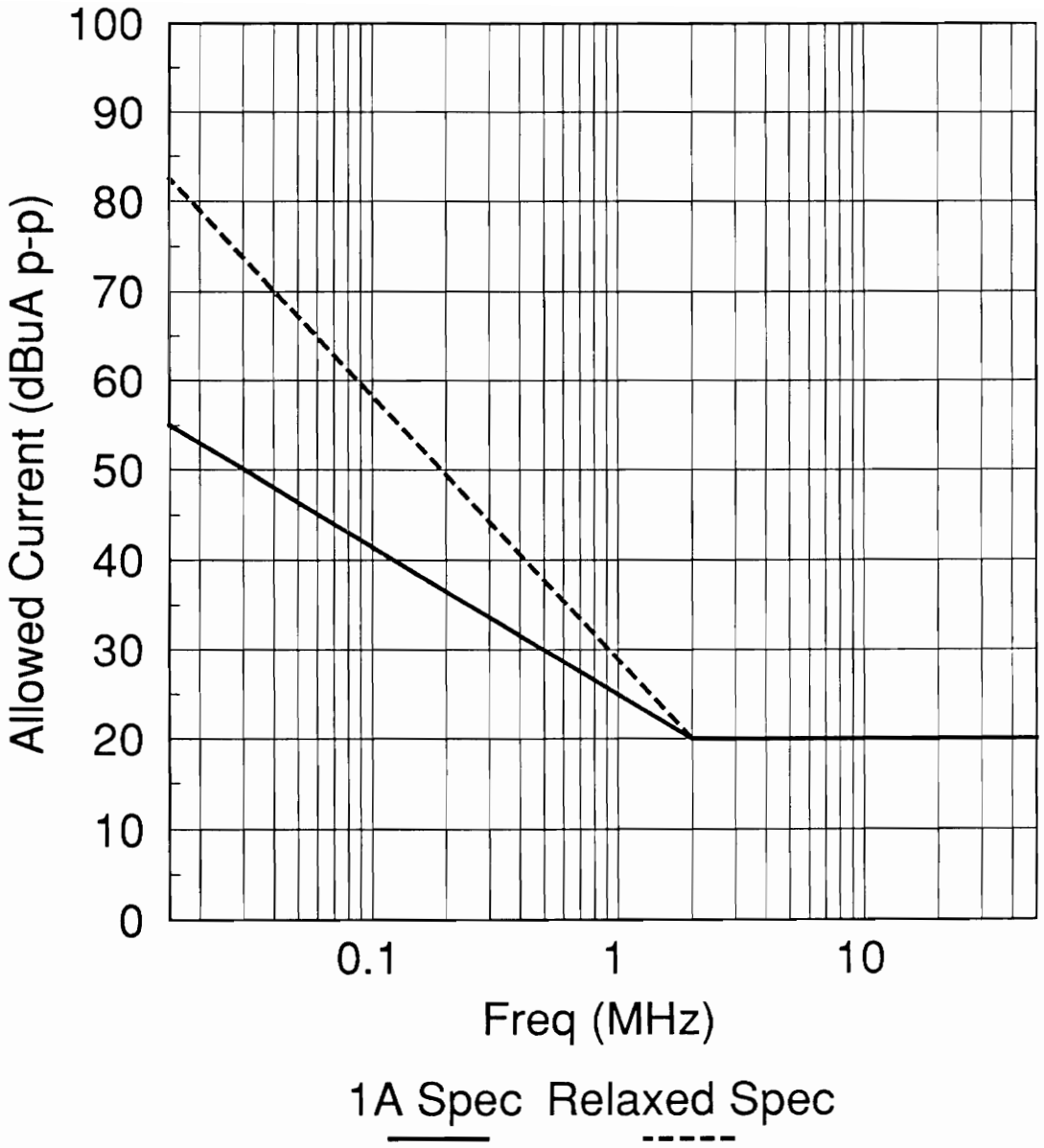

Figure 16. Limit for MIL-STD 461B CE03 Narrowband Emissions

Table 1. Worst-case harmonic magnitude and required attenuation

Frequency (MHz)	Allowed Current (uA p-p)	Load Current (A p-p)	Attenuation (dB)
0.25	224	34.0	103.6
0.50	79	17.1	106.6
0.75	40	11.3	109.1
1.00	28	8.5	109.6
1.25	20	6.8	110.6
1.50	16	5.7	111.0
1.75	13	4.9	111.7
2.00	10	4.3	112.6

To determine the attenuation required of the input filter, we must first find the worst-case current spectrum drawn by the line conditioners. It is obvious that in-phase operation at heavy load will create the largest harmonic currents. However, each harmonic varies differently with the input voltage (or duty cycle). Thus, the worst-case for each harmonic will occur at a different line voltage. For example, the first harmonic at the fundamental frequency is maximum at a line voltage of 180*V* (corresponding to a duty cycle of 0.5). However, the second harmonic has a minimum at that line voltage. To determine the worst-case for each harmonic, the magnitude of each harmonic was plotted versus line voltage for the full range of input voltage. This was done using analytical equations of the Fourier coefficients as derived in [12] for the first eight harmonics. Table 1 shows the worst-case harmonics, the military specification at each harmonic frequency, and the required attenuation at each harmonic frequency.

From Table 1, we see that the filter must provide a minimum of 103.6dB attenuation at 250kHz for the fundamental. Notice that the higher order harmonics require very little additional attenuation compared to the fundamental. Considering the fact that the filter will have at least 6dB/octave attenuation after the fundamental, it is apparent that if the specification is met for the fundamental, it will be met for the higher order harmonics as well. Therefore, the resulting design specification for the input filter is a minimum of 103.6dB attenuation at 250kHz.

3.4.1 Large-signal Considerations

In general, the line input filter consists of two components as shown in Figure 11 on page 41. One filter, common to all modules, is located before a summing junction where the modules are tied in parallel (Filter 1). Another filter is then located directly in front of each regulator module (Filter 2). Filter 2 is needed, otherwise large ripple currents would flow on the distribution lines feeding each line conditioner module. Since the DPS is often used to supply

noise sensitive equipment, these large ripple currents could be problematic. Also, without Filter 2, the large ripple current seen at the summing junction would generate a considerable ripple voltage at the output of Filter 1, which is undesirable for the line conditioners. Therefore, each Filter 2 block should provide enough attenuation so that the ripple current on the distribution lines is reduced to an acceptable level.

With parallel converters, phase-shifted clocks may be used to reduce input and output ripple currents. At the summing junction, ripple cancellation between phases occurs, thus providing attenuation without the associated cost of increased filter size. However, if the filters are to be designed for worst-case attenuation, the conditioners should be assumed to be operating in-phase. It is also assumed that the parallel modules are frequency synchronized, thus eliminating the possibility of sum and difference frequency components.

When designing the system input filter, there are two possible approaches. In one case, we could attempt to design the Filter 1 and Filter 2 blocks independently and then minimize interaction by insuring a wide separation in impedances seen at the summing junction. The overall filter attenuation would then be the product of the individual Filter 1 and Filter 2 attenuations. This approach is not optimal from a filtering viewpoint and might not be practical considering the restrictions placed on the output impedance of Filter 2 (to minimize interaction with the line conditioners). On the other hand, we could design the filters such that they work together. This second design approach would be to design Filter 1 and 2 together, expecting interaction between the two stages. In this case, the impedances seen at the summing junction would overlap for some frequencies (the minor loop gain defined at this point would be greater than 0dB for some frequencies) due to the interaction between stages.

For the required level of attenuation, it was decided to use a fourth-order input filter. A common topology for single module regulators, shown in Figure 17, uses a resistor in series with the first stage capacitor to damp both stages of the filter. The second stage capacitor should have a very low ESR since a large RMS current passes through this capacitor. By distributing

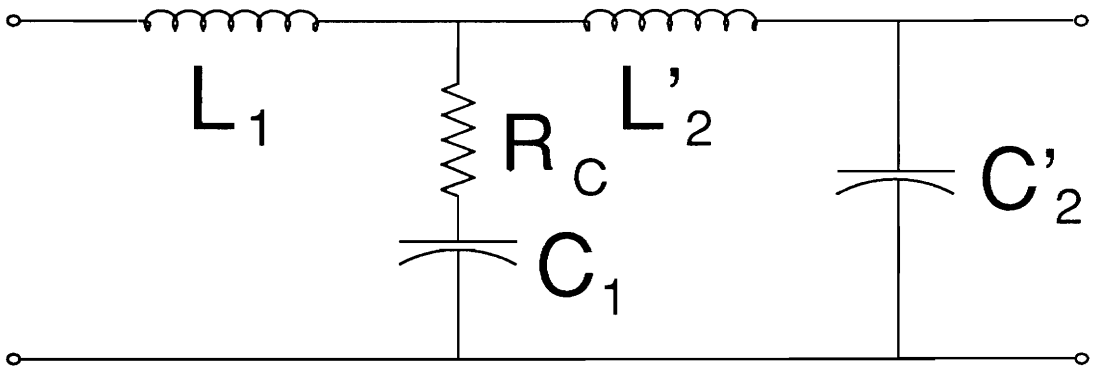

Figure 17. Fourth-order low-pass input filter

various elements of the filter in Figure 17, we may come up with a distributed topology, as represented by the Filter 1 and 2 boxes in Figure 11.

The first filter topology considered for the input filter is shown in Figure 18. In this topology, the second stage capacitance of the fourth-order filter was distributed to the Filter 2 blocks. Distributing the second stage capacitance was intended to reduce the the large ripple current on the distribution lines due to the pulsating input current of the line conditioners. The small-signal analysis predicted good filter performance, but the large-signal simulation brought to light some undesirable features of this topology.

A large-signal model was constructed to test the performance of the input filter. The initial test of this topology used only two parallel modules, and Figure 19 shows the simulation results for in-phase operation. Figure 19(a) and (b) show the in-phase current waveforms drawn by the two line conditioners. Notice that a duty cycle of 0.5 and full load current were chosen for the simulation to provide the worst case fundamental. Shown in Figure 19(c) and (d) are the distribution line currents as defined in Figure 18, which have a low peak-to-peak current ripple. Also shown is the overall input current, which meets the attenuation specification of 103.6dB.

Phase-shifted operation was simulated to observe the effect of ripple cancellation. Figure 20 shows the phase-shifted operation results. The simulation revealed the problem of this topology during phase-shifted operation. Under phase-shifted operation, the potential difference developed across each distributed capacitor C_2 caused large circulating currents to flow between modules [13]. The distributed capacitance, intended to reduce distribution line ripple current, is ineffective for phase-shifted operation. To avoid this problem, the input filter was designed using a distributed second stage inductance.

Figure 21 shows the second topology chosen for the line input filter. Notice that both the second stage capacitance and inductance of the fourth-order filter were distributed to the

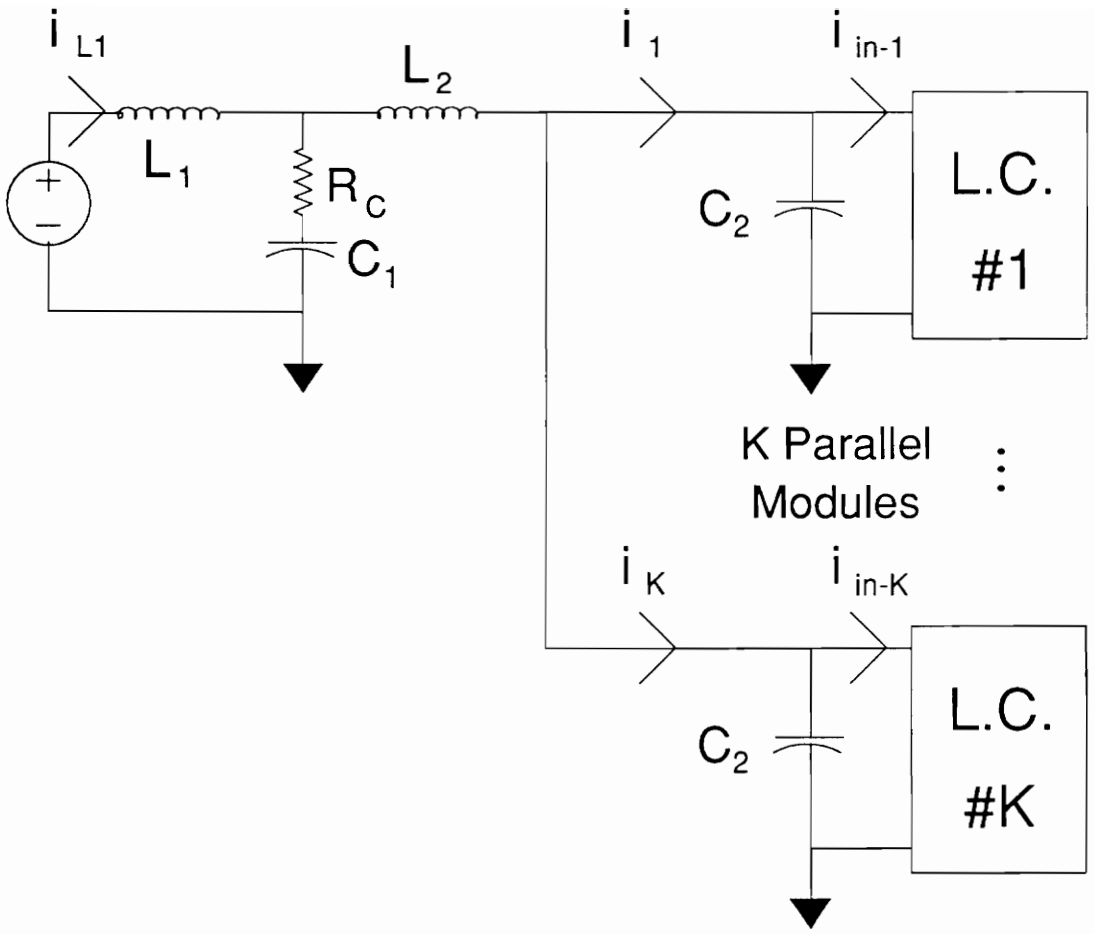

Figure 18. Line input filter with distributed second stage capacitance

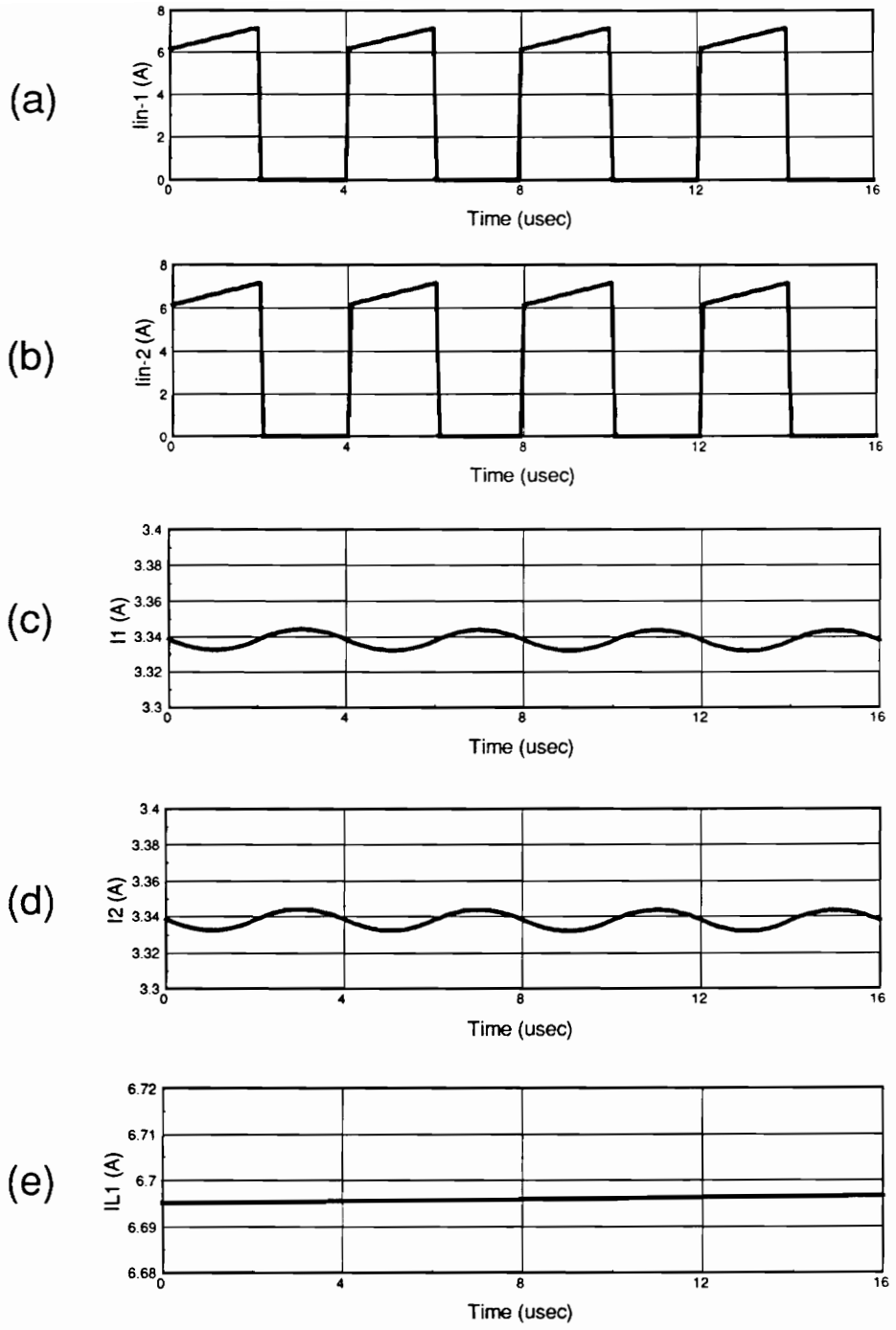

Figure 19. In-phase operation of initial input filter topology: (a) input current drawn by module 1, (b) input current drawn by module 2, (c) distribution line current feeding module 1, (d) distribution line current feeding module 2, (e) overall input current

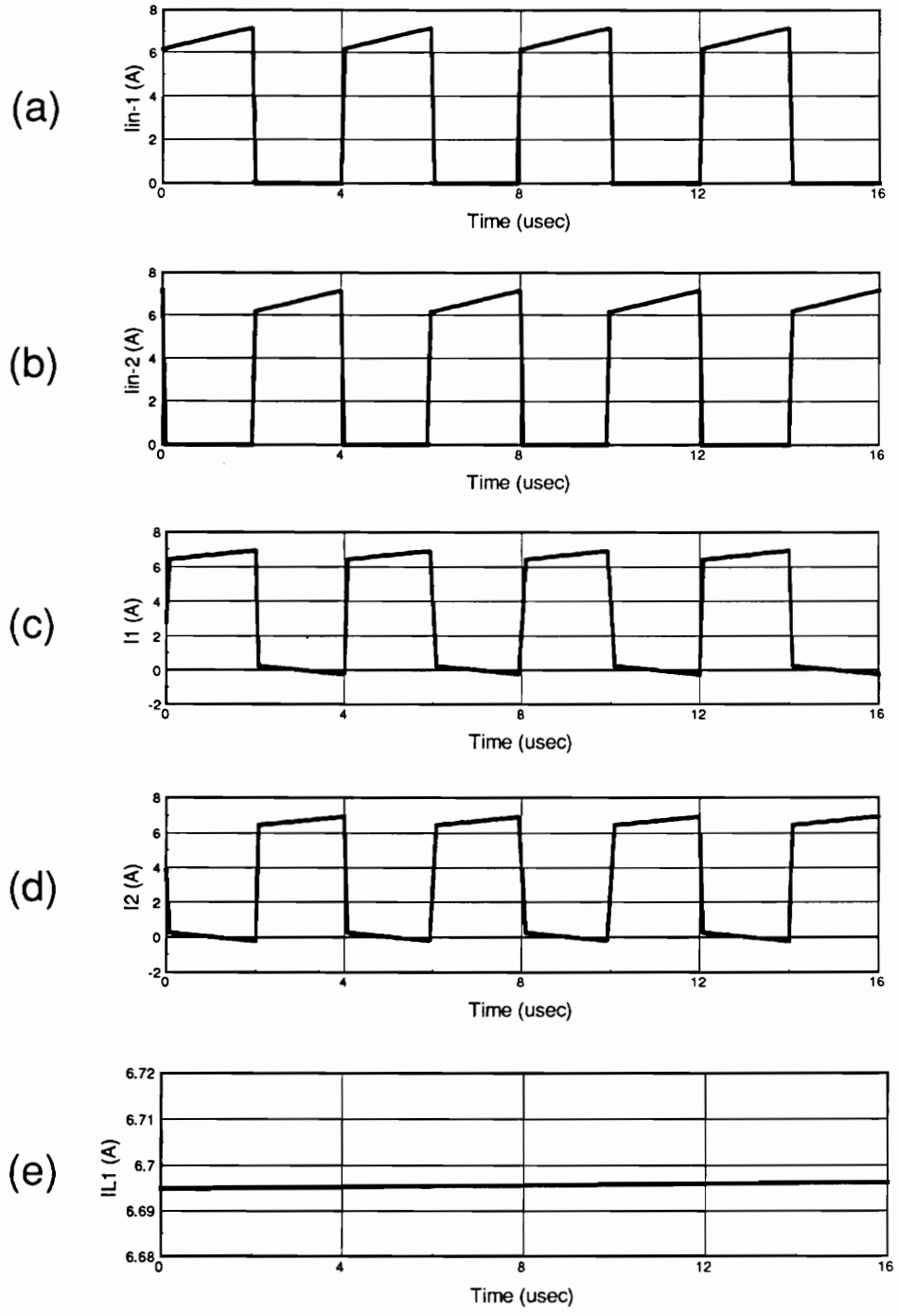

Figure 20. Phase-shifted operation of initial input filter topology: (a) input current drawn by module 1, (b) input current drawn by module 2, (c) distribution line current feeding module 1, (d) distribution line current feeding module 2, (e) overall input current

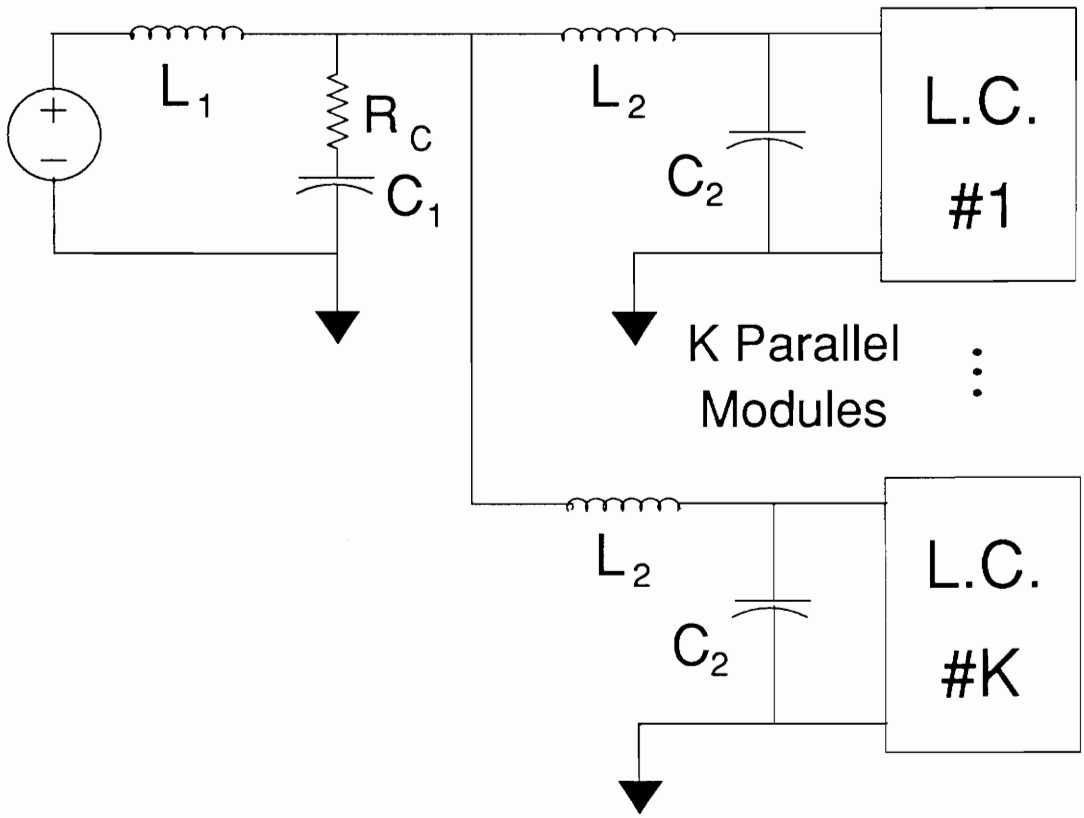

Figure 21. Line input filter with distributed second stage inductance and capacitance

second stage blocks. This filter must be designed to provide 103.6dB of attenuation at 250kHz, while avoiding degradation of the line conditioner performance and maintaining stability.

3.4.2 Stability Analysis

3.4.2.1 Instability Due to Parallel Interaction

To determine the absolute stability of the line input filter and the parallel line conditioner modules, we may use the input filter model derived in Section 3.3.1. Figure 22(a) shows the model of the filter in Figure 21 for K parallel line conditioner modules. The equivalent shunt branch consisting of the elements L_{2eq}, C_{2eq}, and R_{ineq} represents the impedance seen at the summing junction due to $(K-1)$ parallel modules. It is the purpose of this section to estimate the eigenvalue location of the input filter model, and show how instability results due to parallel interaction.

First, we may find four of the eigenvalues by further simplification of the filter model, as shown in Figure 22(b). The system in Figure 22(b) has been discussed previously in [1,14,15]. For stability, it can be shown that $|Z_s(s)| << |R_{in}/K|$ is a sufficient condition to guarantee that the four eigenvalues will lie in the LHP. For a typical design, $C_1 >> KC_2$ and $L_1 >> L_2/K$. One pair of eigenvalues occurs at the first stage resonance. Near the first stage resonant frequency we may assume that C_2 is essentially an open circuit, while L_2 is a short circuit. The eigenvalues due to the first stage resonance can be estimated as the roots of CE_1 shown in Equation (3.29) below.

$$CE_1 = s^2 L_1 C_1 \left(1 + R_c \frac{K}{R_{in}}\right) + s\left(C_1 R_c + L_1 \frac{K}{R_{in}}\right) + 1 = 0 \qquad (3.29)$$

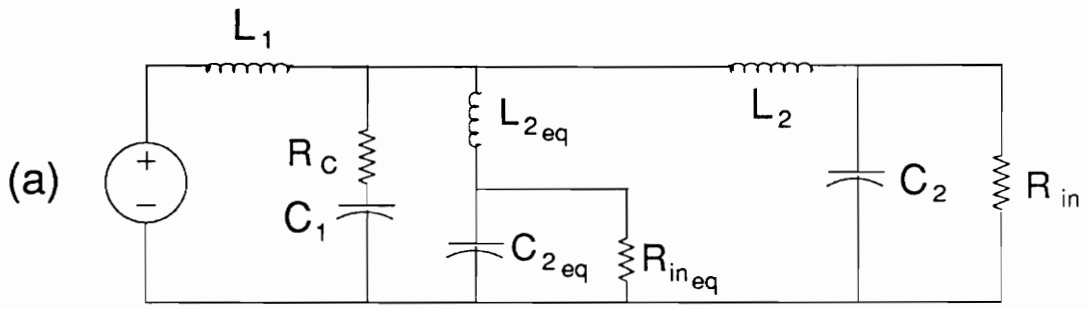

$$L_{2_{eq}} = L_2 /(K-1)$$
$$C_{2_{eq}} = (K-1)C_2$$
$$R_{in_{eq}} = R_{in} /(K-1)$$

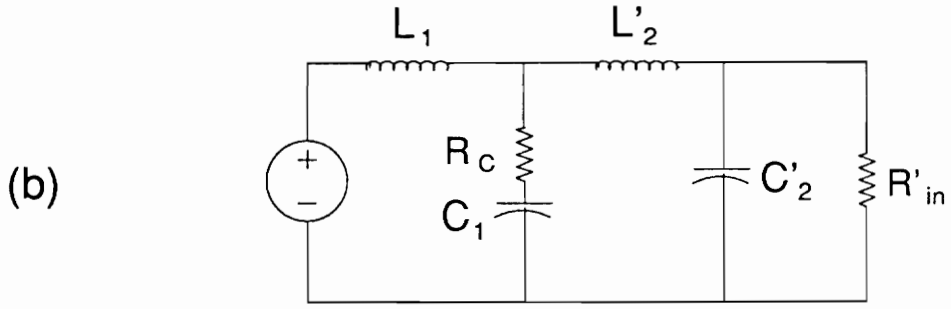

$$L'_2 = L_2 /K$$
$$C'_2 = KC_2$$
$$R'_{in} = R_{in}/K$$

Figure 22. Input filter models for the filter in Figure 21: (a) complete model, (b) simplified model

Another pair of eigenvalues can be found at the second stage resonant frequency. At this frequency, L_1 can be assumed to be an open circuit, while C_1 is a short circuit. Therefore, KC_2 and L_2/K form a resonant loop, and the resulting eigenvalues may be approximated by the roots of CE_2 as shown in Equation (3.30).

$$CE_2 = s^2 L_2 C_2 \left(1 + R_c \frac{K}{R_{in}}\right) + s\left(\frac{KC_2 R_c + \frac{L_2}{R_{in}}}{1 + R_c \frac{K}{R_{in}}}\right) + 1 = 0 \qquad (3.30)$$

Finally, we may find the eigenvalues due to parallel interaction by using the model in Figure 22(a). A resonant loop exists between C_{2eq}, L_{2eq}, C_2, and L_2. The impedance of the equivalent shunt branch will be very low due to series resonance, and therefore the effect of R_c on this resonance will be negligible. In fact, due to the perfect symmetry involved, it can be shown that the elements L_1, C_1, and R_c will have *no effect* on these eigenvalues due to parallel interaction. Thus, the resulting eigenvalues are given by the roots of CE_3 as shown in Equation (3.31).

$$CE_3 = s^2 L_2 C_2 + s\frac{L_2}{R_{in}} + 1 = 0 \qquad (3.31)$$

The combined roots of CE_1, CE_2, and CE_3 are the eigenvalues of the filter model shown in Figure 22(a). For a reasonable value of damping resistance R_c, CE_1 and CE_2 will provide stable eigenvalues. However, due to parallel interaction, CE_3 will always have RHP eigenvalues. Therefore, the filter in Figure 21 will be unstable, with unbounded oscillating currents between modules.

3.4.2.2 *Filter Stabilization with Second Stage Damping*

In order to stabilize the system, some additional damping must be added to the filter such that the eigenvalues due to parallel interaction move into the LHP. Looking at Figure 22(a), it can be seen that a damping resistance could be added in series with each second stage inductance or across each second stage capacitance to damp the eigenvalues due to parallel interaction. The latter method was chosen, and a DC blocking capacitor was used to block DC current through the damping resistor. Figure 23 shows the redesigned filter introducing additional damping. The effect of the additional elements on system stability must now be assessed.

Figure 24(a) shows the model of the filter in Figure 23 for K parallel line conditioner modules. In a manner similar to the last section, we may further simplify the filter model as shown in Figure 24(b) to find five of the eigenvalues. Suppose that the filter is designed such that $C_1 >> KC_d >> KC_2$ and $L_1 >> L_2/K$. In this case, the eigenvalues associated with the first stage resonance are not greatly affected by the additional damping branch. Thus, two of the eigenvalues are given by Equation (3.29). At the second stage resonance, we may assume that KC_d is a short circuit. Thus R_d/K will be seen in parallel with R_{in}/K. Therefore, the resulting eigenvalues may be approximated as the roots of CE_4 in Equation (3.32), where R_p is the parallel combination of R_d and R_{in}.

$$CE_4 = s^2 L_2 C_2 \left(1 + R_c \frac{K}{R_p}\right) + s\left(\frac{KC_2R_c + \dfrac{L_2}{R_p}}{1 + R_c \dfrac{K}{R_p}}\right) + 1 = 0 \qquad (3.32)$$

Also, a single real eigenvalue will appear at approximately the R_dC_d corner.

Finally, the remaining three eigenvalues may be found by examining the filter model in Figure 24(a). Near the second stage resonance, C_d and $C_{d_{eq}}$ are essentially short circuits.

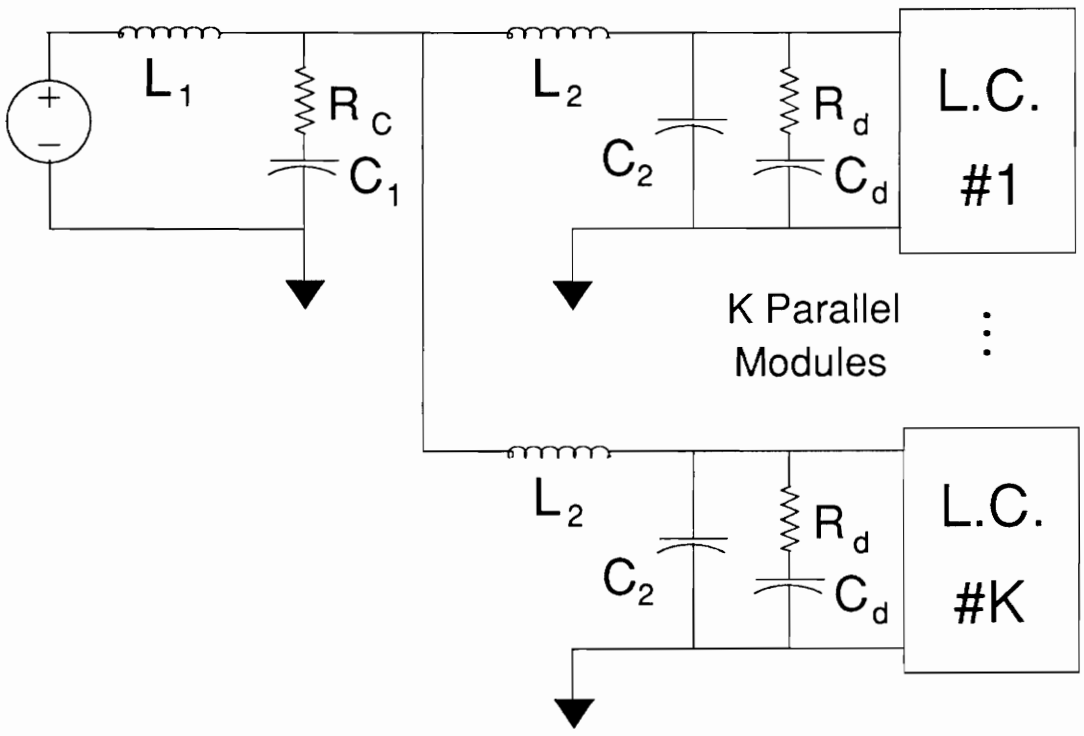

Figure 23. Line input filter with second stage damping

(a)

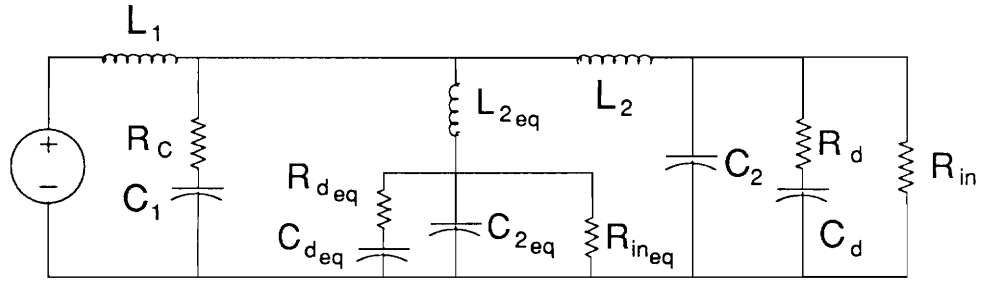

$$L_{2_{eq}} = L_2/(K-1)$$
$$C_{2_{eq}} = (K-1)C_2$$
$$R_{in_{eq}} = R_{in}/(K-1)$$
$$C_{d_{eq}} = (K-1)C_d$$
$$R_{d_{eq}} = R_d/(K-1)$$

(b)

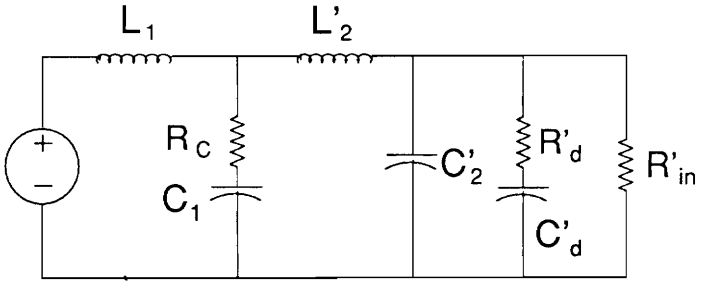

$$L'_2 = L_2/K$$
$$C'_2 = KC_2$$
$$R'_{in} = R_{in}/K$$
$$C'_d = KC_d$$
$$R'_d = R_d/K$$

Figure 24. Input filter model for the filter in Figure 23: (a) complete model, (b) simplified model

Regardless of the values of L_1, C_1, and R_c, the eigenvalues due to parallel interaction can be approximated as the roots of CE_5 in Equation (3.33).

$$CE_5 = s^2 L_2 C_2 + s \frac{L_2(R_d + R_{in})}{R_d R_{in}} + 1 = 0 \tag{3.33}$$

It is obvious that for reasonable values of R_c and R_d, CE_1 and CE_4 will provide well damped eigenvalues in the LHP. The damping term in CE_5 is positive if $R_d < R_{in}$, meaning that the eigenvalues due to parallel interaction can be moved into the LHP by appropriate selection of R_d. Thus, by adding damping to the second stage of the filter, we were able to stabilize a system that was previously unstable due to parallel interaction. Also note that another real eigenvalue will appear at approximately the R_dC_d corner due to parallel interaction.

3.4.2.3 Non-minimal Dimensional Systems and Filter Example

In this section, definitions for non-minimal dimensional systems, observability, and controllability will be given. An example will be given to back up the stability analysis of the previous sections, and it it will be shown how the definitions of observability and controllability translate into circuit behavior. Finally, the implications of non-minimal subsystems on the subsystem interaction analysis presented in Chapter 2 will be discussed.

First, recall the following definitions for a single-input, single-output linear system [3].

> A minimal dimensional system is a system of the least possible dimension (or order) that provides the desired input-to-ouput transfer function.
>
> A non-minimal dimensional system can be reduced to a lower order system which will still provide the same input-to-output transfer function.

If a dynamical system is observable, all the modes of the system can be observed at the output.

If a dynamical system is controllable, all the modes of the system can be excited from the input.

Consider the circuit shown in Figure 25. This is a small-signal model of the filter ($K = 2$) shown in Figure 22 with the line conditioner input impedances approximated with negative resistances R_{IA} and R_{IB}. There are two independent sources which will be used to demonstrate the behavior of this filter.

First, the response of the filter to a sinusoidal input voltage source was simulated using the PSPICE code shown in Figure 25. The voltage source was set to 1*V* peak at 5kHz. The results are shown in Figure 26. Notice that all of the voltages and currents of the system are stable and well behaved. Next, the response of the filter to a sinusoidal output current source was simulated (1*A* peak at 5kHz). These results are shown in Figure 27. It is immediately apparent that the filter is unstable due to unbounded oscillations between the two second stage filters. Also notice that the first stage filter remains stable even when the second stage blows up. This is because the unbounded component of the currents in L_{2A} and L_{2B} are 180° out-of-phase. The unbounded oscillation is predicted exactly by the Equation (3.31). Also notice that the unbounded oscillation occurs at 10kHz, which is the natural frequency of the system's RHP eigenvalue.

At first, one might be confused as to why a system may appear to be stable when excited by one particular source (the input voltage source) and unstable when excited by another (the output current source). This can be explained by observability and controllability. From the input admittance of the filter, the system is neither observable nor controllable. That is, not all of the system eigenvalues can be excited by the input voltage source. For example, examination of the input admittance shown in Figure 28 reveals a stable transfer function.

(a)

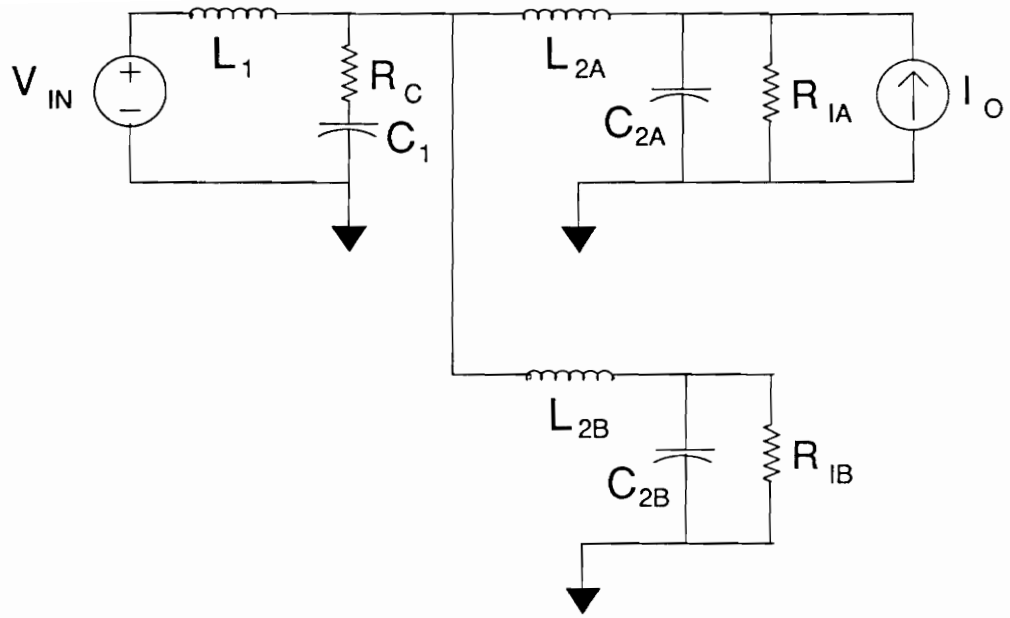

(b)

```
Line Input Filter Model

* Sources
VIN     1     0     DC  0  AC   0   SIN(0  1  5E3)
IO      0     4     DC  0  AC   0

* Filter 1
L1      1     2     80U  IC=0
C1      3     0     320U  IC=0
RC      2     3     0.5

* Filter 2A
L2A      2     4     42.5U  IC=0
C2A      4     0     6.8U  IC=0
RIA      4     0     -26

* Filter 2B
L2B      2     5     42.5U  IC=0
C2B      5     0     6.8U  IC=0
RIB      5     0     -26

.TRAN   20U  10M   UIC
.PRINT   TRAN   V(4)   I(L1)   I(L2A)   I(L2B)
.PROBE
.END
```

Figure 25. Unstable filter example: (a) circuit model, (b) PSPICE code

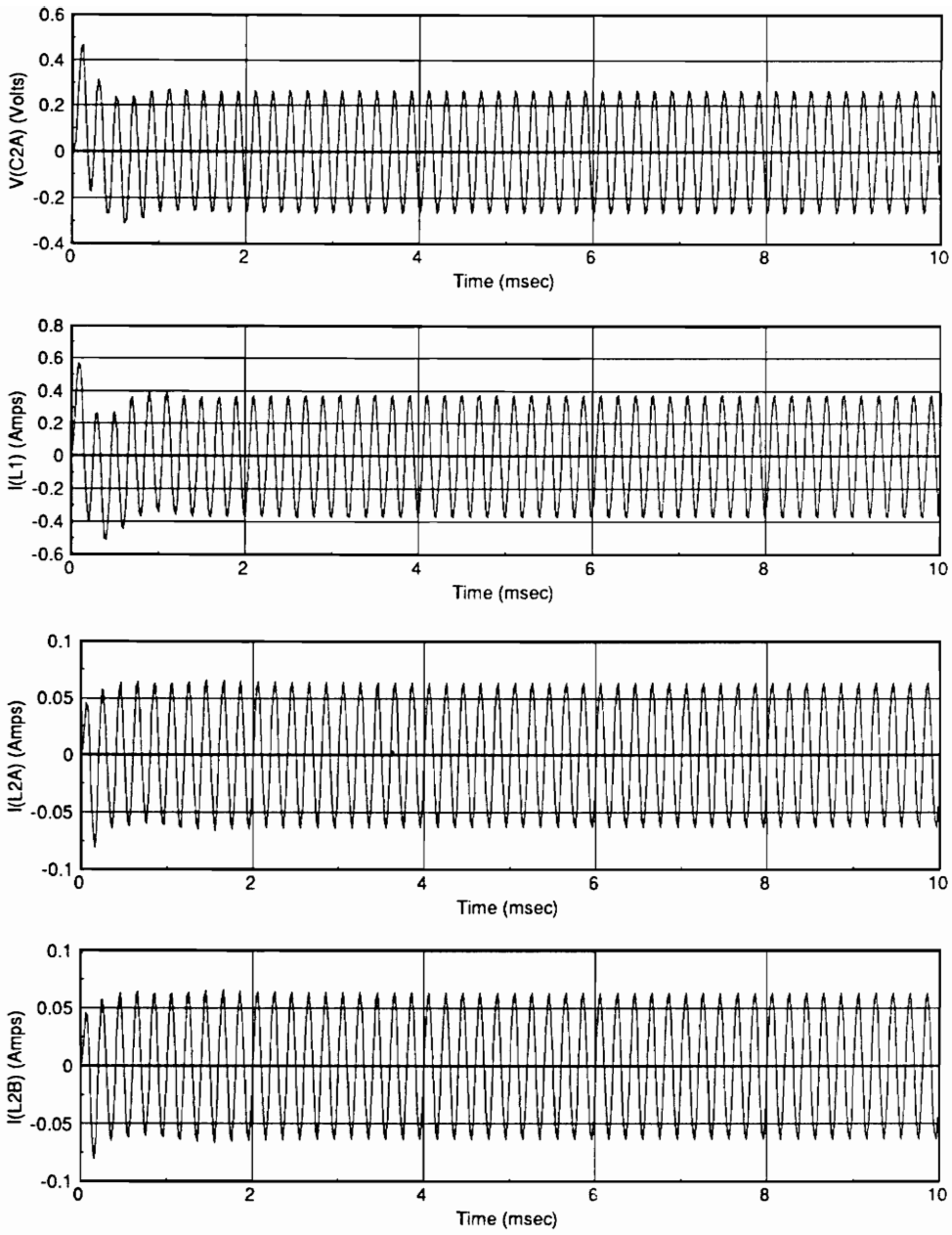

Figure 26. Response to input voltage excitation: (a) voltage across C_{2A}, (b) current through L_1, (c) current through L_{2A}, (d) current through L_{2B}

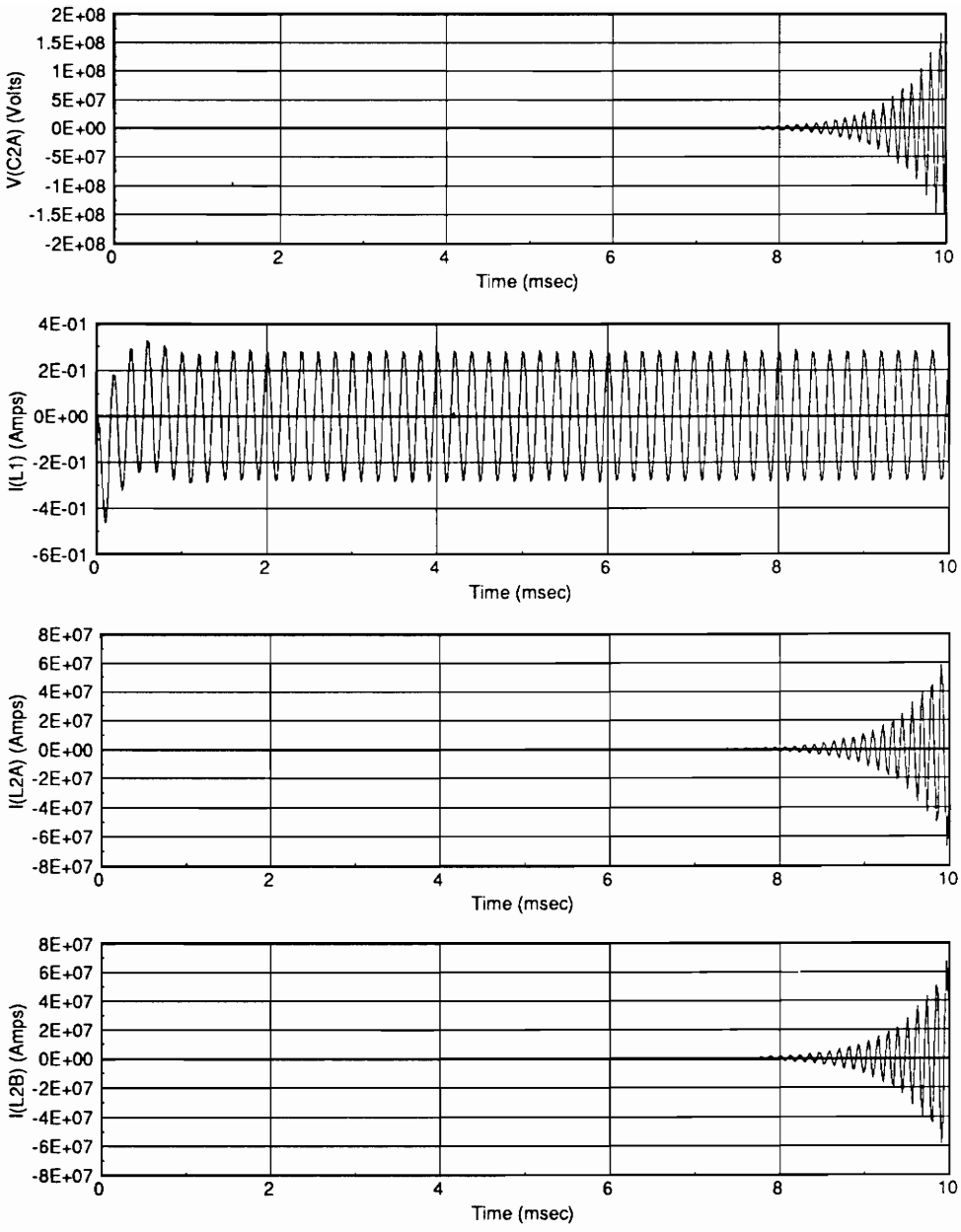

Figure 27. Response to output current excitation: (a) voltage across C_{2A}, (b) current through L_1, (c) current through L_{2A}, (d) current through L_{2B}

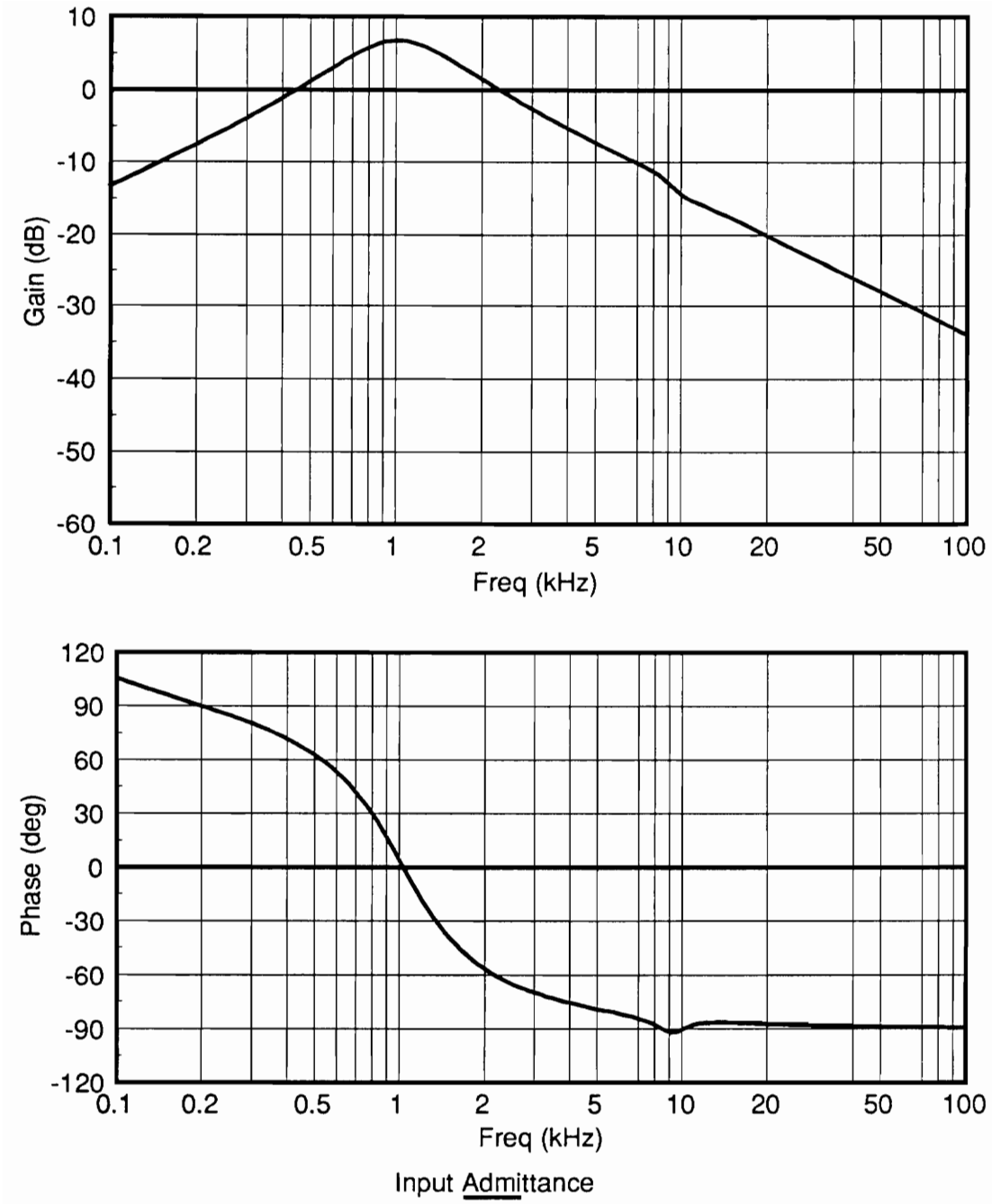

Figure 28. Input admittance of the filter

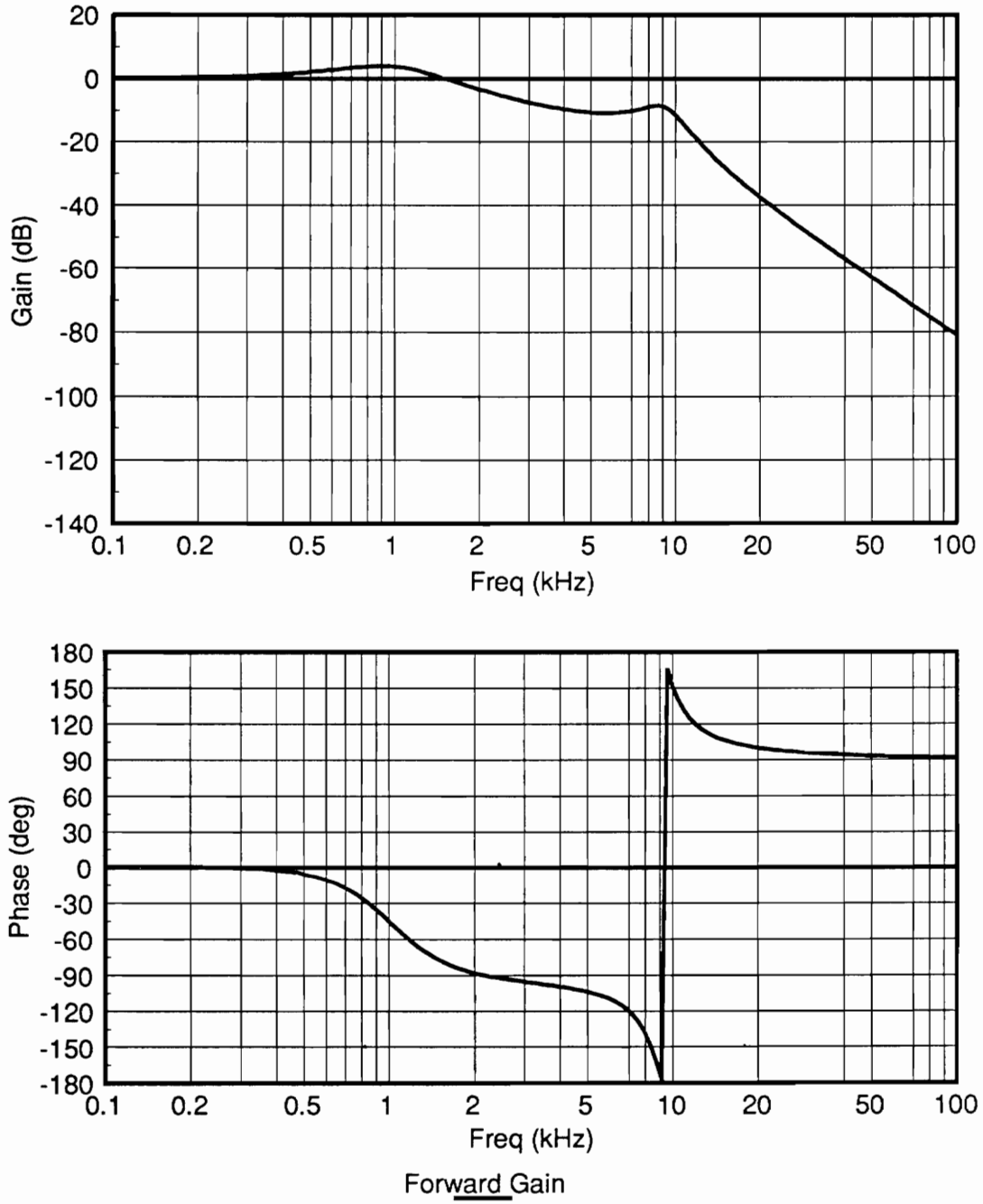

Figure 29. Forward voltage gain of the filter

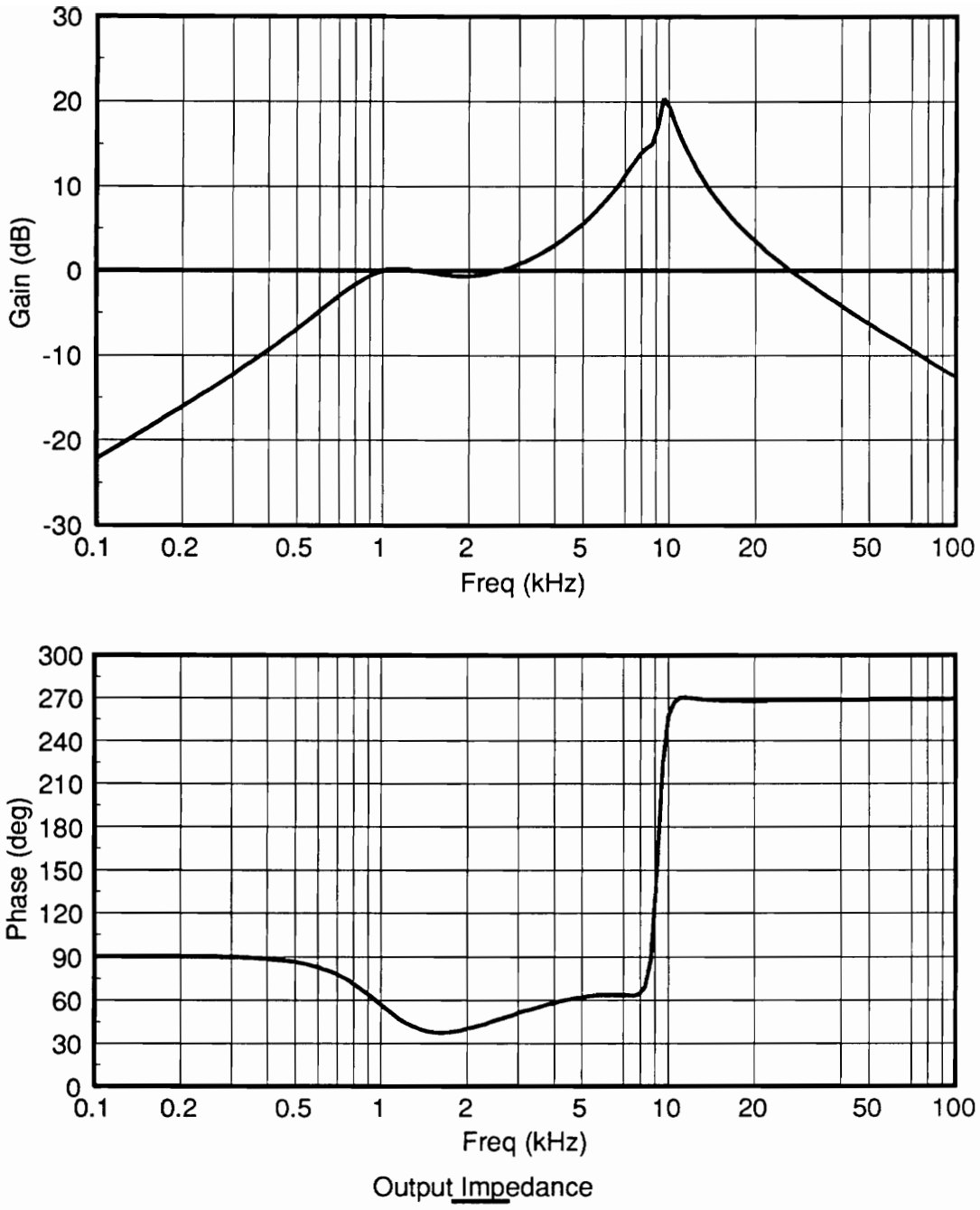

Figure 30. Output impedance of the filter showing unstable characteristics

Similarly, the forward voltage gain of the filter shown in Figure 29 is also a stable transfer function. As far as these two transfer functions are concerned, the system is non-minimal and a lower order network could provide the same transfer functions. However, when we examine the output impedance of the filter as shown in Figure 30, all of the system eigenvalues are exposed, and the system is seen to be unstable (complex RHP pole pair at 10kHz). From this point the system is minimal, and all of the system dynamics are revealed.

Now consider the circuit shown in Figure 31. This is a small-signal model of the redesigned input filter shown in Figure 24 which has additional second-stage damping. Again, we would like to examine the system response to input voltage and output current sources. Figure 32 shows the system response to the 1*V*peak, 5kHz input voltage source excitation. As before, the system seems stable and well behaved. Figure 33 shows the system response to the 1*A*, 5kHz output current source. The redesigned system is seen to be stable even from the output current excitation. This is explained by examination of the filter output impedance, shown in Figure 34, which has been stabilized by the additional damping in the system as described by Equation (3.33).

We have just seen in the previous example that due to the parallel modules in a distributed power system, the system may be unobservable and uncontrollable from a particular point in the system. Recall the development of the subsystem interaction analysis developed in Chapter 2. In many practical examples, either the source or the load subsystem (or both) is non-minimal dimensional. Without loss of generality, we shall consider the integration of two subsystems where the source is minimal dimensional, and the load is non-minimal dimensional. It will be assumed that the load subsystem is both unobservable and uncontrollable at the interface bus.

From the definition of observability, it is apparent that the load subsystem input admittance, $Y_i(s)$, does not contain any information on the unobservable modes due to pole/zero cancellation in that transfer function. Therefore, knowledge of $Y_i(s)$ is not sufficient to determine the

(a)

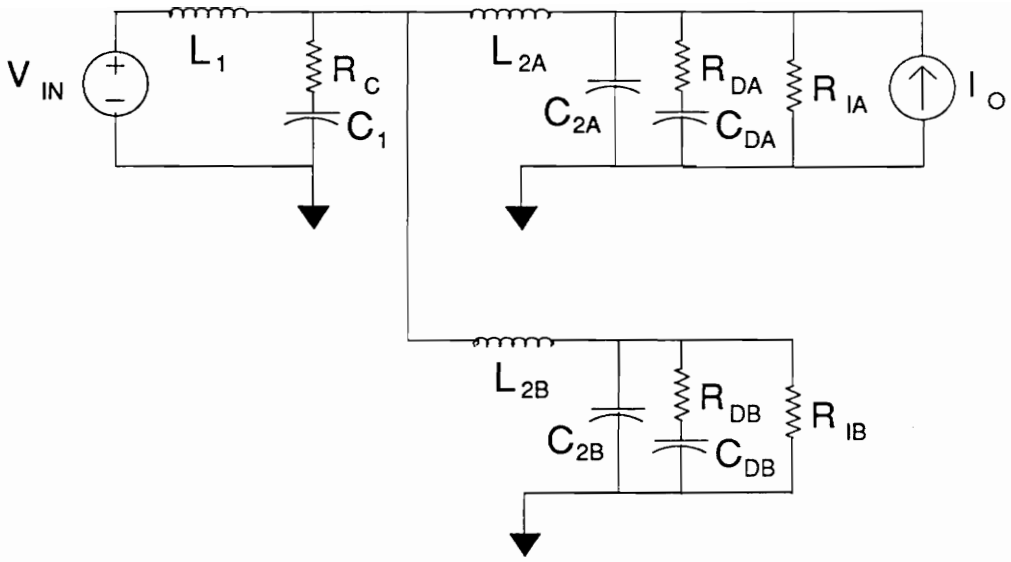

(b)

```
Line Input Filter Model with Second Stage Damping

* Sources
VIN     1     0     DC  0  AC   0   SIN(0  1  5E3)
IO      0     4     DC  0  AC   0

* Filter 1
L1      1     2     80U  IC=0
C1      3     0     320U  IC=0
RC      2     3     0.5

* Filter 2A
L2A     2     4     42.5U  IC=0
C2A     4     0     6.8U  IC=0
RIA     4     0     -26
CDA     6     0     22U  IC=0
RDA     4     6     5

* Filter 2B
L2B     2     5     42.5U  IC=0
C2B     5     0     6.8U  IC=0
RIB     5     0     -26
CDB     7     0     22U  IC=0
RDB     5     7     5

.TRAN   20U  10M   UIC
.PRINT   TRAN   V(4)   I(L1)   I(L2A)   I(L2B)
.PROBE
.END
```

Figure 31. Stabilized filter example: (a) circuit model, (b) PSPICE code

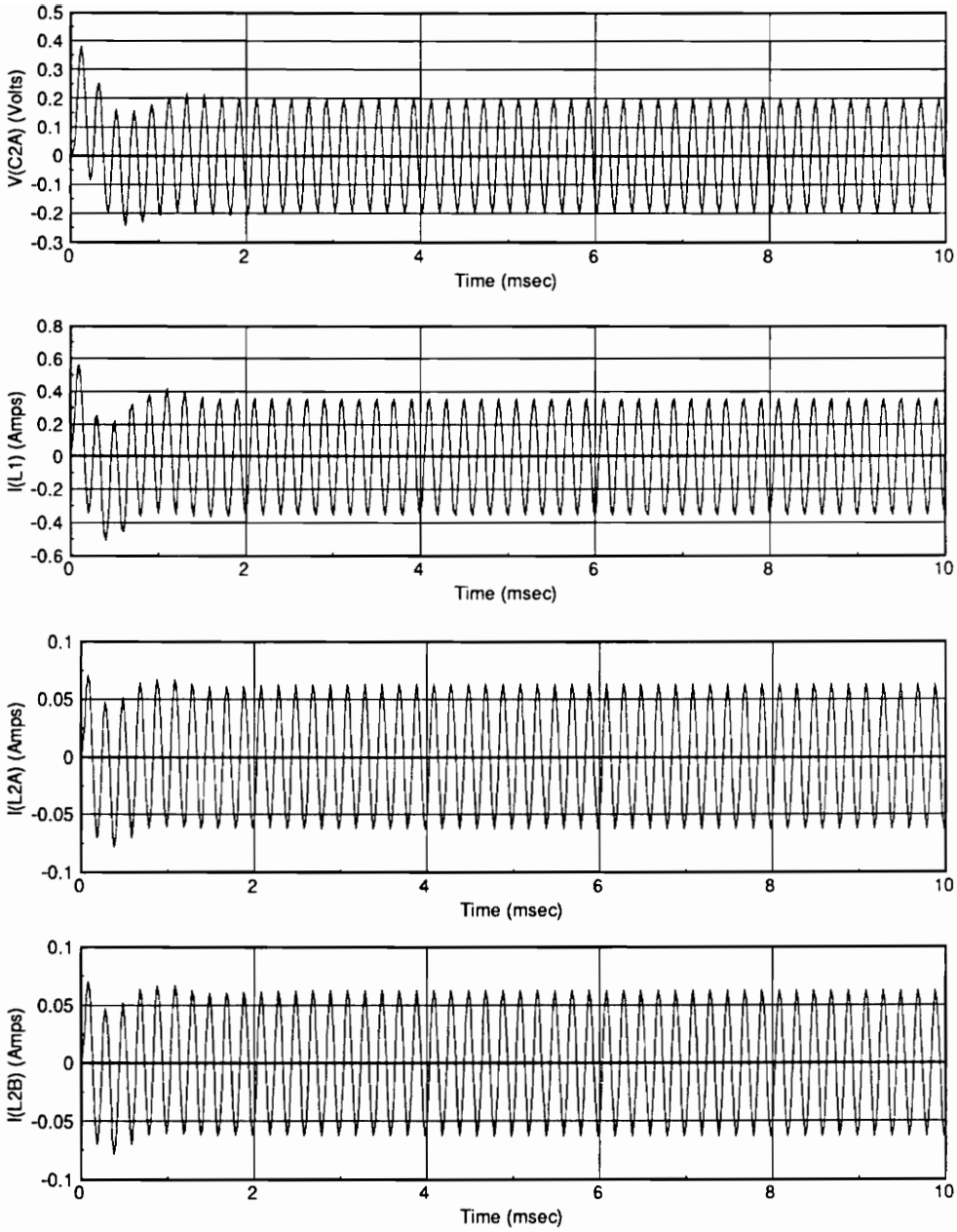

Figure 32. Response to input voltage excitation: (a) voltage across C_{2A}, (b) current through L_1, (c) current through L_{2A}, (d) current through L_{2B}

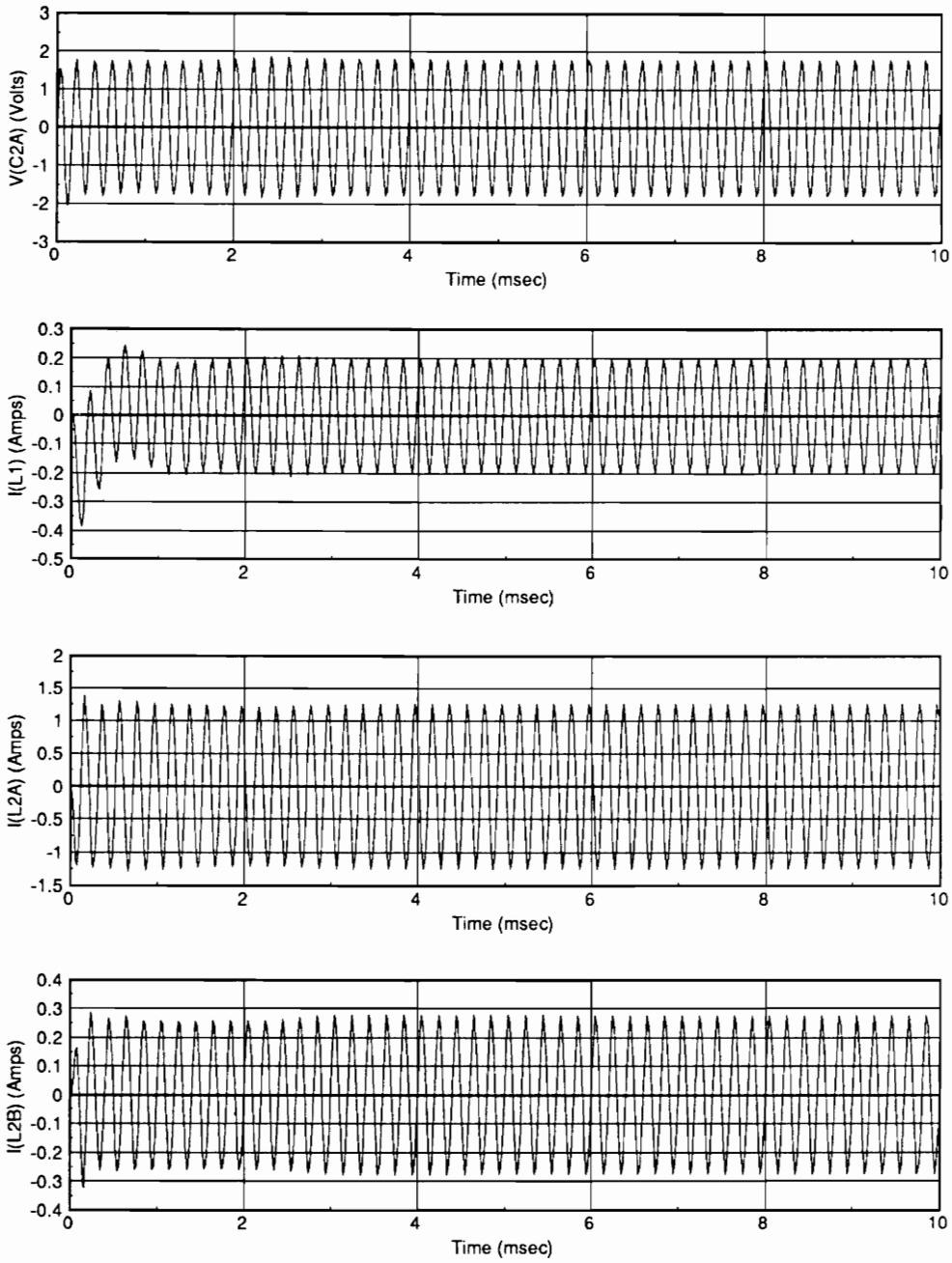

Figure 33. Response to output current excitation: (a) voltage across C_{2A}, (b) current through L_1, (c) current through L_{2A}, (d) current through L_{2B}

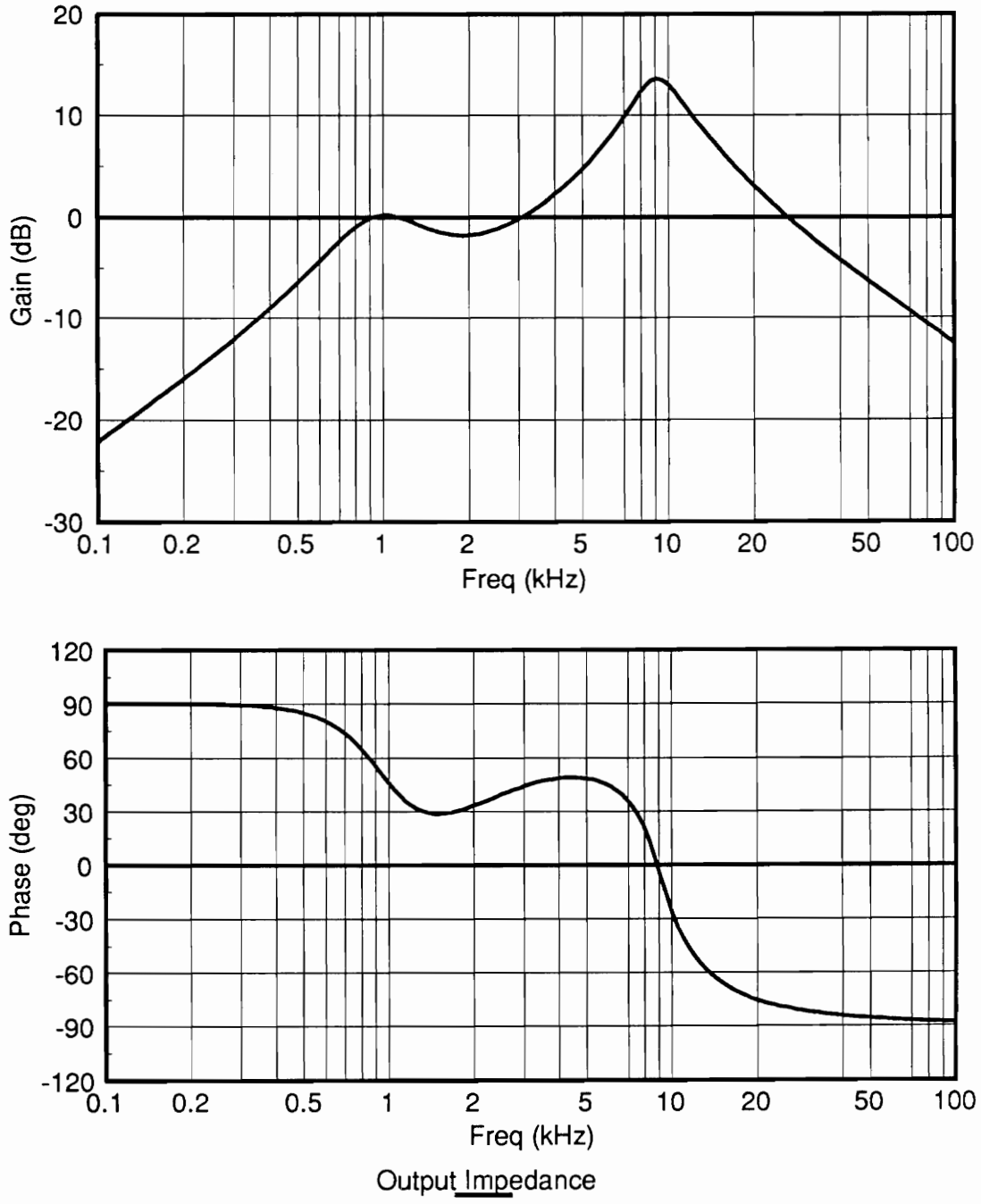

Figure 34. Output impedance of filter showing stable characteristics

stability of the unobservable load subsystem modes. However, $Y_l(s)$ can still be used to predict interaction with the source for the observable modes.

From the definition of controllability, it can be seen that the source output impedance, $Z_s(s)$, will have no effect on the uncontrollable modes of the load subsystem upon integration. The effect of the source on the controllable modes of the load can still be determined with the impedance comparison technique.

To summarize the above discussion, two important conclusions can be drawn for the general case. One, the unobservable/uncontrollable modes of either subsystem will not be affected by the subsystem integration. Two, under the assumption that each independent subsystem is known to be stable, then the presence of unobservable/uncontrollable modes in either subsystem will not prevent one from using the impedance comparison technique to determine the integrated system stability.

When faced with non-minimal dimensional subsystems, one must identify the unobservable/uncontrollable modes of the subsystems and insure that they are stable before integration. For example, in Section 3.4.2.2, we designed the line input filter such that the eigenvalues due to parallel interaction (which are unobservable and uncontrollable from the filter input) are well damped and in the LHP. In Chapter 4, a non-ideal generator source will be added to the DPS in front of the line input filter. There, it is shown that the generator source has no effect on the filter eigenvalues due to parallel interaction.

3.4.3 Design Guidelines

In this section, a set of design guidelines are provided for the design of the line input filter shown in Figure 23. The filter must be designed keeping several considerations in mind.

First, the filter must provide 103.6dB of attenuation to meet the MIL-STD 461 CE03 specification. Secondly, the ripple voltage generated at the filter output (or the input to the line conditioner module) should be kept to a minimum. Thirdly, the filter should not degrade the system's loop gains, audio, or output impedance. Finally, the eigenvalues due to parallel interaction should be well damped in the LHP. Before proceeding, it should be noted that many other topologies could be selected for the input filter, but only one will be discussed here for brevity.

Shown in Figure 35 is the single module model of the line conditioner stage with the line input filter. The dynamic load impedance seen by the line conditioners is the input impedance of the load converter stage, modeled here with a negative resistance. Shown boxed in Figure 35 is the equivalent input filter which must be designed to provide the required attenuation and filter output impedance. The equivalent input filter is a fifth-order circuit. To simplify the design, we may assume that KC_d and R_d/K are chosen so that they have a negligible effect on the unloaded equivalent input filter forward gain $H_s(s)$ and output impedance $Z_s(s)$. In this case, the circuit can be assumed to be fourth-order. The sufficient conditions for KC_d and R_d/K to satisfy the above assumptions are:

$$C_1 >> KC_d >> KC_2 \quad \text{and} \quad \frac{R_d}{K} > \frac{1}{K}\sqrt{\frac{L_2}{C_2}} \tag{3.34}$$

If the conditions in Equation (3.34) are satisfied, then the straight-line approximations to $H_s(s)$ and $Z_s(s)$ are as shown in Figure 36. Notice that the two resonant frequencies are assumed to be well-separated. As discussed in [1], having the two resonant frequencies close together will result in large peaking of $Z_s(s)$ and a very low filter input impedance, both of which are undesirable. The filter transfer functions may be approximated as follows:

$$H(s) \simeq \frac{1 + sR_cC_1}{\left(\frac{s^2}{\omega_1^2} + \frac{s}{Q_1\omega_1} + 1\right)\left(\frac{s^2}{\omega_2^2} + \frac{s}{Q_2\omega_2} + 1\right)} \tag{3.35}$$

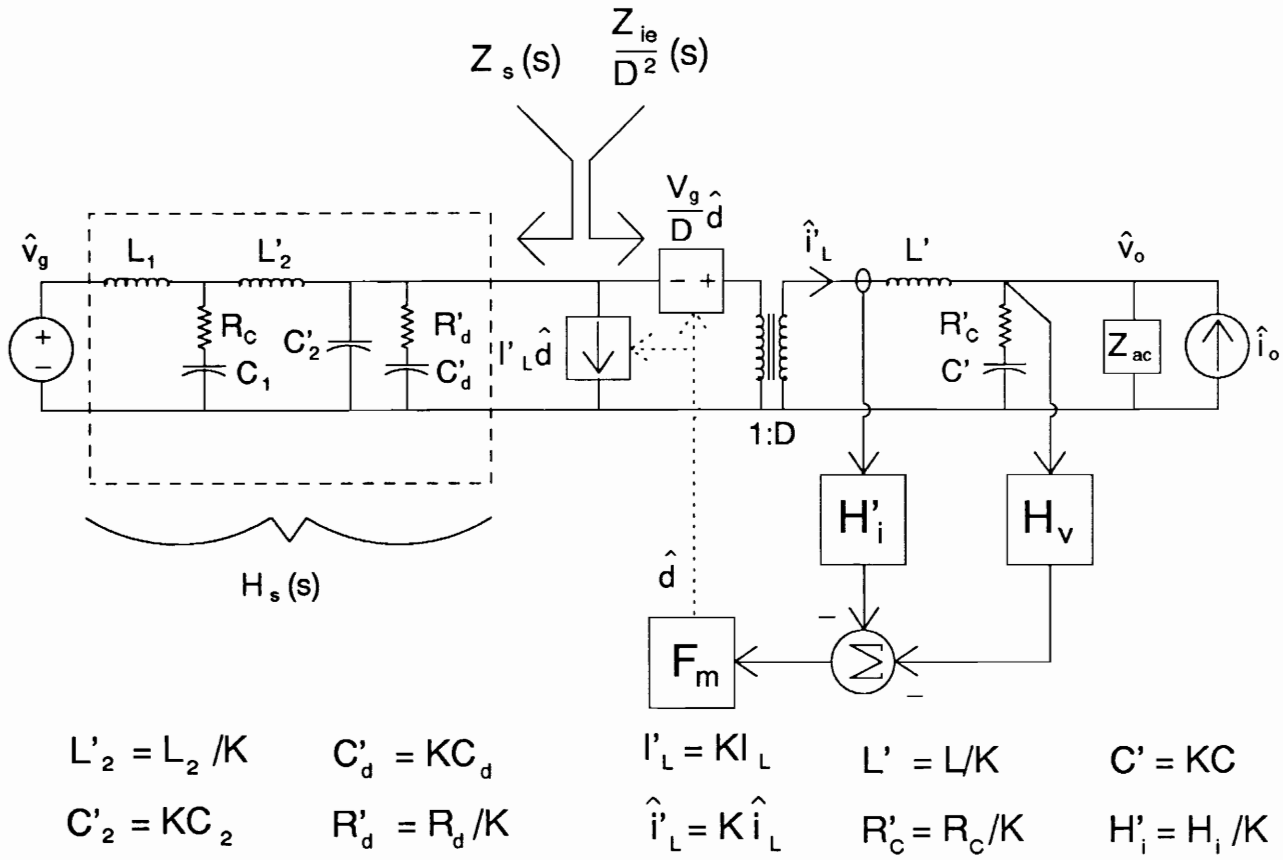

Figure 35. Single module model of line conditioner stage with line input filter

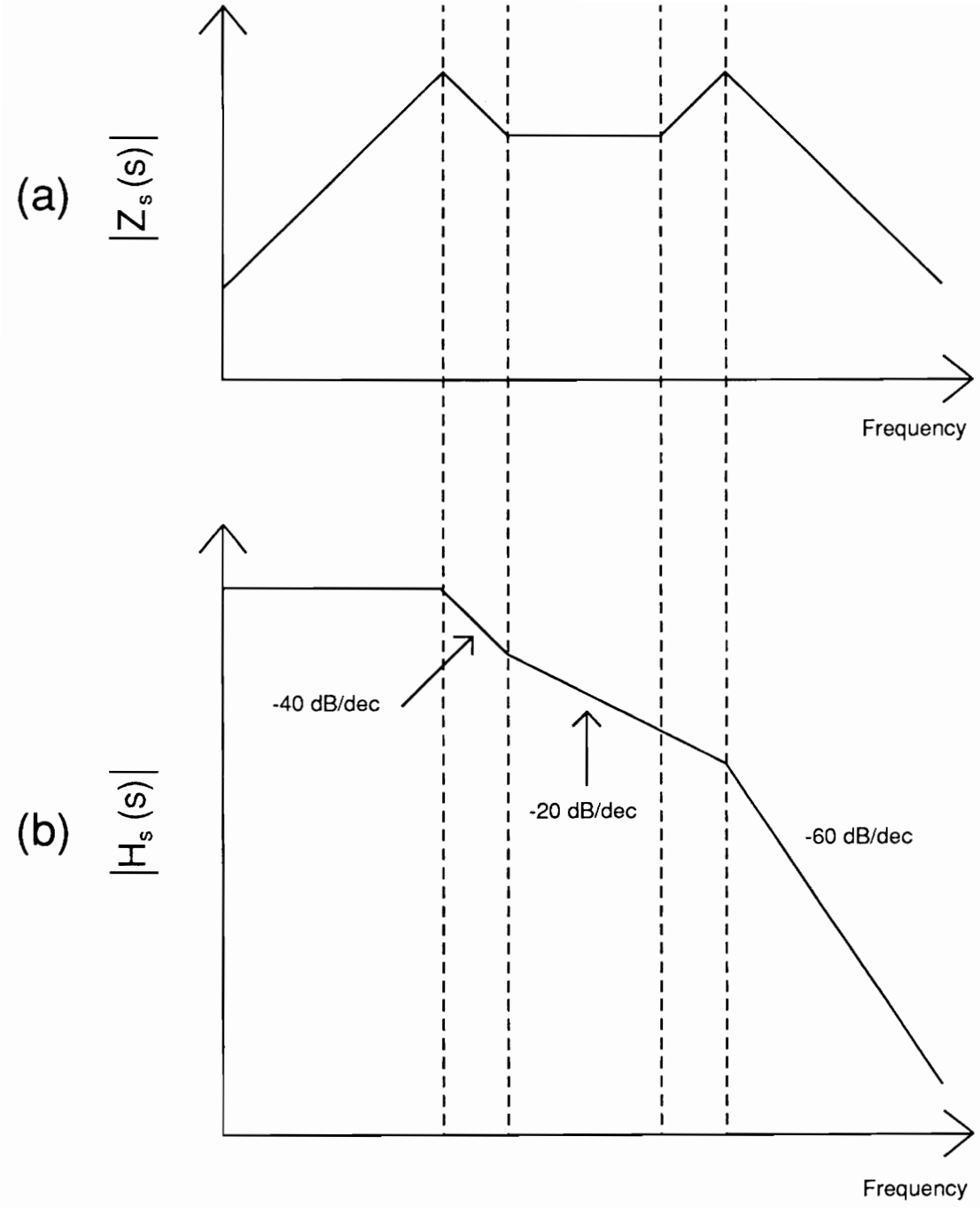

Figure 36. Straight-line approximations for equivalent input filter (high Q): (a) output impedance, (b) attenuation

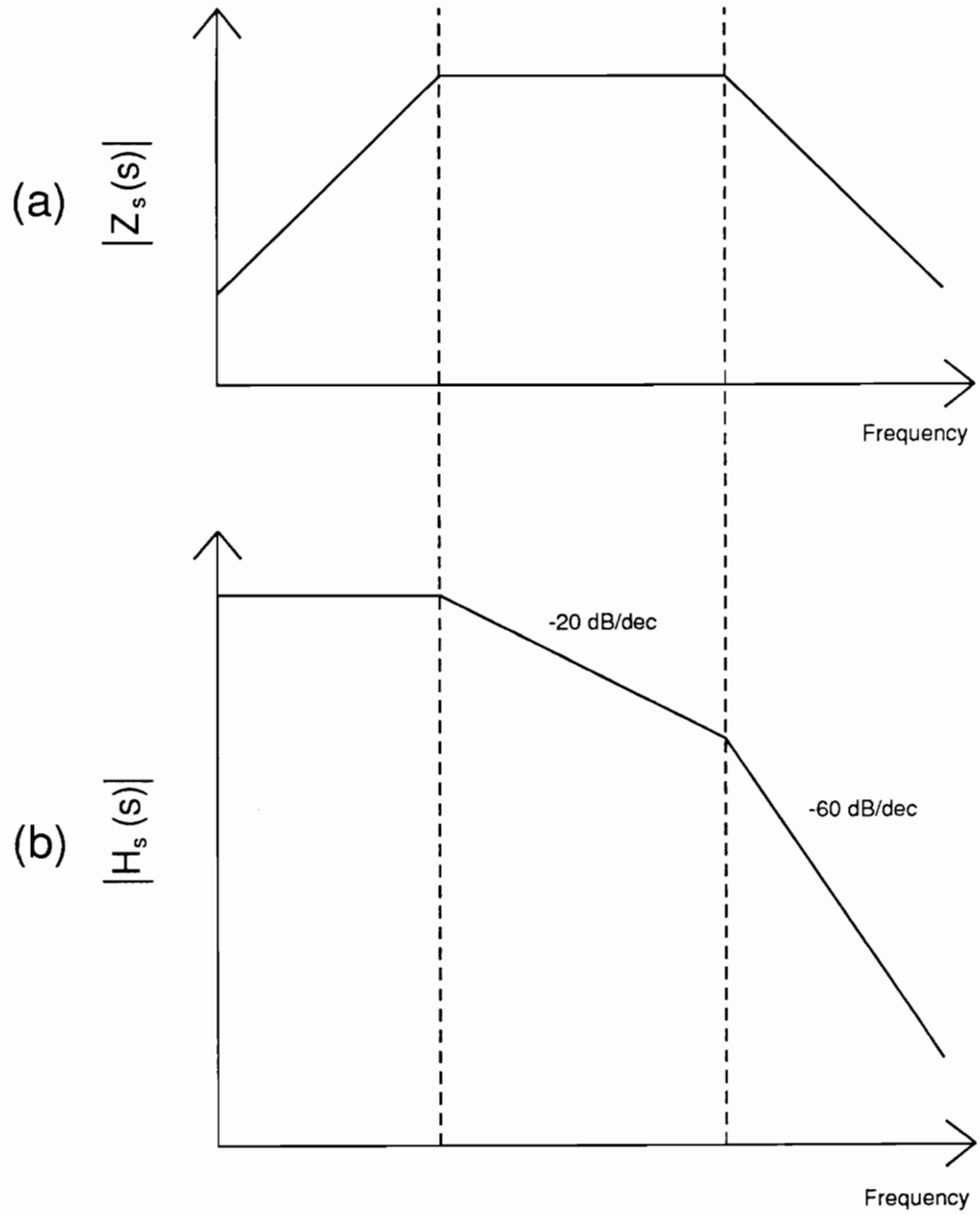

Figure 37. Straight-line approximations for equivalent input filter when $Q_1 \simeq 1$ and $Q_2 \simeq 1$: (a) output impedance, (b) attenuation

$$Z_s(s) \simeq \frac{sL_1(1+sR_cC_1)\left(1+s\frac{L_2}{K}R_c\right)}{\left(\frac{s^2}{\omega_1^2}+\frac{s}{Q_1\omega_1}+1\right)\left(\frac{s^2}{\omega_2^2}+\frac{s}{Q_2\omega_2}+1\right)} \tag{3.36}$$

Where:

$$\omega_1 \simeq \frac{1}{\sqrt{L_1C_1}} \quad \text{and} \quad Q_1 \simeq \frac{1}{R_c}\sqrt{\frac{L_1}{C_1}} \tag{3.37}$$

$$\omega_2 \simeq \frac{1}{\sqrt{L_2C_2}} \quad \text{and} \quad Q_2 \simeq \frac{1}{KR_c}\sqrt{\frac{L_2}{C_2}} \tag{3.38}$$

Equations (3.35) to (3.38) assume that $C_1 >> KC_2$ and $L_1 >> L_2/K$. Notice that $H_s(s)$ has one zero and four poles, giving a high frequency slope of -60dB/dec. To further simplify the design, we may assume that the R_cC_1 zero lies at ω_1. If additionally we assume that the L_2/KR_c zero lies at ω_2, then the straight-line approximation of $Z_s(s)$ will be the same as a second-order transfer function and $H_s(s)$ the same as a third-order transfer function. These two conditions are equivalent to setting $Q_1 \simeq Q_2 \simeq 1$. The straight-line approximations will then appear as in Figure 37. This assumption is quite practical, and greatly eases the design.

The following steps detail one procedure that may be used to determine the filter parameters.

1. Find the minimum value of KC_2 to satisfy the voltage ripple specification at the filter output.

2. Choose R_c, which approximately determines the peak value of $Z_s(s)$.

3. Choose ω_1 for a desired settling time. This fixes the values of L_1 and C_1.

4. From ω_1 and the required attenuation, find ω_2.

5. From ω_2, find L_2/K and KC_2. KC_2 should be greater than or equal to the value found in step 1.

6. Choose KC_d and R_d/K to satisfy Equation (3.34) and place the roots of Equation (3.33) in the LHP.

For the system under consideration, the following filter parameters were found as shown in Appendix A:

$L_1 = 80\mu H$

$C_1 = 320\mu F$

$R_c = 0.5\Omega$

$L_2 = 42.5\mu H$

$C_2 = 6.8\mu F$

$C_d = 22\mu F$

$R_d = 5\Omega$

Figure 38 shows the simulated Z_{ie}/D^2 and $Z_s(s)$ for five line conditioners. Notice that the two impedances impedances overlap near the power stage output filter corner frequency. This does not necessarily mean that the line conditioner performance will be degraded. Since the interaction occurs at a frequency where $Z_s(s)$ is nearly resistive, the only effect will be additional damping of the power stage output filter. Also note that C_d and R_d had a negligible effect on $Z_s(s)$.

Figure 39 shows the reverse current gain $H_s(s)$ of the line input filter. It can be seen that the fitler provides 105dB of attenuation at 250kHz. Also, C_d and R_d have little effect on this transfer function. Figure 40 shows the line conditioner overall loop gain with and without the input filter. Figure 41 shows the line conditioner outer loop gain with and without the input filter, while Figure 42(a) and (b) show the audio and output impedance with and without the input

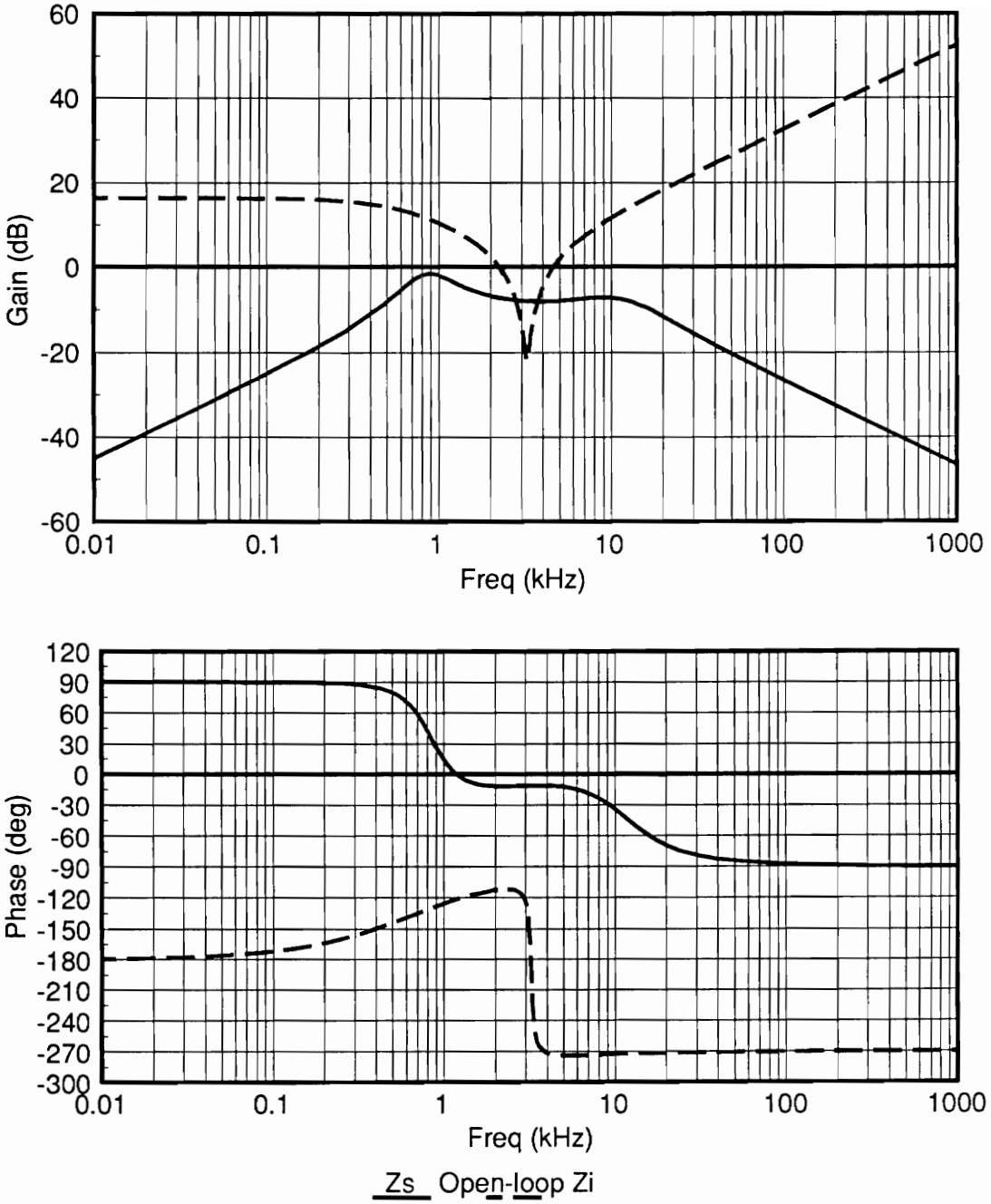

Figure 38. Open-loop $Z_{io}(s)/D^2$ and $Z_s(s)$

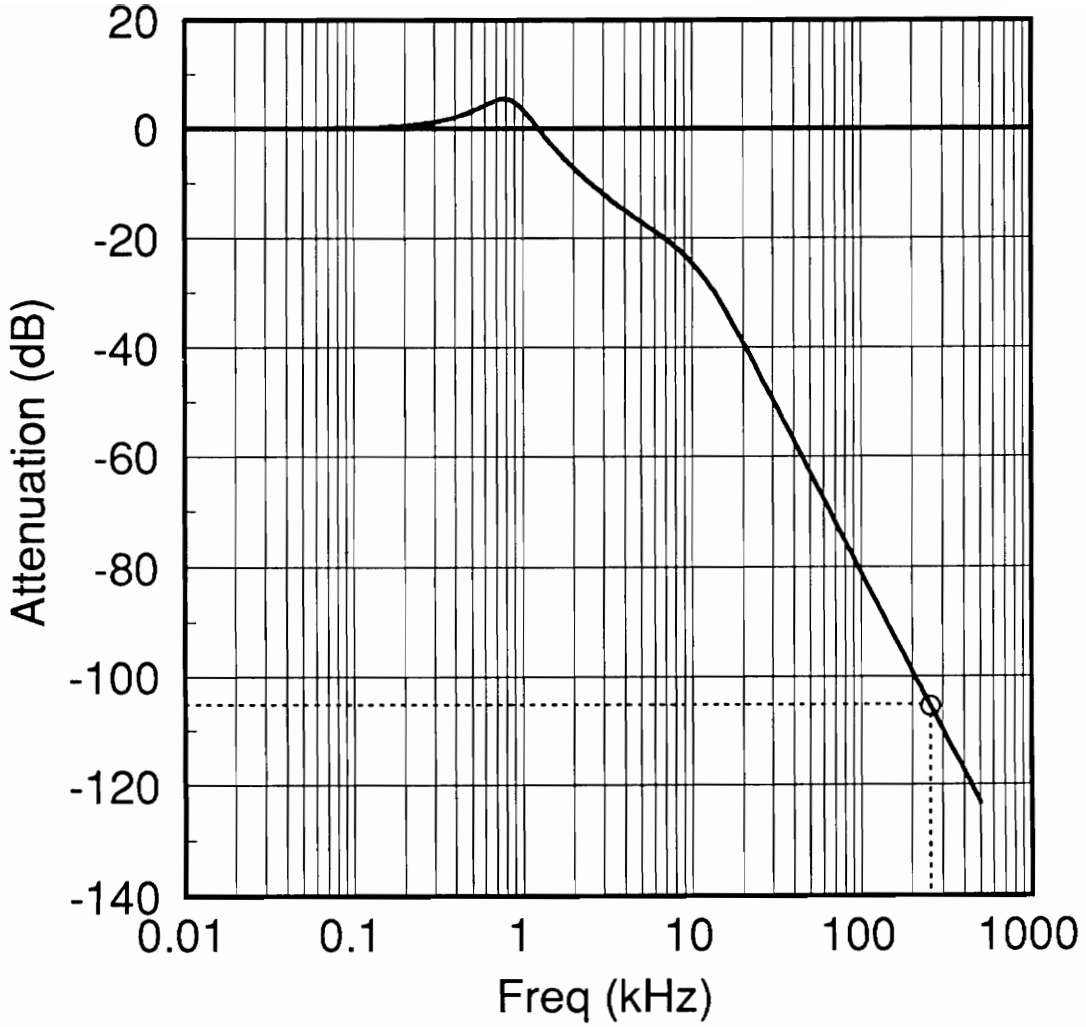

Figure 39. Reverse current gain of the line input filter

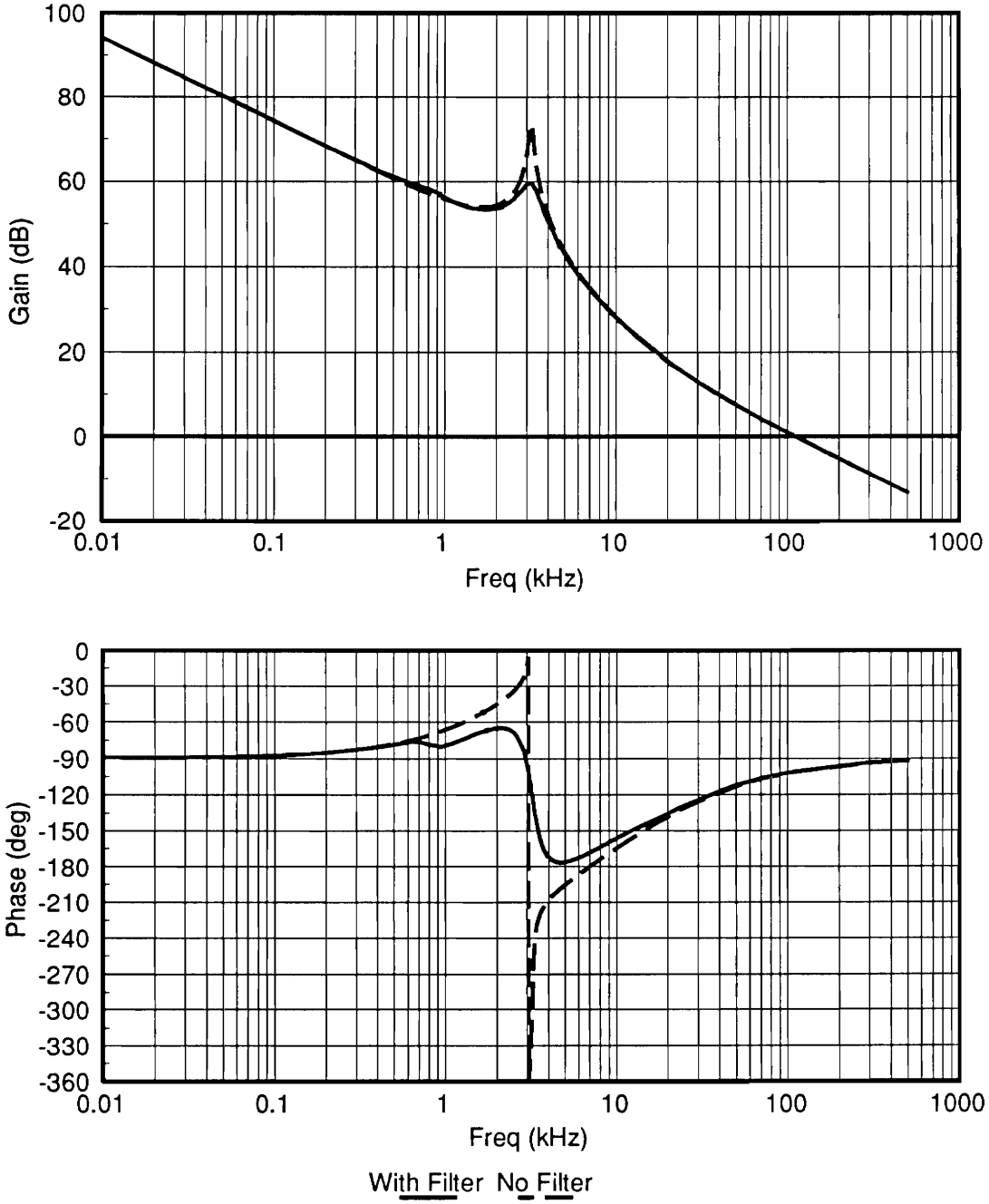

Figure 40. Overall loop gain of line conditioners with and without line input filter

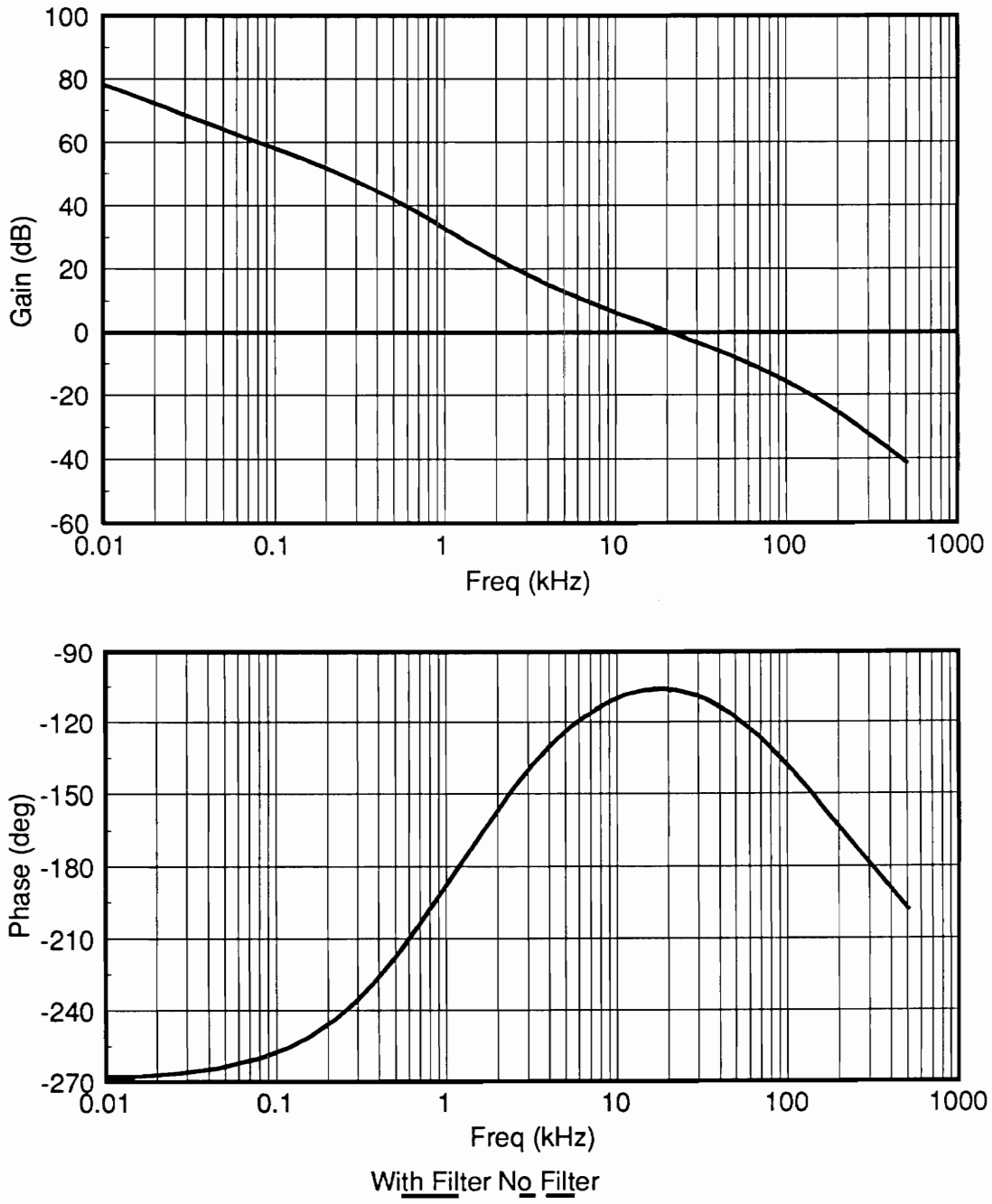

Figure 41. Outer loop gain of line conditioners with and without line input filter

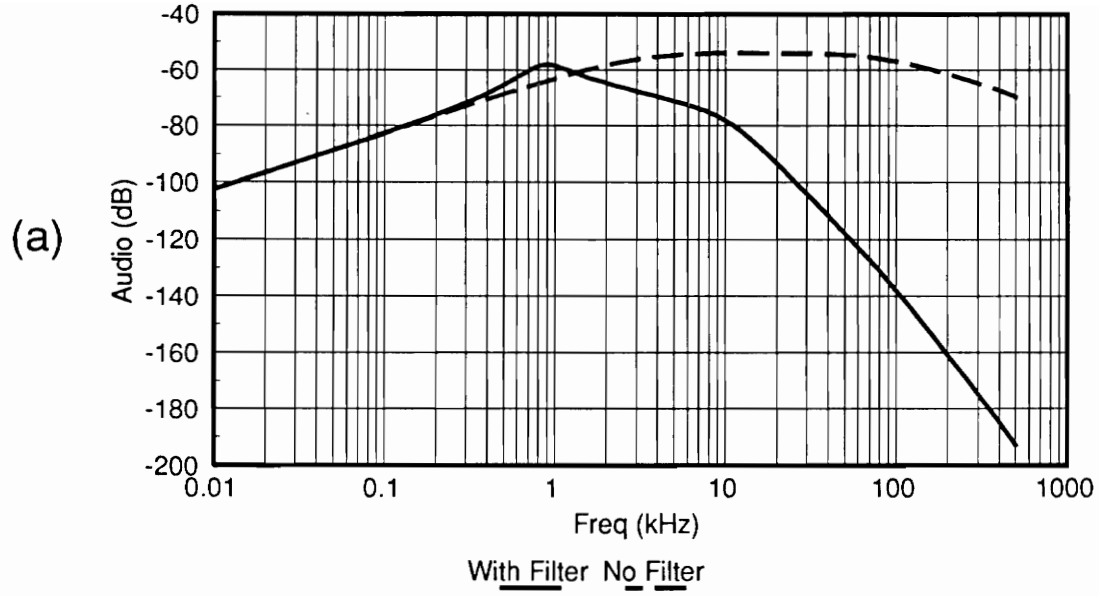

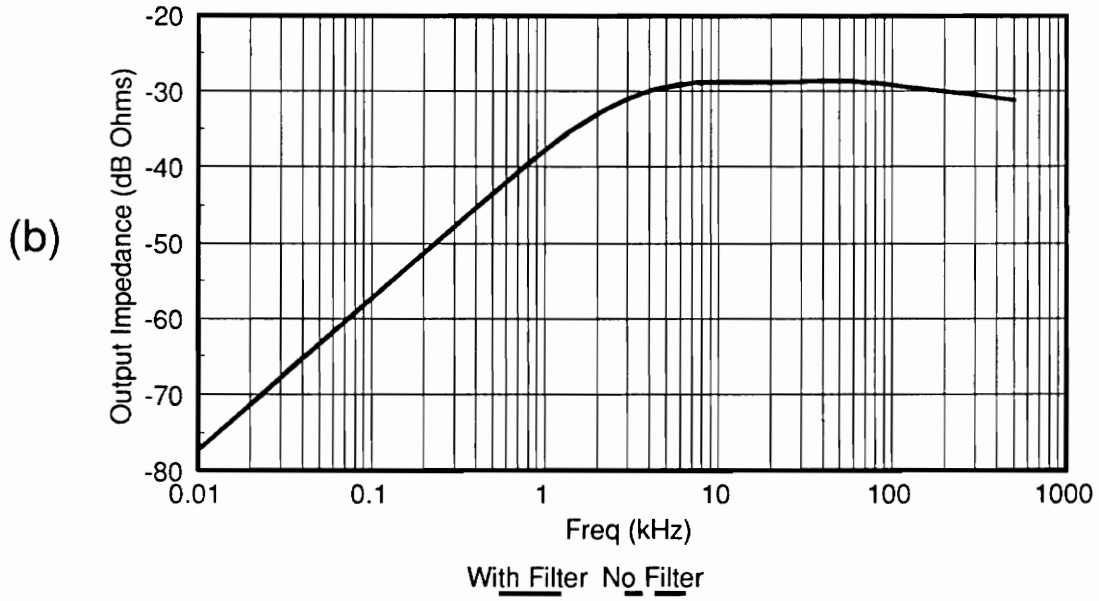

Figure 42. Performance of line conditioners with and without line input filter: (a) audio, (b) output impedance

Table 2. Comparison of filter eigenvalues

Table 2(a). 5 Line Conditioners					
Mode	Mult	Real Part	Imaginary Part	Natural Frequency	Damping Ratio
1	1	-18282.1	0.00E+00	18282.1	1.00
2	1	-92635.7	0.00E+00	92635.7	1.00
3	4	-133333.	0.00E+00	133333.	1.00
7	1	-244162.	0.00E+00	244162.	1.00
8	1	-478320.	0.00E+00	478320.	1.00
9	4	-703570.	0.00E+00	703570.	1.00
13	1	-6.612969E+06	0.00E+00	6.612969E+06	1.00
14	1	-3.582154E+07	0.00E+00	3.582154E+07	1.00

Table 2(b). 5 Line Conditioners with Line Input Filter					
Mode	Mult	Real Part	Imaginary Part	Natural Frequency	Damping Ratio
1	1	-1772.25	±5159.42	5455.32	0.324867
2	1	-8358.46	0.00E+00	8358.46	1.00
3	4	-9890.79	0.00E+00	9890.79	1.00
7	4	-12296.3	±54873.6	56234.4	0.218662
11	1	-18295.8	0.00E+00	18295.8	1.00
12	1	-43429.0	±54954.2	70043.1	0.620031
13	1	-92643.1	0.00E+00	92643.1	1.00
14	4	-133333.	0.00E+00	133333.	1.00
18	1	-242242.	0.00E+00	242242.	1.00
19	1	-485019.	0.00E+00	485019.	1.00
20	4	-707589.	0.00E+00	707589.	1.00
24	1	-6.612984E+06	0.00E+00	6.612984E+06	1.00
25	1	-3.582154E+07	0.00E+00	3.582154E+07	1.00

Table 2(c). Filter Model in Figure 24(a)					
Mode	Mult	Real Part	Imaginary Part	Natural Frequency	Damping Ratio
1	1	-1772.32	±5158.92	5454.87	0.324906
2	1	-8358.41	0.00E+00	8358.41	1.00
3	1	-9889.32	0.00E+00	9889.32	1.00
4	1	-12047.9	±55097.2	56399.0	0.213618
5	1	-43578.6	±55151.0	70290.3	0.619980
6	1	-1.999941E+09	0.00E+00	1.999941E+09	1.00

filter. It is apparent that the input filter did not degrade the system performance, even though there was interaction at the power stage output filter corner. It can be seen how the interaction damped the output filter corner by examining the overall loop gain. Notice that the interaction did not show up in T_2, the audio, or the output impedance. Finally, Table 2 compares the filter eigenvalues for five line conditioners with no input filter, five line conditioners with input filter, and those of the filter model in Figure 24(a). First, notice that the addition of the input filter does not have any significant effect on the line conditioner eigenvalues (compare Table 2(a) with Table 2(b)). Also, it can be seen that the filter model of Figure 24(a) predicts the filter eigenvalues very closely (compare Table 2(b) with Table 2(c)). Eigenvalues with a multiplicity of four are due to parallel interaction between modules. The high frequency eigenvalue listed in Table 2(c) as mode 6 is due to modelling constraints, and will not appear in the actual system. In conclusion, the system is stable, with very little interaction occurring between the regulator and input filter.

3.5 *Intermediate Bus Filter Design*

Since each load converter draws a pulsating input current, problems may arise if no input filter is used. Pulsating current on the intermediate bus can generate unwanted noise or cause interaction with the line conditioners. For these reasons, an input filter should be used to attenuate the high ripple current drawn by the load converters. While no specification was given for the harmonic content of the load converters' input current, it was decided to adopt the MIL-STD 461B CE03 spec. Since each line conditioner can supply three load converters, the filter will be designed such that three parallel load converters operating in-phase meet the specification. Using the same procedure described in Section 3.4, it was found that the intermediate bus filter should provide 35dB of attenuation at 500kHz. A single-stage filter placed at the input to each load converter was found to be sufficient to provide the necessary attenuation. An RC damping branch was used to avoid peaking in the output impedance and input admittance of the filter which could cause interaction and stability problems. Figure 43 shows the intermediate bus filters and placement of the damping branch.

The intermediate bus filter is quite different from the line input filter in that it not only sees a switching regulator load, but it is also supplied by a switching regulator source. When designing the intermediate bus filter, we must meet the required attenuation specification while avoiding interaction with both the line conditioners and the load converters [14,16]. Therefore, restrictions will not only be placed on the filter output impedance, but also on its input impedance as well. To minimize filter interaction with the load converters, we would like to minimize the output impedance of the intermediate bus filter. To minimize filter interaction

with the line conditioners, we would like to maximize the input impedance of the intermediate bus filter. These two criteria can be applied to the design of the intermediate bus filter. However, the design goals of large input impedance and low output impedance of the filter are conflicting. For the example of the single stage LC filter, large input impedance requires a large inductance and small capacitance, while low output impedance requires a small inductance and large capacitance. With careful design, it will be shown that both attenuation and minimum interaction can be achieved with little compromise.

3.5.1 Interaction with Line Conditioner and Stability

In order to apply the results of Section 3.3, we may think of the line conditioner stage as the Filter 1 block in Figure 11 on page 41. The entire line conditioner stage can be represented by its unloaded output impedance $Z_{sb}(s)$ (the source impedance seen at the intermediate bus) as defined in Figure 43. The load impedance seen at the intermediate bus is the fitler input impedance $Z_{ib}(s)$. By design, the filter should satisfy the following condition:

$$|Z_{ib}| << |Z_{sb}| \tag{3.39}$$

When the condition in Equation (3.39) is satisfied, the interaction between the line conditioner stage and the intermediate bus filter will be minimal. In this case, the filter can be thought of as being supplied by an ideal source. Since this filter topology is of the single-stage type and does not rely on $Z_{sb}(s)$ for damping, the eigenvalues due to parallel interaction will be almost identical to those provided by the single module model. Therefore, the single module model will provide all of the necessary information needed to design the filter and determine stability.

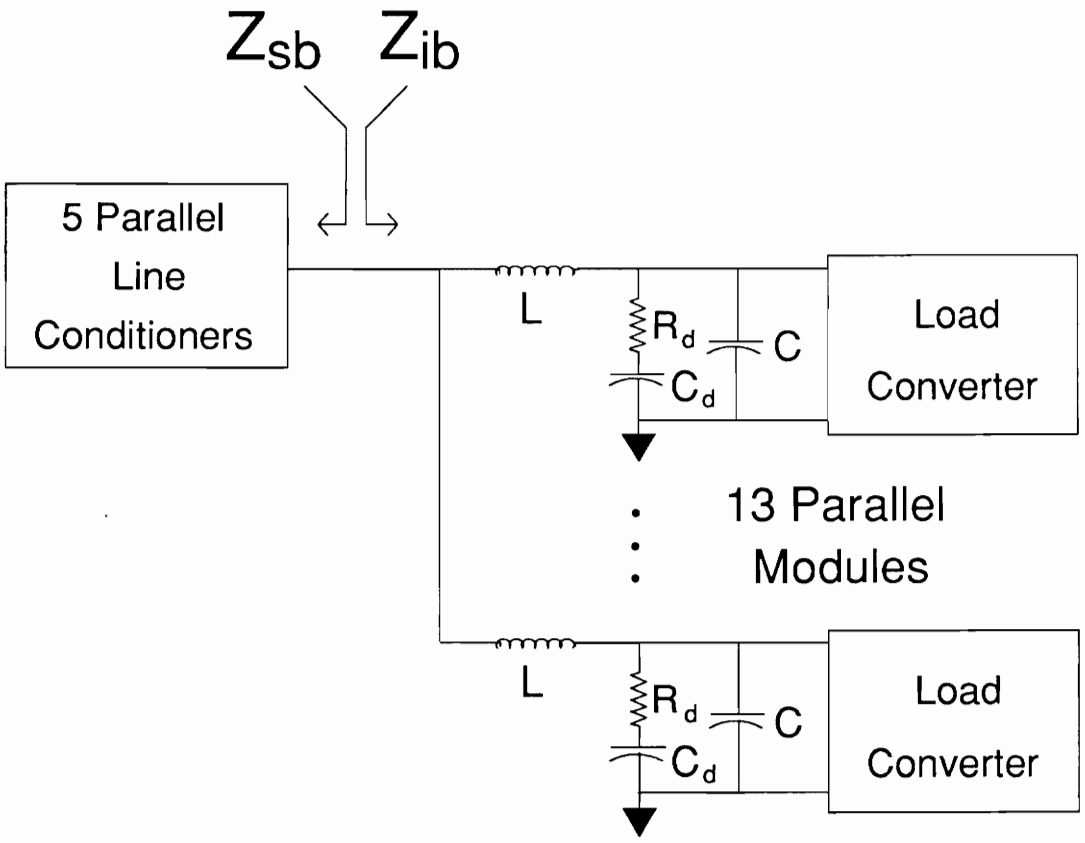

Figure 43. Intermediate bus filter

It is possible that in some cases Equation (3.39) cannot be met due to certain system constraints. In this case, the impedance comparison technique developed in Chapter 2 can be used with $Z_{sb}(s)$ and $Z_{ib}(s)$ to assess the interaction between the line conditioners and the load converters/intermediate bus filter. Also, the analysis of Section 3.2 could be applied to determine the effect of interaction on the loop gains and performance indices of the regulators. However, in most cases, Equation (3.39) can be satisfied with a good design. Therefore, the case of interaction at the intermediate bus will not be considered here, and the reader is referred to [10] for an example.

3.5.2 Design Guidelines

As discussed in the previous section, the single module model will provide all of the design information needed for the intermediate bus filter as long as interaction with the line conditioner is avoided. Figure 44 shows the singe module model of the load converter stage supplied by the intermediate bus filter. Notice that the line conditioner stage is completely represented by $Z_{sb}(s)$. Shown boxed in the figure is the equivalent filter which must be designed to provide the required attenuation and input and output impedances. Notice that the filter is third-order. In order to simplify the design of the filter, we may use the following assumptions:

$$C_d >> C \quad \text{and} \quad \frac{L}{R_d} \geq CR_d \tag{3.40}$$

If the conditions in Equation (3.40) are satisfied, then the transfer functions for the ideally terminated filter can be approximated by the following second-order equations:

$$H(s) \simeq \frac{1}{\left(\frac{s^2}{\omega_o^2} + \frac{s}{Q\omega_o} + 1\right)} \tag{3.41}$$

$$Z_s(s) \simeq \frac{s\frac{L}{K}}{\left(\frac{s^2}{\omega_o^2} + \frac{s}{Q\omega_o} + 1\right)} \tag{3.42}$$

Where:

$$\omega_o \simeq \frac{1}{\sqrt{LC}} \quad \text{and} \quad Q \simeq R_d\sqrt{\frac{C}{L}} \tag{3.43}$$

The load impedance seen at the intermediate bus can be approximated as follows:

$$Z_{ib}(s) \simeq \frac{-R_L(1 + sR_dC_d)\left(\frac{s^2}{\omega_o^2} + \frac{s}{Q\omega_o} + 1\right)}{(1 - sR_LKC_d)(1 + sR_dC)} \tag{3.44}$$

The straight-line approximations for these transfer functions appear in Figure 45. The following steps outline a design which sets $Q \simeq 1$.

1. Find the minimum value of KC to satisfy the voltage ripple specification at the filter output.

2. Plot the line conditioner stage output impedance $Z_{sb}(s)$ and the load converter stage open-loop input impedance Z_{ie}/D^2.

3. Choose the desired value $Z_{i_{min}}(s)$ and $Z_{s_{max}}$ to minimize interaction with both the line conditioner and the load converter. This gives the value of R_d/K

4. From the required attenuation, find ω_o.

5. Find L by setting the L/R_d corner to ω_o.

6. Find C by setting the R_dC corner to ω_o. KC should be greater than or equal to the value found in step 1.

7. Choose the value of C_d to be much greater than the value of C.

For the system under consideration, the following filter parameters were found as shown in Appendix B:

$L = 6\mu H$

$C = 1\mu F$

$C_d = 10\mu F$

$R_d = 2.5\Omega$

Figure 46 shows the source and load impedance seen at the intermediate bus. The 10dB of separation will insure that interaction between the line conditioners and the intermediate bus filter is minimal. Shown in Figure 47 is the source imedance $Z_s(s)$ seen by the load converter single module model, and the single module model open-loop input impedance Z_{ie}/D^2. The wide separation of impedances predicts little interaction between the load converters and filter. Figure 48 shows the reverse current gain of the equivalent filter. Notice that the filter appears to be second-order, and that it provides 35dB of attenuation at 500kHz. Shown in Figure 49 is the overall loop gain T_1 of the line conditioner for the system with and without the intermediate bus filter. Figure 50 shows the line conditioner outer loop gain T_2 with and without the intermediate bus filter. It can be seen that the filter has very little effect on the line conditioner loop gains. Finally, Figure 51 and Figure 52 show the load converter overall loop gain and outer loop gain, respectively, with and without the intermediate bus filter. From these two loop gains, it is apparent that the filter does not interact with the load converter

stage. Thus, appropriate design of the intermediate bus filter can avoid unwanted interactions with both stages of regulators in a two-stage DPS.

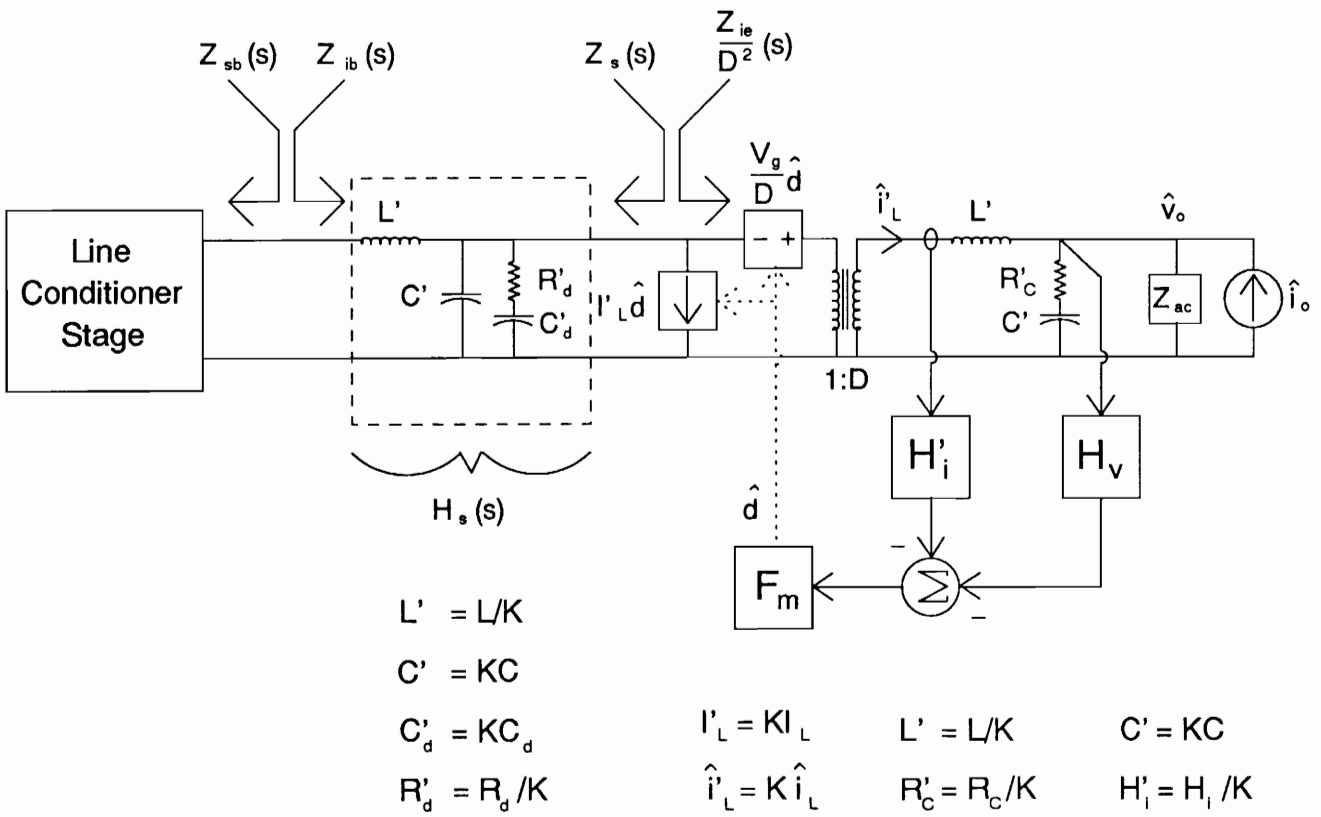

Figure 44. Single module model of load converter stage and intermediate bus filter

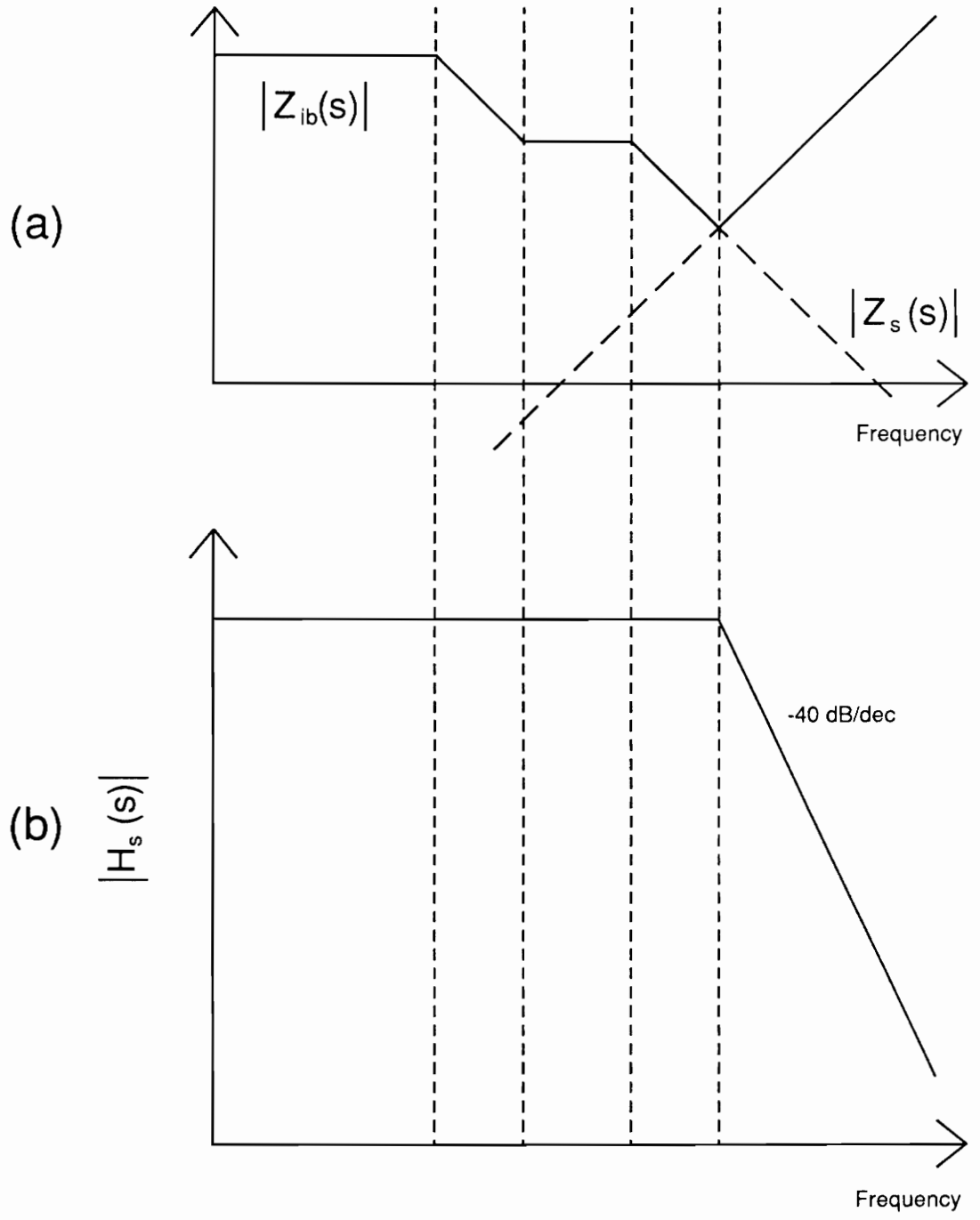

Figure 45. Straight-line approximations for intermediate bus equivalent filter: (a) filter input and output impedance, (b) attenuation

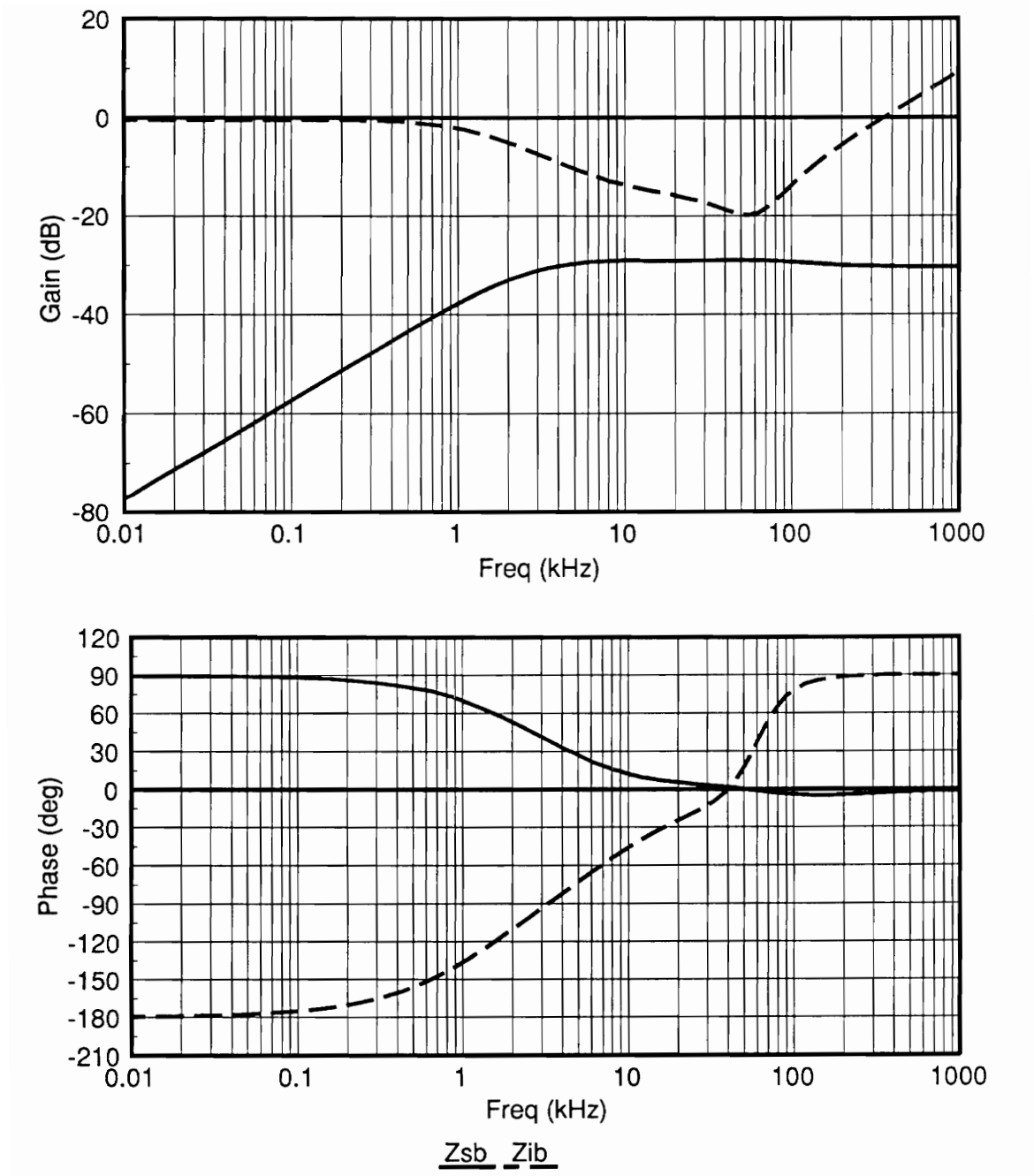

Figure 46. Source and load impedances seen at the intermediate bus

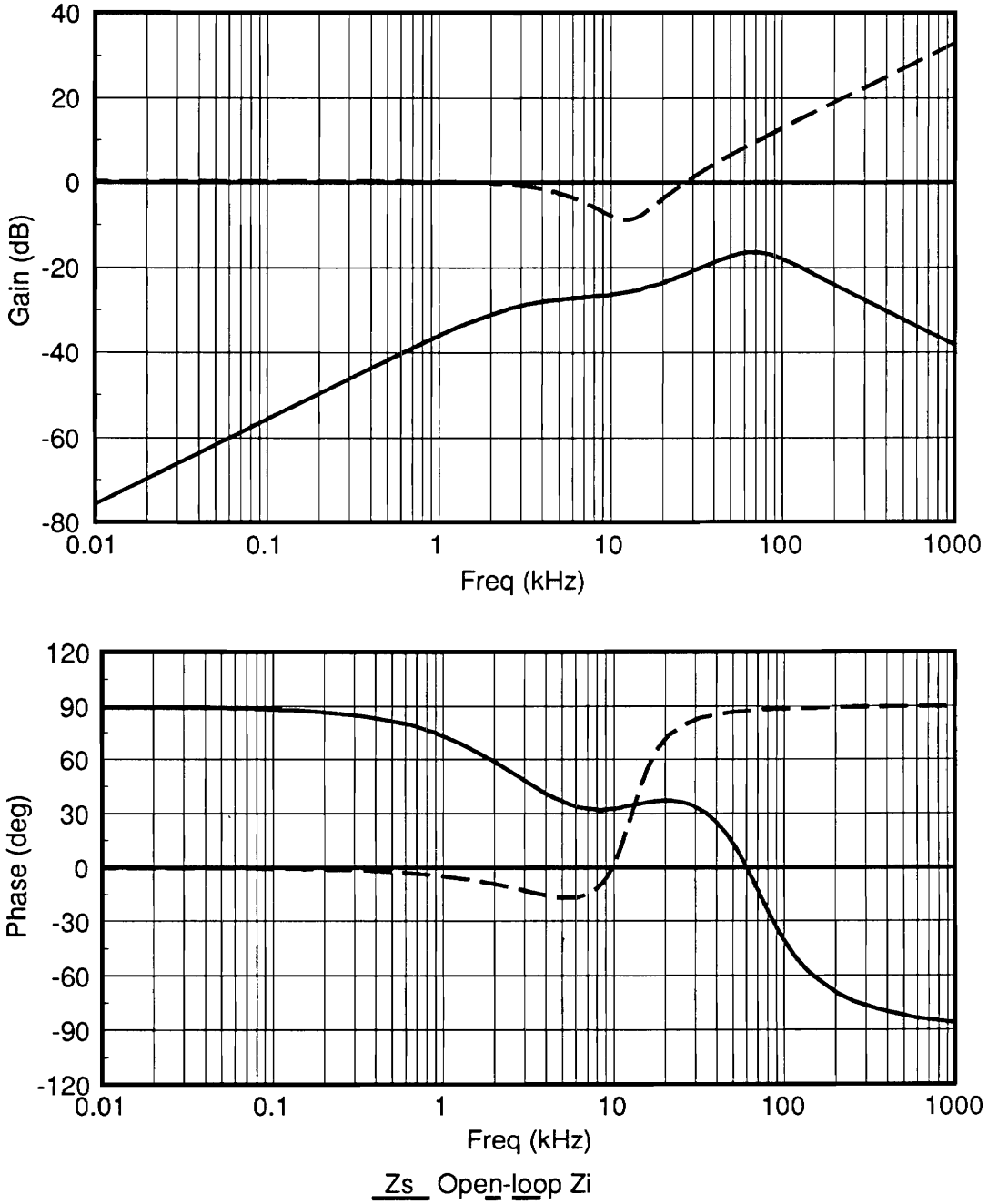

Figure 47. Source impedance seen by and the open-loop input impedance of the single module model

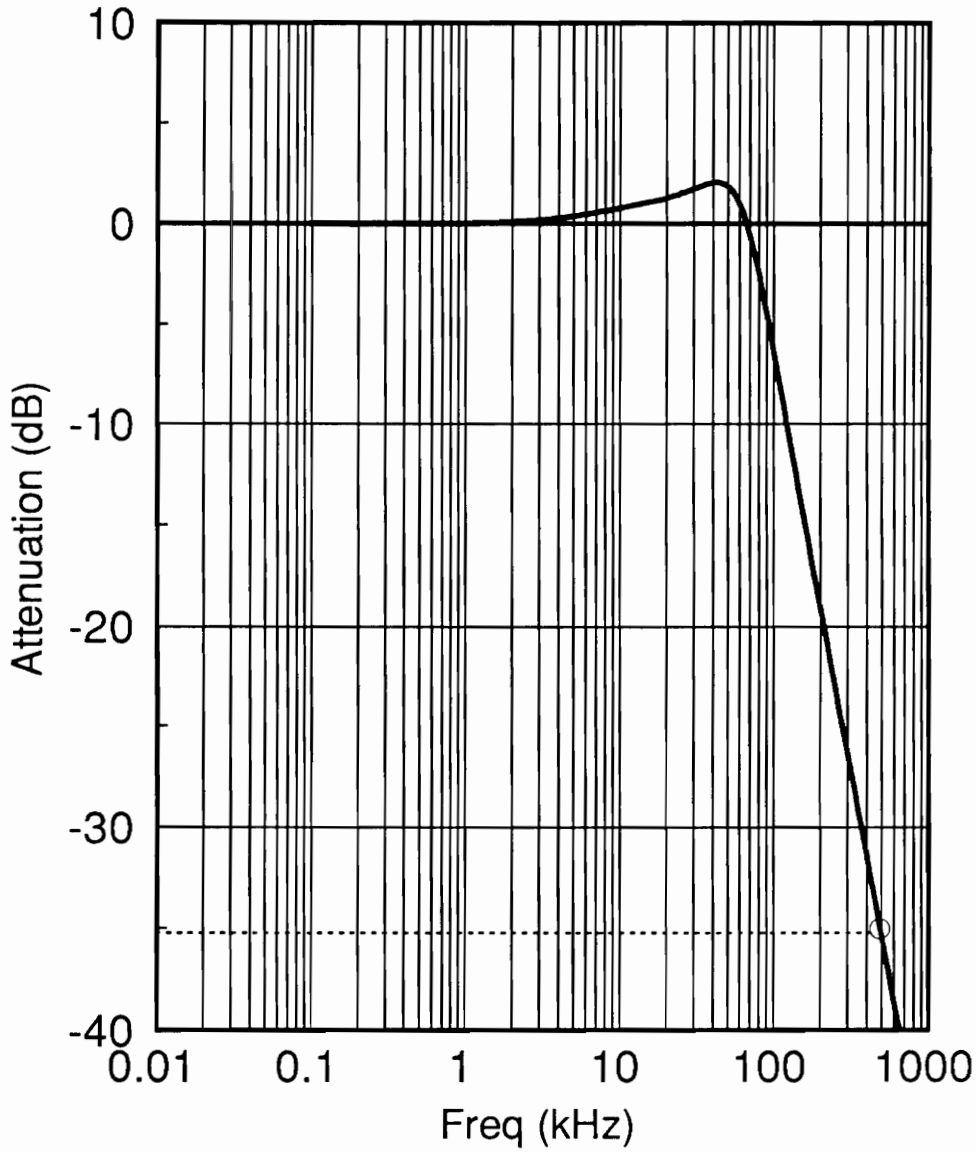

Figure 48. Reverse current gain of the intermediate bus filter

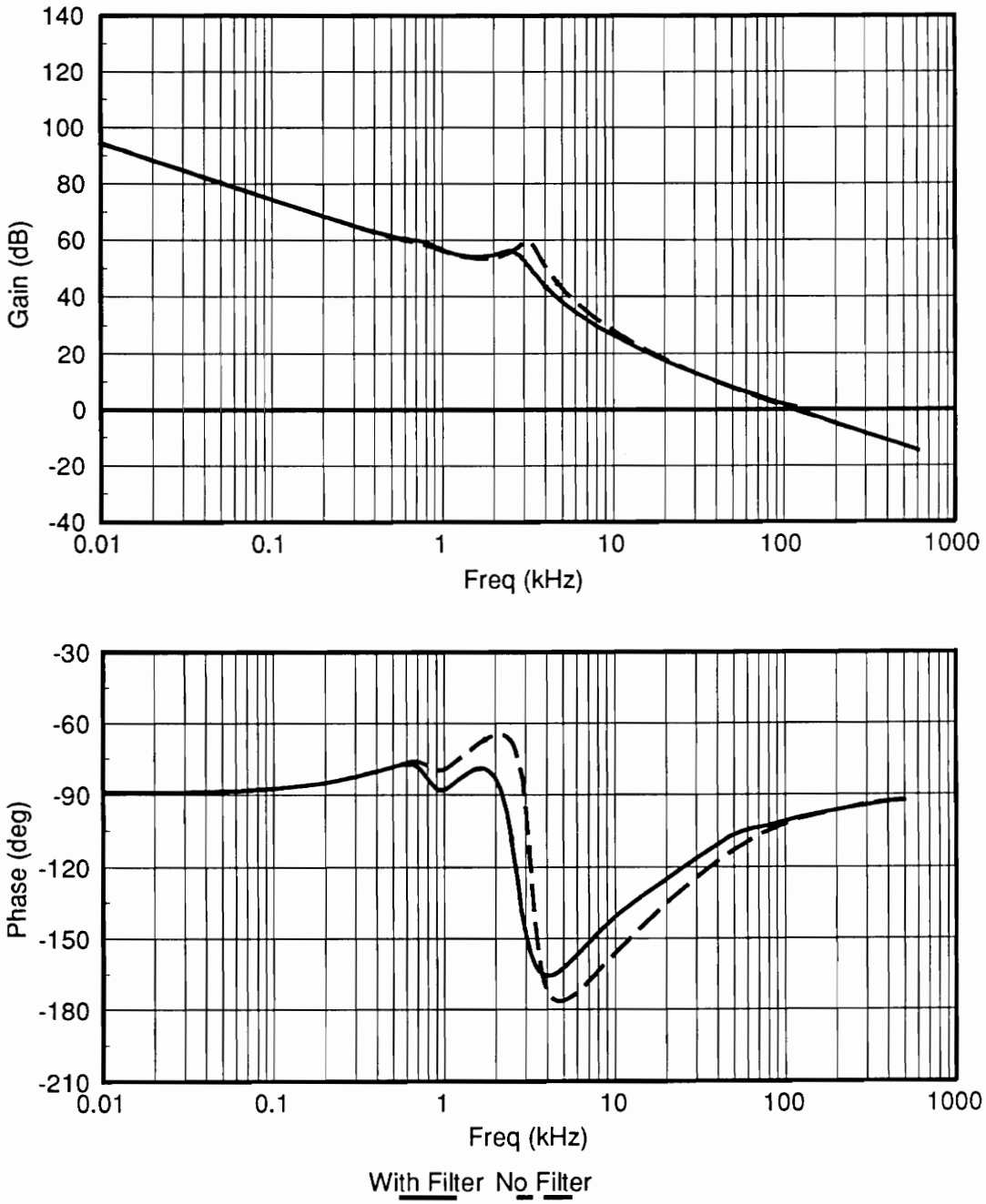

Figure 49. Overall loop gain of the line conditioner with and without the intermediate bus filter

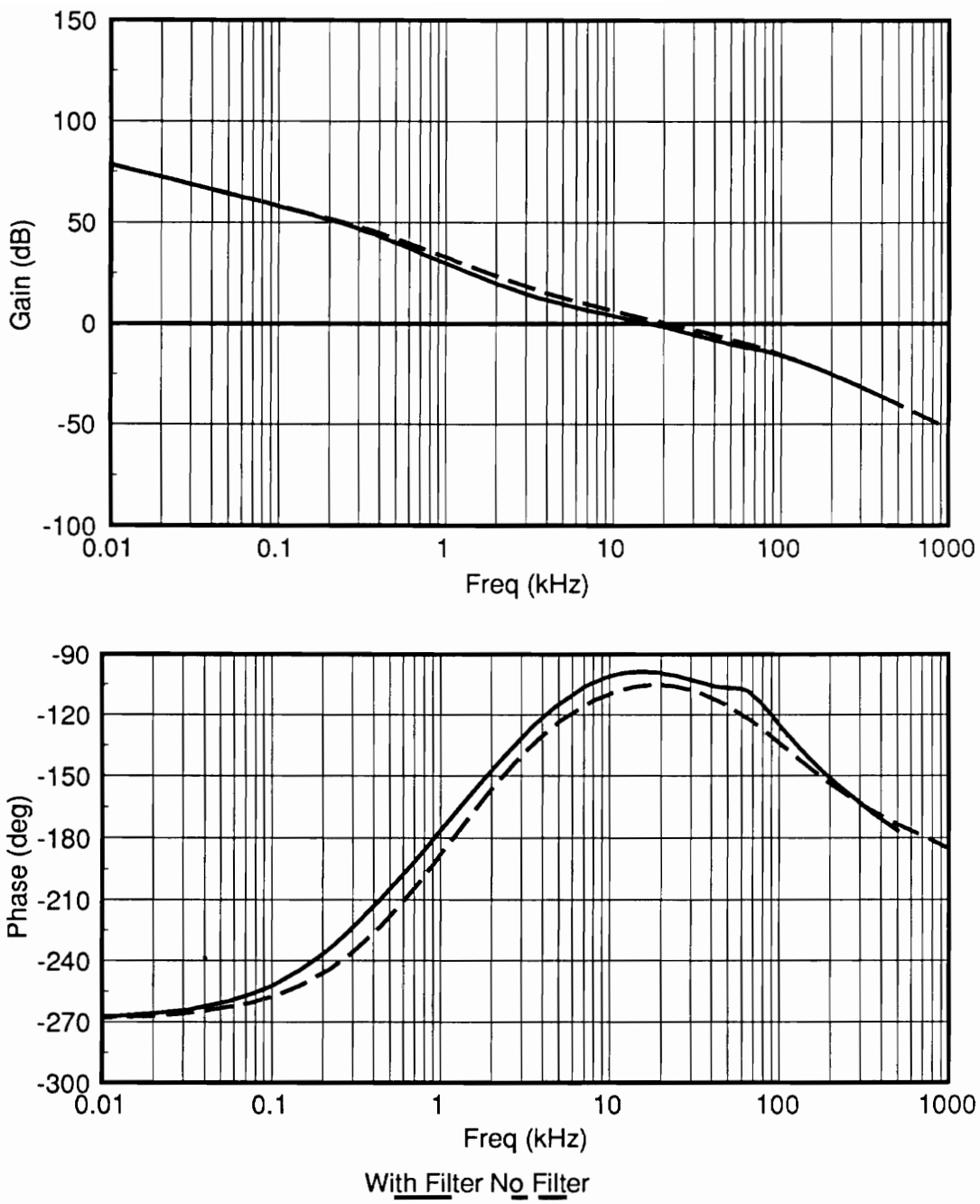

Figure 50. Outer loop gain of the line conditioner with and without the intermediate bus filter

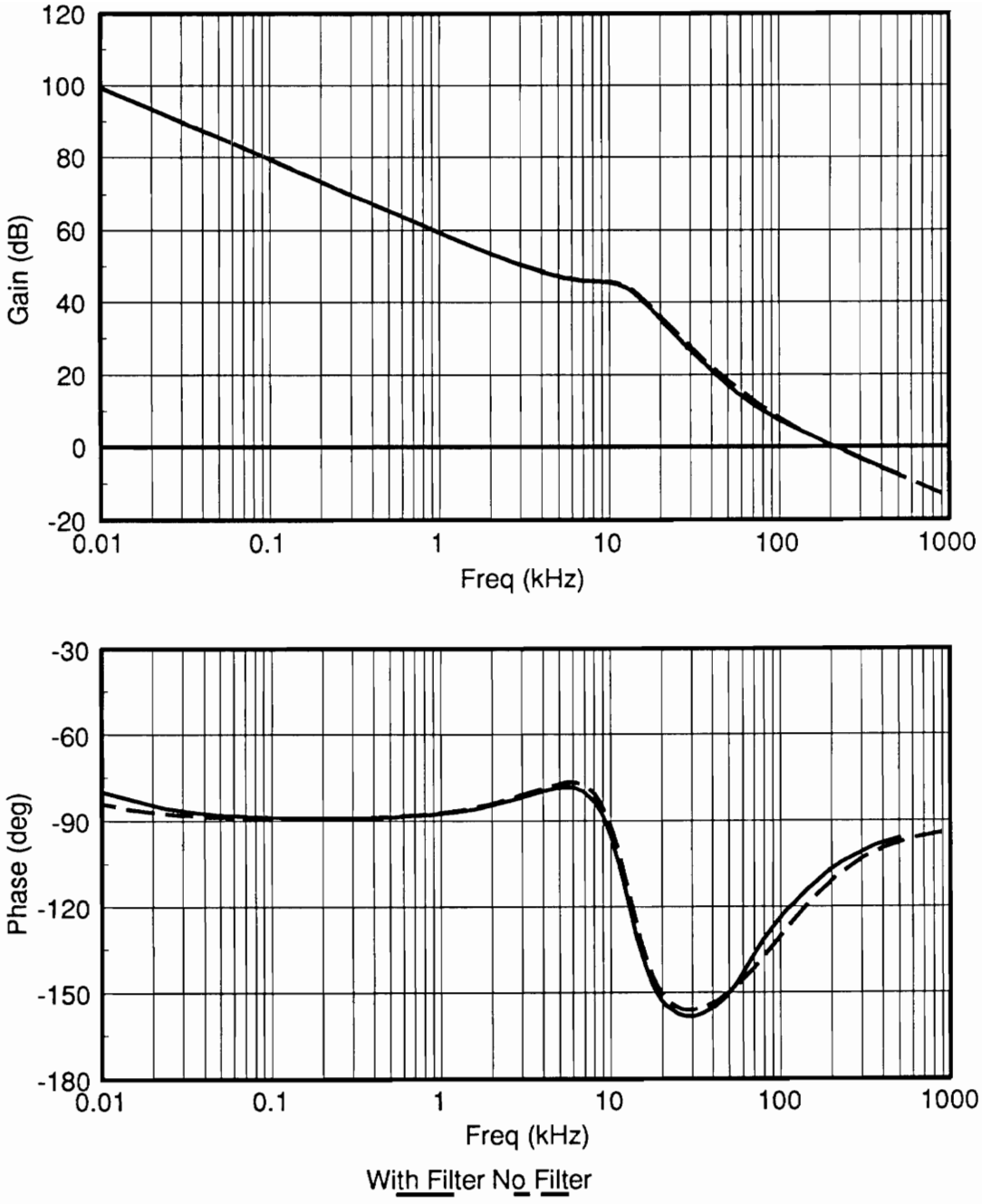

Figure 51. Overall loop gain of the load converter with and without the intermediate bus filter

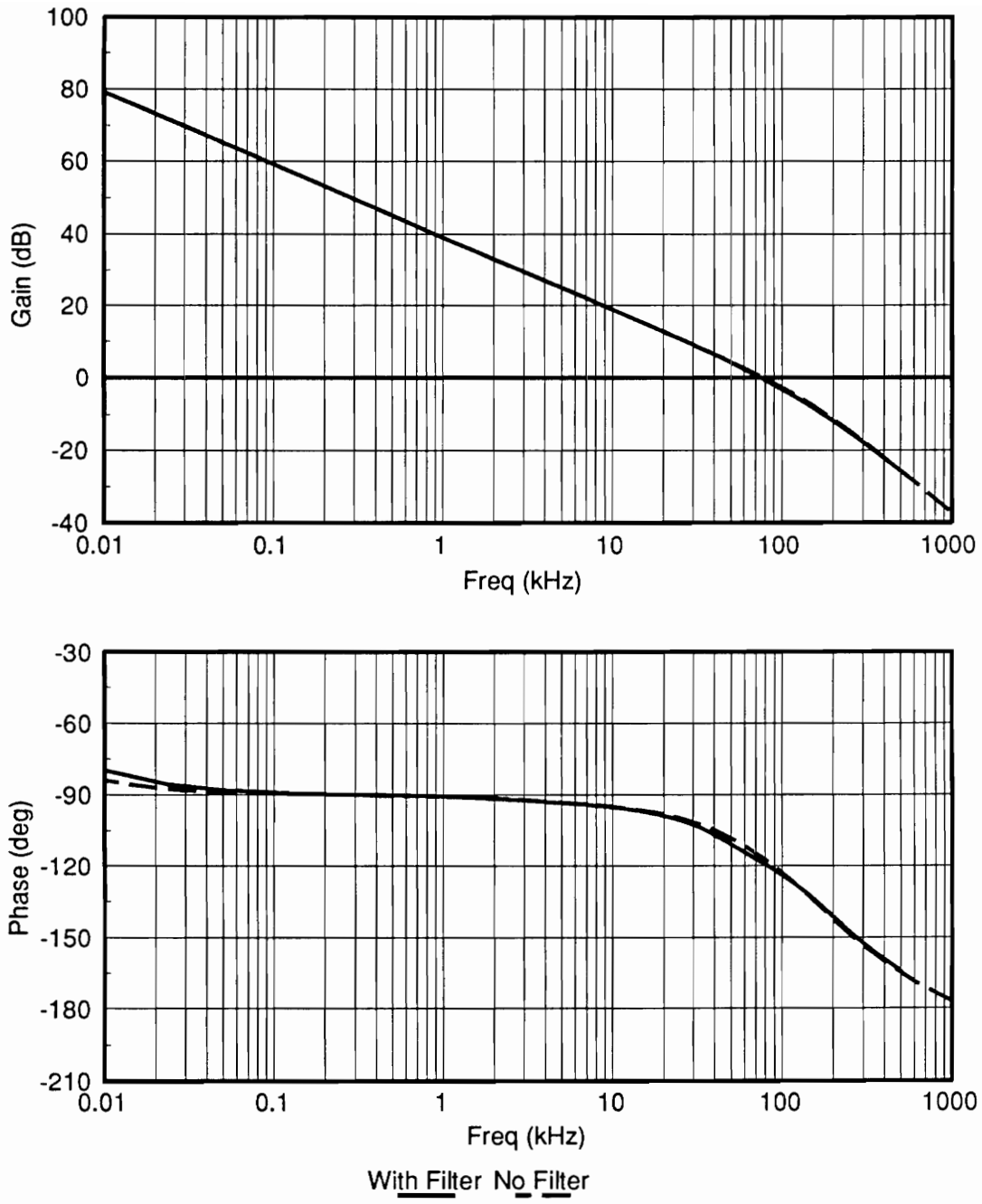

Figure 52. Outer loop gain of the load converter with and without the intermediate bus filter

3.6 Summary

This chapter addressed the design of filters for the DPS. Before discussing the DPS filtering, a discussion of input filters for current-mode controlled single module regulators was presented. It was shown how a non-ideal source impedance seen by a switching regulator affects the regulators loop gains, audiosusceptibility, and output impedance. Criteria were developed which can be used to design the source impedance such that interaction with the regulator is minimized.

In Section 3.3, a discussion of the design considerations for input filters in distributed power systems was given. A method of determining the eigenvalue location of the filter was given, and the use of a single module model was discussed. Of major importance, was the ability to determine the eigenvalues due to parallel interaction. These eigenvalues are not predicted by the single module model.

In Section 3.4, the design of the line input filter was considered. First, large-signal considerations were discussed, and then a small-signal stability analysis was performed. It was shown that the eigenvalues due to parallel interaction can cause instability in an improperly designed filter. A method of stabilizing a previously unstable filter was presented. The definitions for non-minimal systems, observability, and controllability were given, and their impact on the subsystem interaction analysis of Chapter 2 was discussed. Finally, design guidelines for the line input filter were given, along with a practical design example.

The last section in this chapter discussed the design of the intermediate bus filter. It was shown that a compromise between low filter output impedance and high filter input impedance must be made to avoid interaction with both stages of regulators. Design guidelines were given, and a design example was presented.

Chapter 4

POWER SOURCE INTERACTION ANALYSIS

4.1 Introduction

It is common practice to design switching regulators assuming an ideal voltage source supply. This assumption simplifies the design process a great deal. However, as it is well known, a non-ideal source impedance can cause a previously stable regulator to oscillate. In practice, the addition of a differential mode EMI noise filter often results in regulator instability. The instability is caused by interaction between the filter and regulator (see examples in Section 2.2.2 and Section 3.4.2.3). By careful design of the EMI filter, interaction can be minimized, instability can be avoided, and the filter will not markedly affect the regulator performance. Chapter 3 covered the design of filters for the DPS which minimized interaction between the filters and regulators.

Instability can also be caused by other equipment located upstream from the power supply. For instance, cable impedance or impedance of the actual power source can cause the problems. In this chapter, we are concerned with the addition of a non-ideal power source to the DPS. Since the addition of the source will change the impedance seen by the regulators, it is necessary to determine if system stability or performance will be adversely affected. Using the techniques developed in Chapter 2, the effects of the non-ideal source on the DPS will be investigated. It will be shown that while two subsystems may interact, the system performance will not necessarily be compromised. In Section 4.2, the characteristics of the source will be defined. Sections 4.3 and 4.4 will investigate the effects of the non-ideal source from two different points in the system. Finally, Section 4.5 summarizes the results of this chapter.

4.2 Generator Source Characteristics

The DPS under consideration has been designed such that it may operate from a variety of power sources. In this section we will examine the potential interaction between one these sources and the DPS. The non-ideal source consists of a three-phase generator, transformer, rectifier, and bus filter. This particular source provides a DC output of 155V. In order to proceed with the dynamic interaction analysis, it is first necessary to obtain a model of the source dynamic characteristics. The source model (as determined by EG&G) is shown in Figure 53. The source parameters have been modified slightly for this thesis to provide a useful example of source interaction. Shown in Figure 54 is the output impedance of the source. At very high frequencies, the ESL of the bus capacitance causes the source impedance to rise, but at frequencies of interest, the impedance remains less than 10Ω. It should be noted here that the emphasis of this chapter is not on modelling of the source, but rather on determining the effect of a given source characteristic on the system performance and stability.

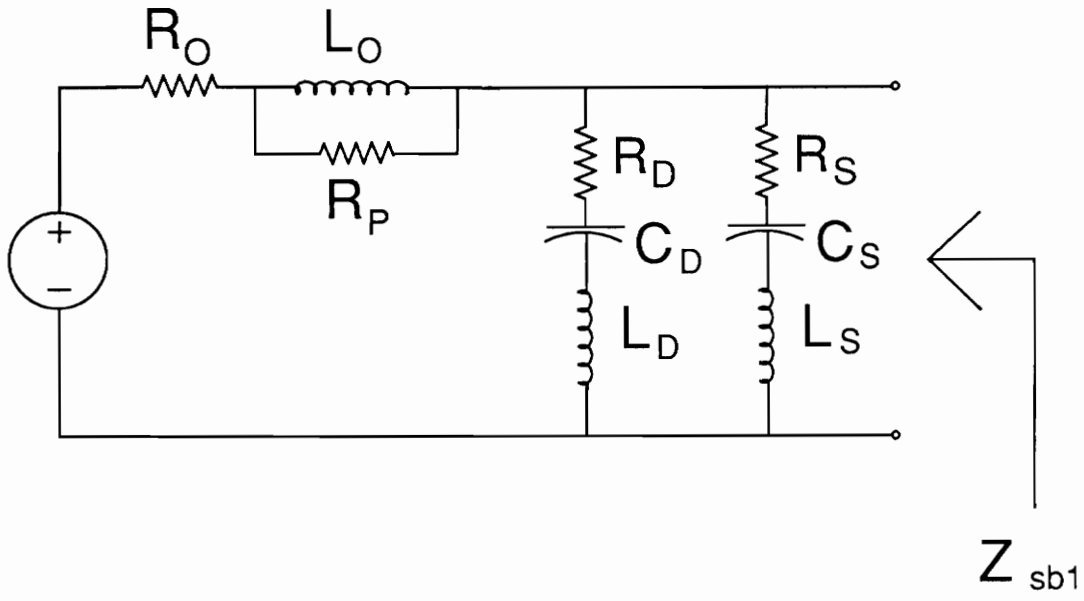

Figure 53. Small-signal dynamic model of non-ideal generator source

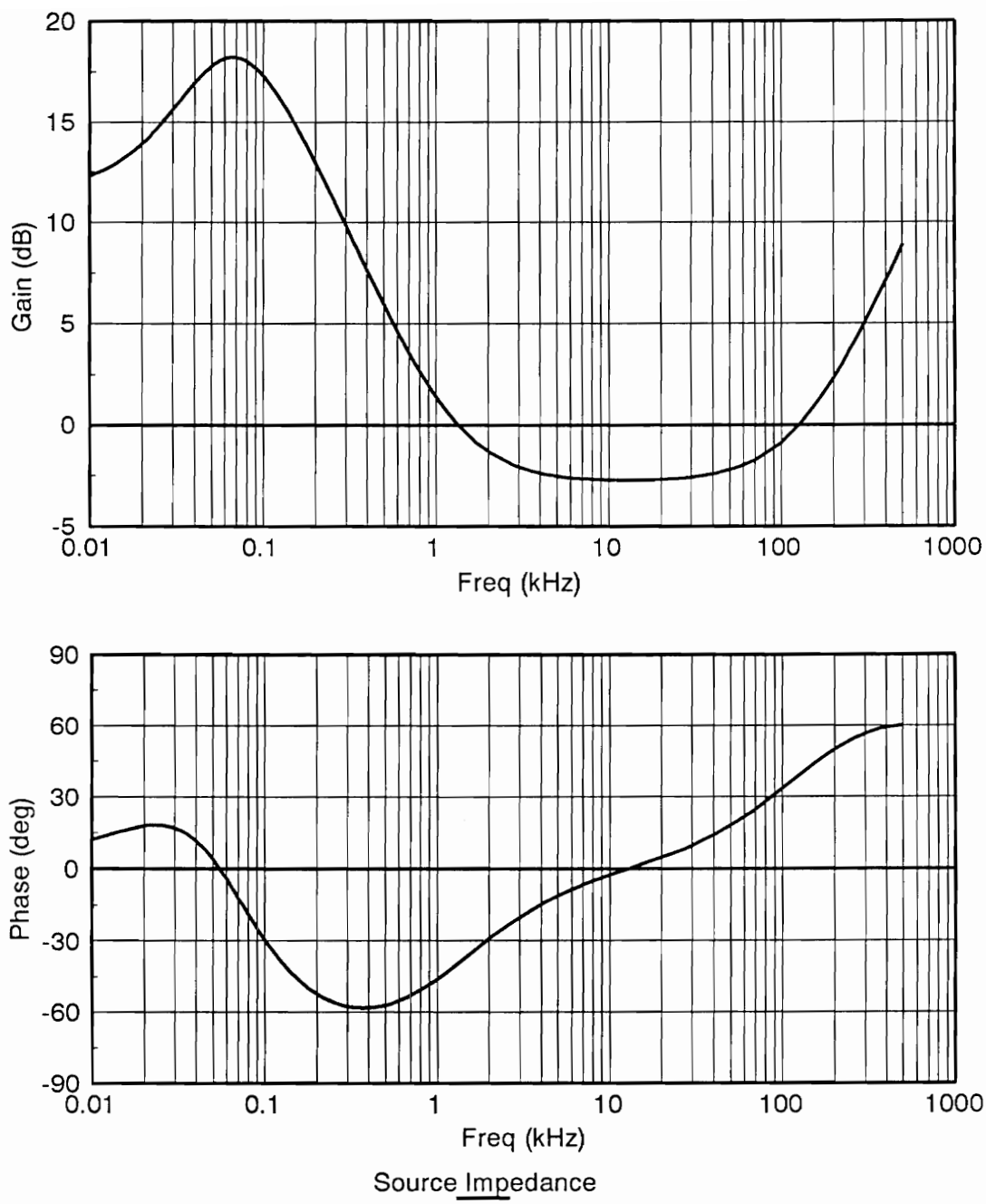

Figure 54. Output impedance of non-ideal generator source

We may first ask whether the generator source is compatible with the line conditioners in the absence of any intermediate EMI filtering (the line input filter developed in Chapter 3). This is facilitated by extending the results of Chapter 2. A comparison of the source impedance with the input impedance of the line conditioner stage of parallel regulators can provide the necessary information. For example, we may approximate the input impedance of the line conditioner stage as a negative resistance. At 155V input voltage and 2.4kW output power, the input impedance is 20dBΩ with a phase of -180 degrees. From Figure 54, we find that $|Z_s| < 20\text{dB}\Omega$ for all frequencies. Therefore, stability of the integrated system is assured. However, at 64Hz the peak of $|Z_s|$ comes very close to the 20dBΩ line conditioner input impedance, and slight interaction is expected at that point. The result of the interaction will be less damping of the source eigenvalue at 64Hz. For a practical application, the degree of interaction may not be acceptable, and additional filtering of the source may be required to lower the source impedance at low frequencies.

The next step is to determine the compatibility of the DPS with line input filter to the generator source. Figure 55 shows the circuit diagram of the source side of the DPS with the addition of the non-ideal power source. Examining Figure 55, it can be seen that there are two buses of interest on the source side. Bus 1 naturally separates the regulator/input filter subsystem from the generator subsystem. Bus 2 is the summing junction and is immersed in the line input filter. It will be shown that either of these two buses may be used to predict the integrated system stability and performance.

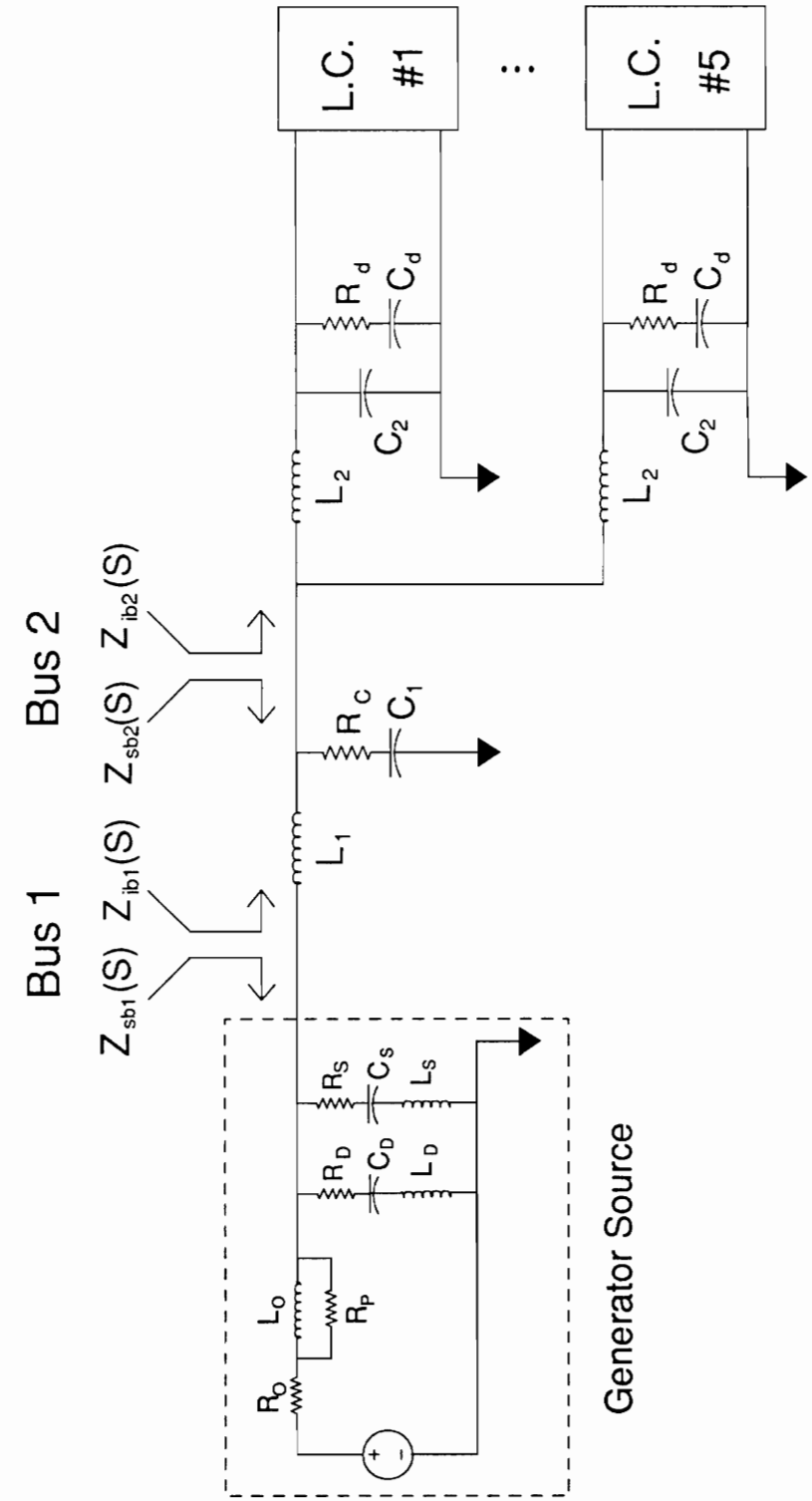

Figure 55. Circuit diagram of source side of the DPS including non-ideal power source

4.3 Bus 2 Analysis

Shown in Figure 56 are the source and load impedances seen at bus 2 for a power level of 2.4kW. The large overlap in impedances predicts interaction between the two subsystems defined at that point. We would first like to demonstrate how the information at bus 2 can predict system stability. It should be stated that the overlap in impedances does not imply instability. We must make use of the techniques developed in Chapter 2 to determine the system stability.

Shown in Figure 57 is the Bode plot of the minor loop gain, T_{m2}, defined at bus 2. Since T_{m2} is greater than 0dB from 4.4kHz to 15kHz, we expect interaction in this frequency range. To determine the stability of the system, we may now determine the system phase margins as defined in Equations (2.8) and (2.9). From Figure 57, we see that $PM_1 = 138°$ at 4.4kHz and $PM_2 = 98°$ at 15kHz. Thus, the eigenvalues of the integrated system introduced due to subsystem interaction should be well damped and in the LHP.

An alternative method to determine stability would be to apply the Nyquist criterion to the polar plot of T_{m2}. This is shown in Figure 58. Since the (-1,0) point is not encircled and both decoupled subsystems defined at bus 2 are stable, then the integrated system is also stable.

The overlap of impedances in Figure 56 can be explained by recalling the design of the line input filter. The single damping resistor in the first stage of the filter was used to provide damping to eigenvalues in both stages of the filter (see Section 3.4.2). At frequencies above 2kHz, the impedance Z_{sb2} is essentially resistive, being dominated by R_c. The dip in Z_{ib2} at 9kHz is due to the resonance of L_2 and C_2 of the second stage filter. The overlap in impedances represents the damping effect of R_c on the L_2C_2 corner.

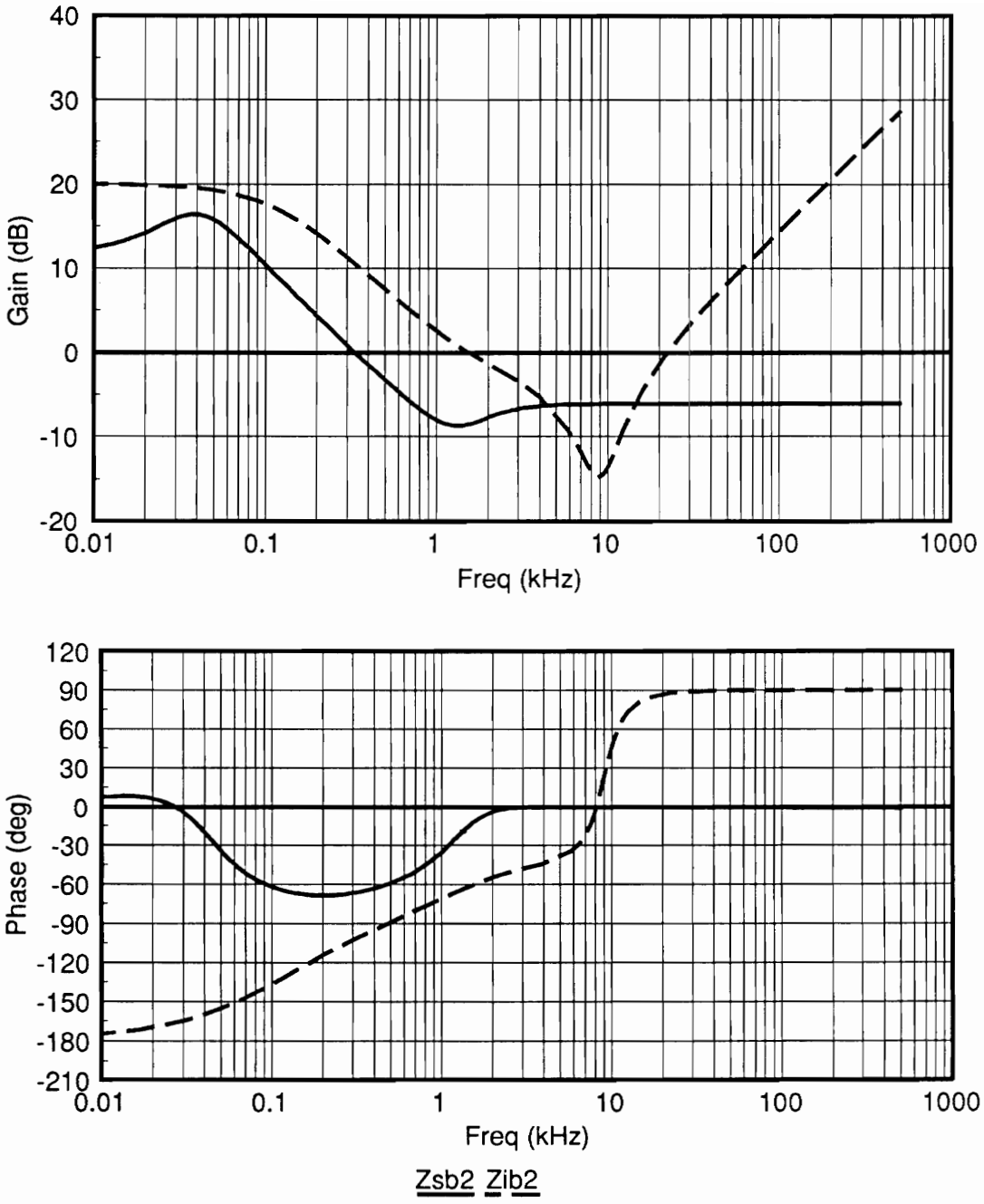

Figure 56. Source and load impedances seen at bus 2

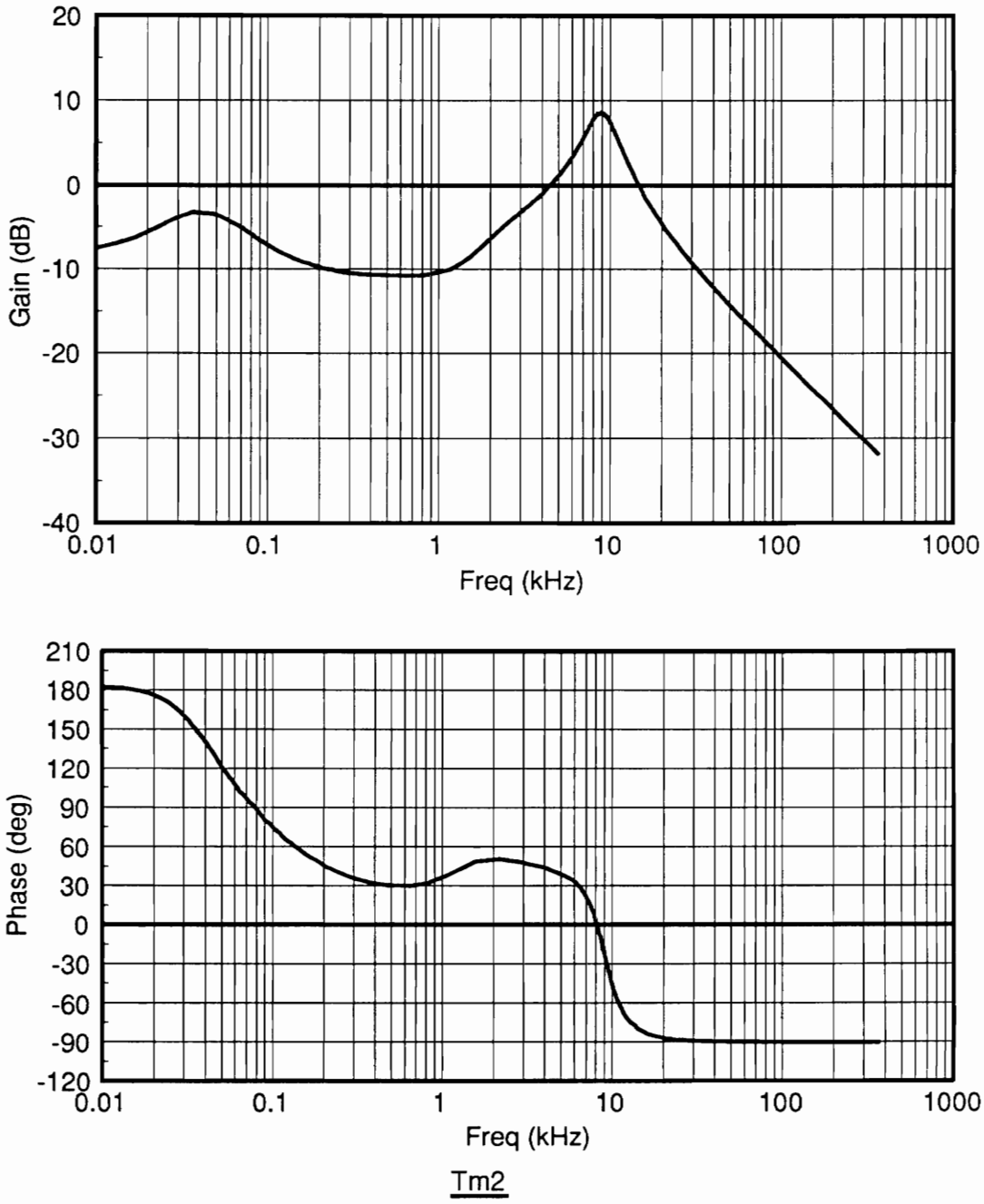

Figure 57. Bode plot of bus 2 minor loop gain

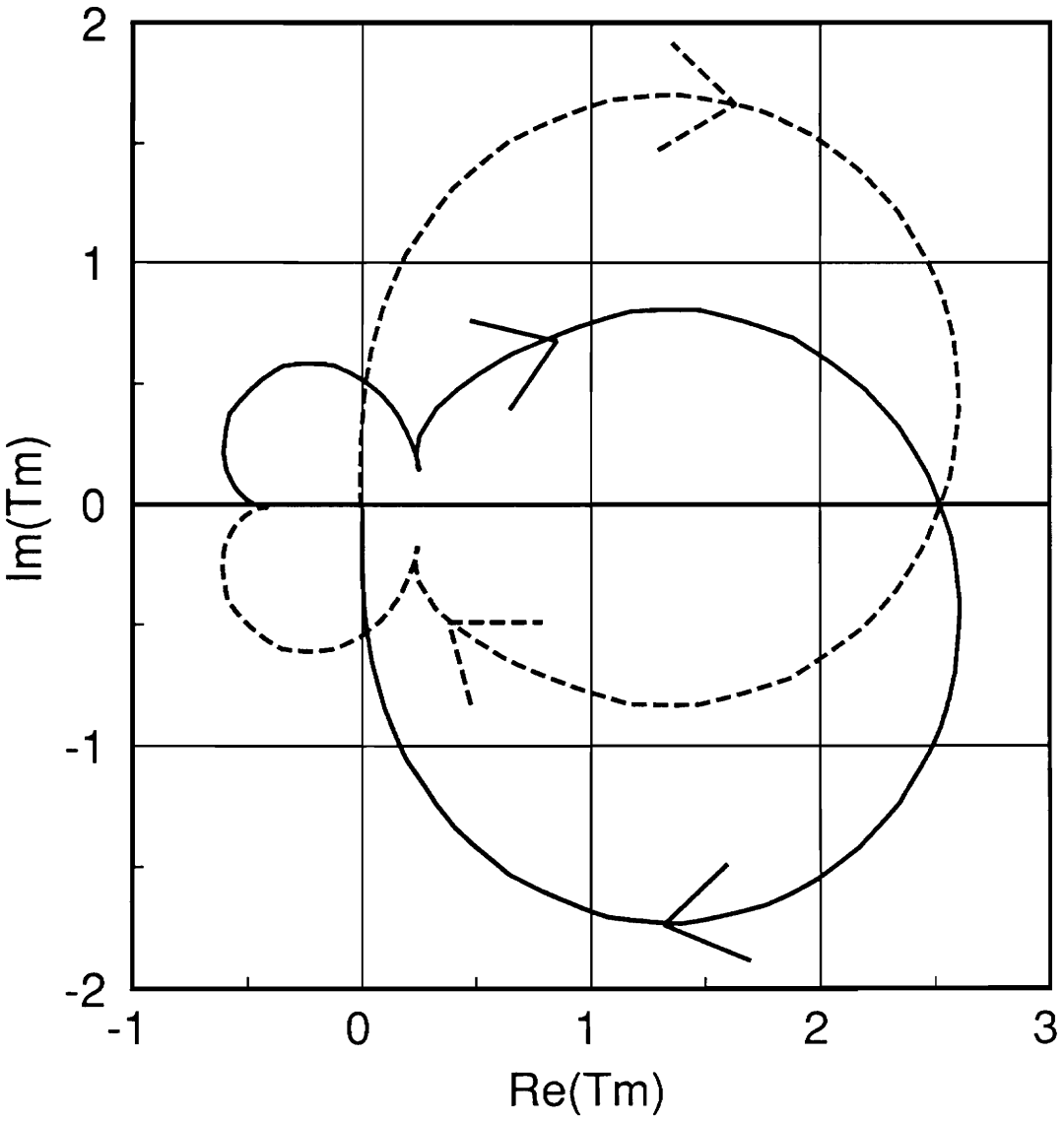

Figure 58. Polar plot of bus 2 minor loop gain

When designing the line input filter, one might attempt to design the Filter 1 and Filter 2 blocks independently. In that case, if minimal interaction between the two stages was insured by a wide separation in impedances at bus 2, then the overall filter attenuation would simply be the product of the two filter forward gains. However, this approach is not optimal from a filtering viewpoint and might not be practical considering the restrictions that are placed on the Filter 2 output impedance. Therefore, the two filters were designed to interact, and that interaction is apparent in the damping effect of R_c on the second stage L_2C_2 resonance.

For the design under consideration, the interaction at bus 2 may cause peaking of the bus impedance. However, due to the large phase margins at the points of intersection, there should be no problem with peaking. The bus impedance, Z_{B2}, is shown in Figure 59. No peaking is apparent at the points of intersection of $|Z_{sb2}|$ and $|Z_{ib2}|$. If fewer line conditioner modules were used, the Z_{ib2} gain curve would change. To determine the effect of the number of line conditioners on the bus 2 impedance, shown in Figure 60 is Z_{B2} for 4 and 5 line conditioners. The bus impedance shows a slight increase in the region of interaction, but there is still no problem with peaking at the frequencies where $|T_{m2}| \simeq 1$. Thus, the removal of a single line conditioner from the system will not threaten stability.

We may now show how the subsystem eigenvalues change location upon system integration at bus 2. Table 3 lists the eigenvalues of the subsystems defined at bus 2. The eigenvalue listed as mode 4 in Table 3(a) is due to modelling constraints, and will not apper in the actual system (this eigenvalue also appears in Table 4 and Table 5 and should be ignored). Table 4 lists the eigenvalues of the integrated system. One interesting point is that the eigenvalues of the load subsystem due to parallel interaction of the parallel modules are not affected by the non-ideal source. Since the eigenvalues due to parallel interaction are unobservable and uncontrollable from bus 2, they are not affected by the non-ideal source, as explained in Section 3.4.2.2. Load subsystem eigenvalues in Table 3 with a multiplicity of 4 are due to parallel interaction of the line conditioner stage, and will not be affected by the sub-

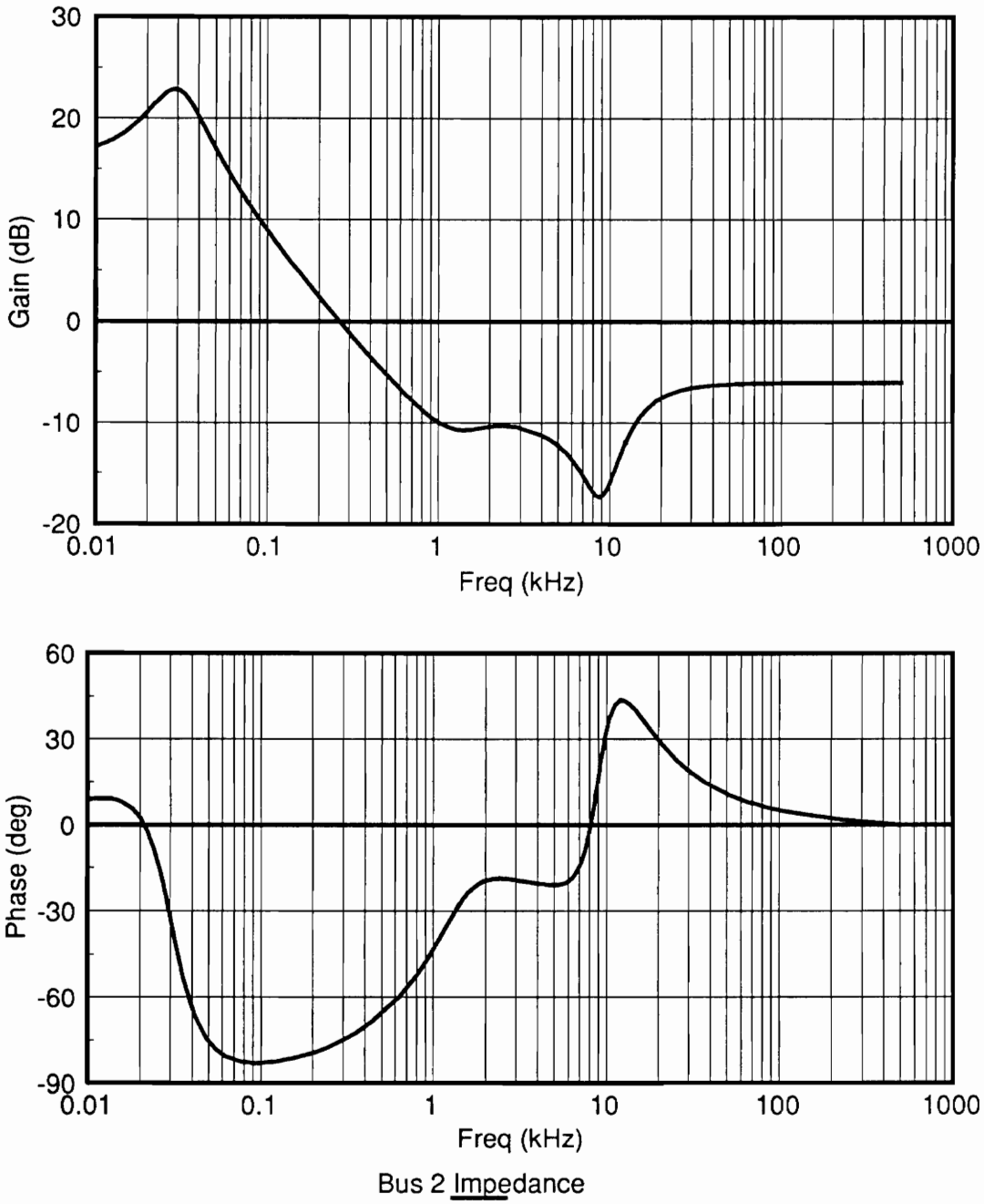

Figure 59. Bus 2 impedance for 5 line conditioners

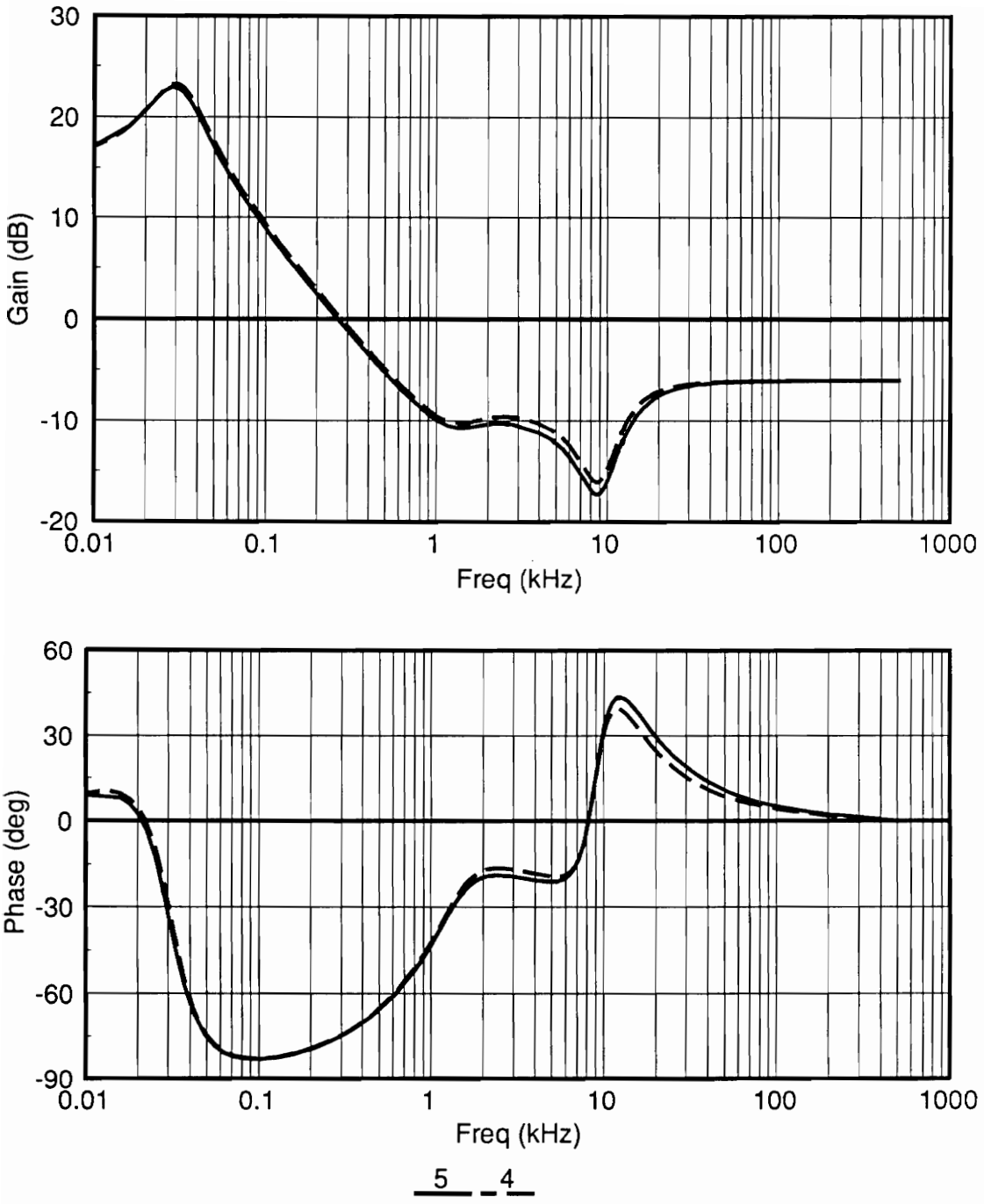

Figure 60. Bus 2 impedance for 4 and 5 line conditioners

system integration. Similarly, eigenvalues with a multiplicity of 12 are due to parallel interaction of the load converter stage, and are also unaffected by subsystem integration.

From the previous discussion, we know that R_c will tend to damp the second stage corner at 9kHz. This eigenvalue is shown as mode 6 in the bus 2 load subsystem eigenvalue listing, and has a relatively high Q of 2.2 before integration. As a result of interaction, this eigenvalue shifts to 11.2kHz and is damped to a Q of 0.8. This is found from mode 14 of the integrated system eigenvalues. Mode 1 of the load subsystem is shifted to a slightly lower frequency, and is found as mode 4 of the integrated system. Mode 1 of the source subsystem, which is seen as the complex pole at 42Hz in Z_{sb2} with a Q of 0.81, is shifted down to 30Hz with an increase in Q to 1.4. This is due to the fact that Z_{sb2} and Z_{ib2} are separated by only a few dBΩ at low frequencies. The result is seen as the slight peaking in Z_{B2} in Figure 59. The remaining subsystem eigenvalues are not greatly affected by the interaction. The results obtained here show that the analysis techniques presented in Chapter 2 can be very useful in analyzing subsystem interaction.

Table 3. Eigenvalues for subsystems defined at bus 2

Table 3(a). Bus 2 Source Subsystem Eigenvalues					
Mode	Mult	Real Part	Imaginary Part	Natural Frequency	Damping Ratio
1	1	-285.268	±239.916	372.743	0.765320
2	1	-322.811	0.00E+00	322.811	1.00
3	1	-3782.89	±5868.32	6981.94	0.541811
4	1	-2.9127E+06	±3.9678E+07	3.9785E+07	7.3212E-02
5	1	-5.4846E+06	0.00E+00	5.4846E+06	1.00
6	1	-2.00E+08	0.00E+00	2.00E+08	1.00

Table 3(b). Bus 2 Load Subsystem Eigenvalues					
Mode	Mult	Real Part	Imaginary Part	Natural Frequency	Damping Ratio
1	1	-9893.64	0.00E+00	9893.64	1.00
2	4	-9894.48	0.00E+00	9894.48	1.00
6	1	-12766.2	±54772.1	56240.2	0.226995
7	4	-13008.1	±54748.4	56272.6	0.231163
11	1	-24928.8	±4547.59	25340.2	0.983765
12	12	-44634.1	0.00E+00	44634.1	1.00
24	1	-50214.6	0.00E+00	50214.6	1.00
25	1	-100534.	0.00E+00	100534.	1.00
26	4	-133333.	0.00E+00	133333.	1.00
30	12	-155327.	±341199.	374891.	0.414326
42	1	-188761.	±379901.	424212.	0.444969
43	1	-235791.	0.00E+00	235791.	1.00
44	1	-437733.	0.00E+00	437733.	1.00
45	1	-511276.	±498554.	714114.	0.715958
46	4	-654746.	0.00E+00	654746.	1.00
50	12	-1.219512E+06	0.00E+00	1.219512E+06	1.00
62	1	-1.326560E+06	0.00E+00	1.326560E+06	1.00
63	12	-1.434710E+06	0.00E+00	1.434710E+06	1.00
75	1	-3.344046E+07	0.00E+00	3.344046E+07	1.00
76	1	-3.578612E+07	0.00E+00	3.578612E+07	1.00
77	1	-5.286940E+07	0.00E+00	5.286940E+07	1.00
78	1	-5.403712E+08	0.00E+00	5.403712E+08	1.00

Table 4. Eigenvalues of the integrated system

Table 4. Full DPS Eigenvalues					
Mode	Mult	Real Part	Imaginary Part	Natural Frequency	Damping Ratio
1	1	-246.967	±261.920	359.993	0.686034
2	1	-305.523	0.00E+00	305.523	1.00
3	1	-2532.00	±5732.66	6266.93	0.404026
4	1	-8359.58	0.00E+00	8359.58	1.00
5	4	-9894.48	0.00E+00	9894.48	1.00
9	4	-13008.1	±54748.4	56272.6	0.231163
13	1	-24887.8	±4687.46	25325.3	0.982722
14	1	-44283.6	±55189.8	70759.8	0.625830
15	12	-44634.1	0.00E+00	44634.1	1.00
27	1	-50214.6	0.00E+00	50214.6	1.00
28	1	-100538.	0.00E+00	100538.	1.00
29	4	-133333.	0.00E+00	133333.	1.00
33	12	-155327.	±341199.	374891.	0.414326
45	1	-188761.	±379901.	424212.	0.444968
46	1	-235819.	0.00E+00	235819.	1.00
47	1	-437720.	0.00E+00	437720.	1.00
48	1	-511276.	±498554.	714114.	0.715958
49	4	-654746.	0.00E+00	654746.	1.00
53	12	-1.219512E+06	0.00E+00	1.219512E+06	1.00
65	1	-1.326560E+06	0.00E+00	1.326560E+06	1.00
66	12	-1.434710E+06	0.00E+00	1.434710E+06	1.00
78	1	-2.912744E+06	±3.967814E+07	3.978490E+07	7.321E-02
79	1	-5.484650E+06	0.00E+00	5.484650E+06	1.00
80	1	-3.344046E+07	0.00E+00	3.344046E+07	1.00
81	1	-3.578612E+07	0.00E+00	3.578612E+07	1.00
82	1	-5.286940E+07	0.00E+00	5.286940E+07	1.00
83	1	-1.999412E+08	0.00E+00	1.999412E+08	1.00
84	1	-5.403712E+08	0.00E+00	5.403712E+08	1.00

4.4 Bus 1 Analysis

This section will address the source interaction analysis as viewed from bus 1. Figure 61 shows the source and load impedances seen at bus 1. As with bus 2, the impedances overlap, predicting interaction. While interaction was expected at bus 2 due to the line input filter design, it was not necessarily expected at bus 1. First, we will predict the stability using the phase margins and also the Nyquist Criterion as applied to the minor loop gain, and then we will discuss the integrated system eigenvalue location.

Shown in Figure 62 is the minor loop gain at bus 1. The plot predicts the interaction in the low frequency range, since its gain is greater than 0dB from 35Hz to 2kHz. It can be seen that $PM_1 = 34°$ and $PM_2 = 80°$. Notice that the phase margins defined at bus 1 are considerably smaller than those defined at bus 2. While the phase margins defined at buses 1 and 2 describe the same system, they represent the stability of different eigenvalues. Figure 63 shows the polar plot which verifies system stability. The large phase margin at 2kHz predicts little peaking in the bus impedance at that frequency. However some peaking is expected at around 30Hz due to the low phase margin there. This is confirmed in Figure 64.

As the number of line conditioners is decreased, no degradation in the bus 1 impedance is expected since Z_{ib1} is relatively insensitive to the number of line conditioner modules. Shown in Figure 65 is Z_{B1} for 4 and 5 line conditioners. The bus impedance is not compromised by the number of line conditioners.

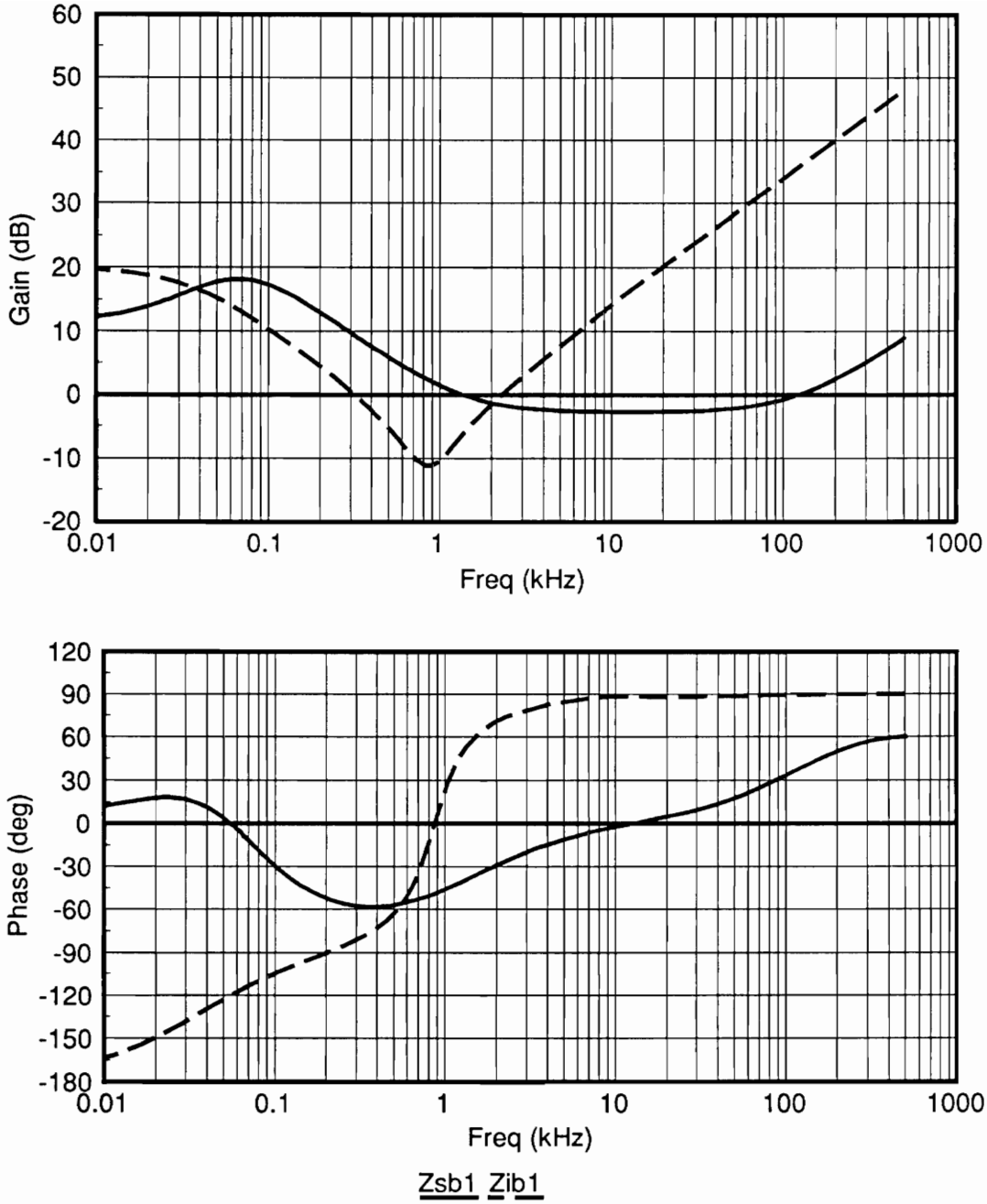

Figure 61. Source and load impedances seen at bus 1

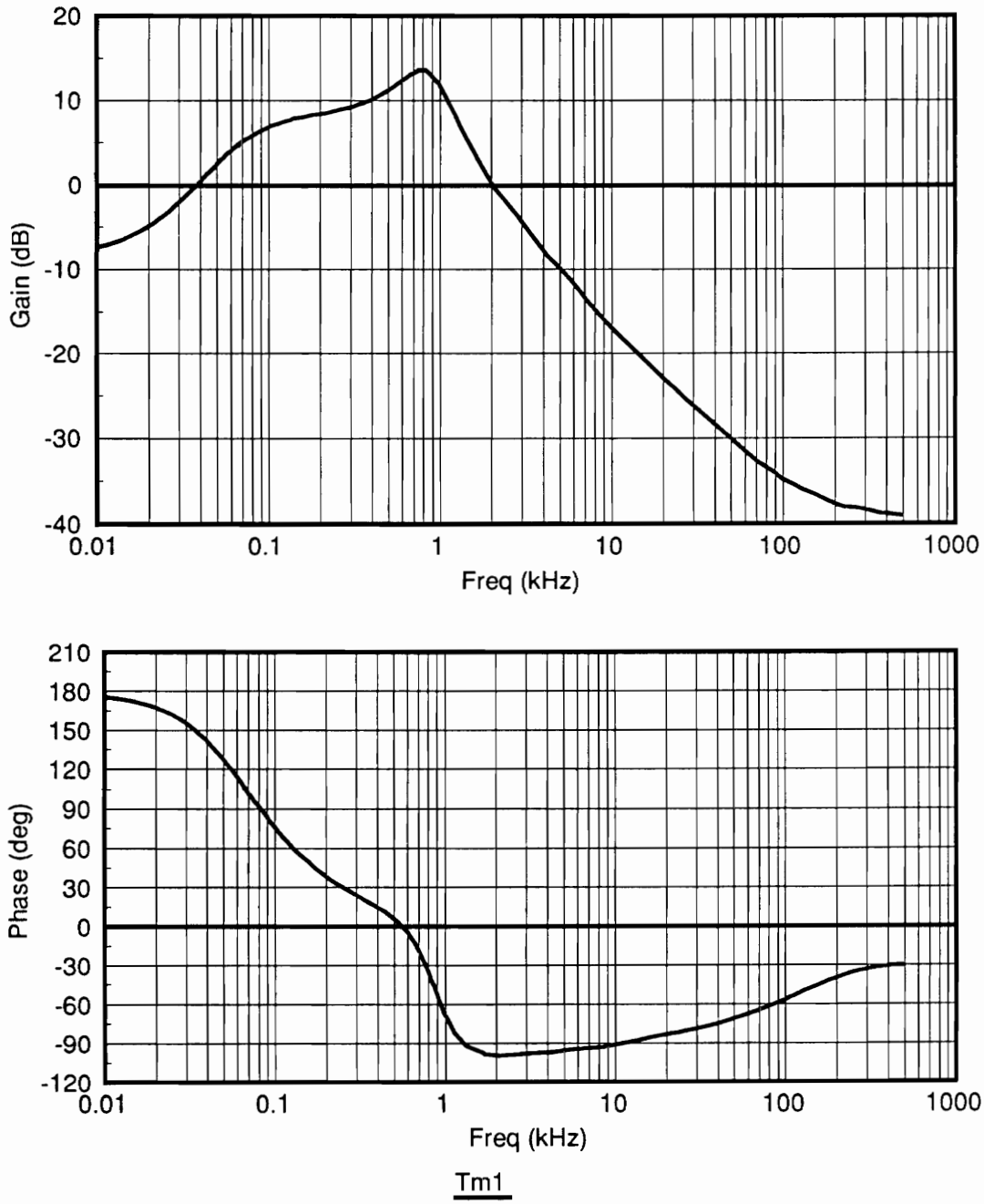

Figure 62. Bode plot of bus 1 minor loop gain

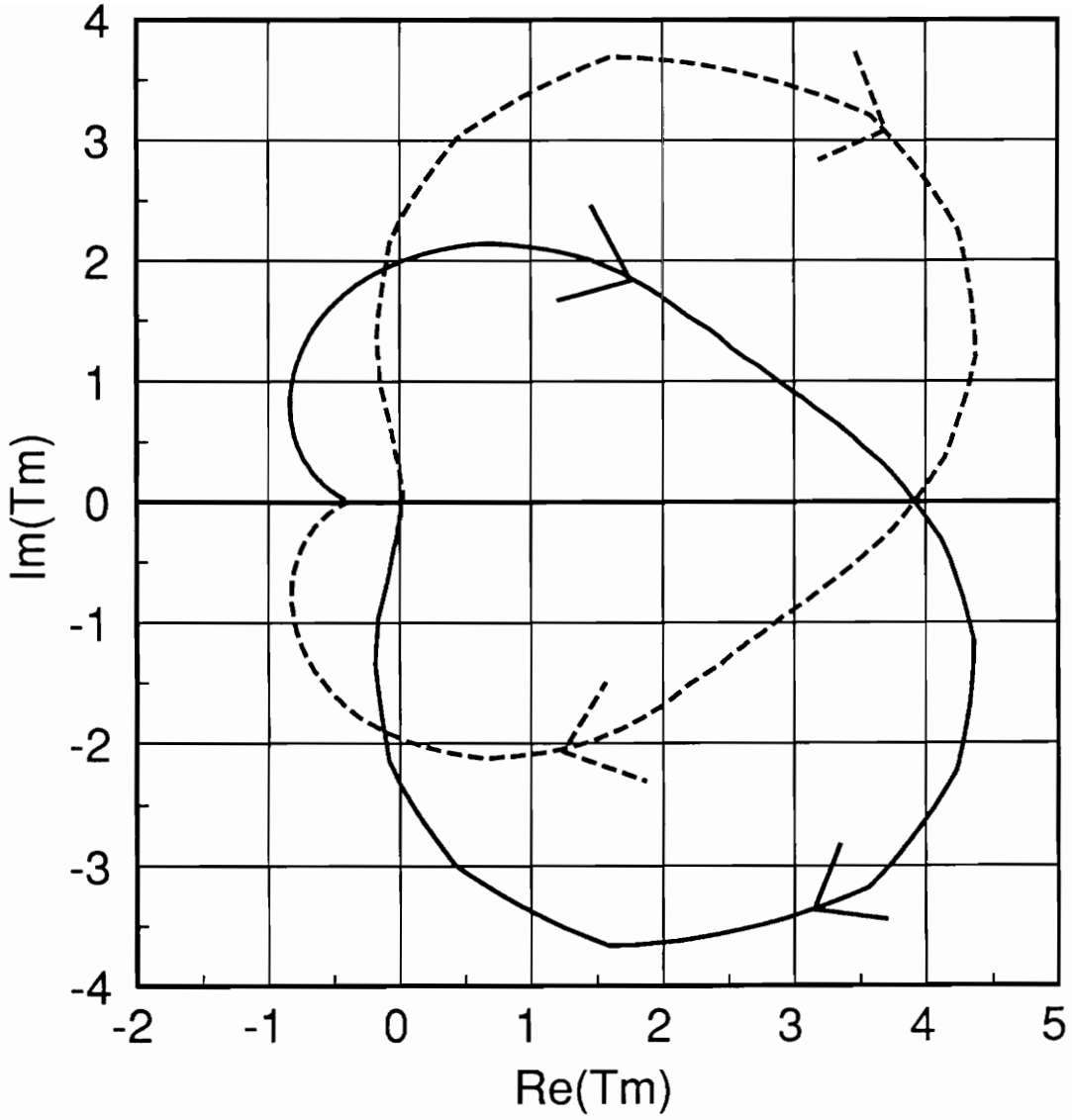

Figure 63. Polar plot of bus 1 minor loop gain

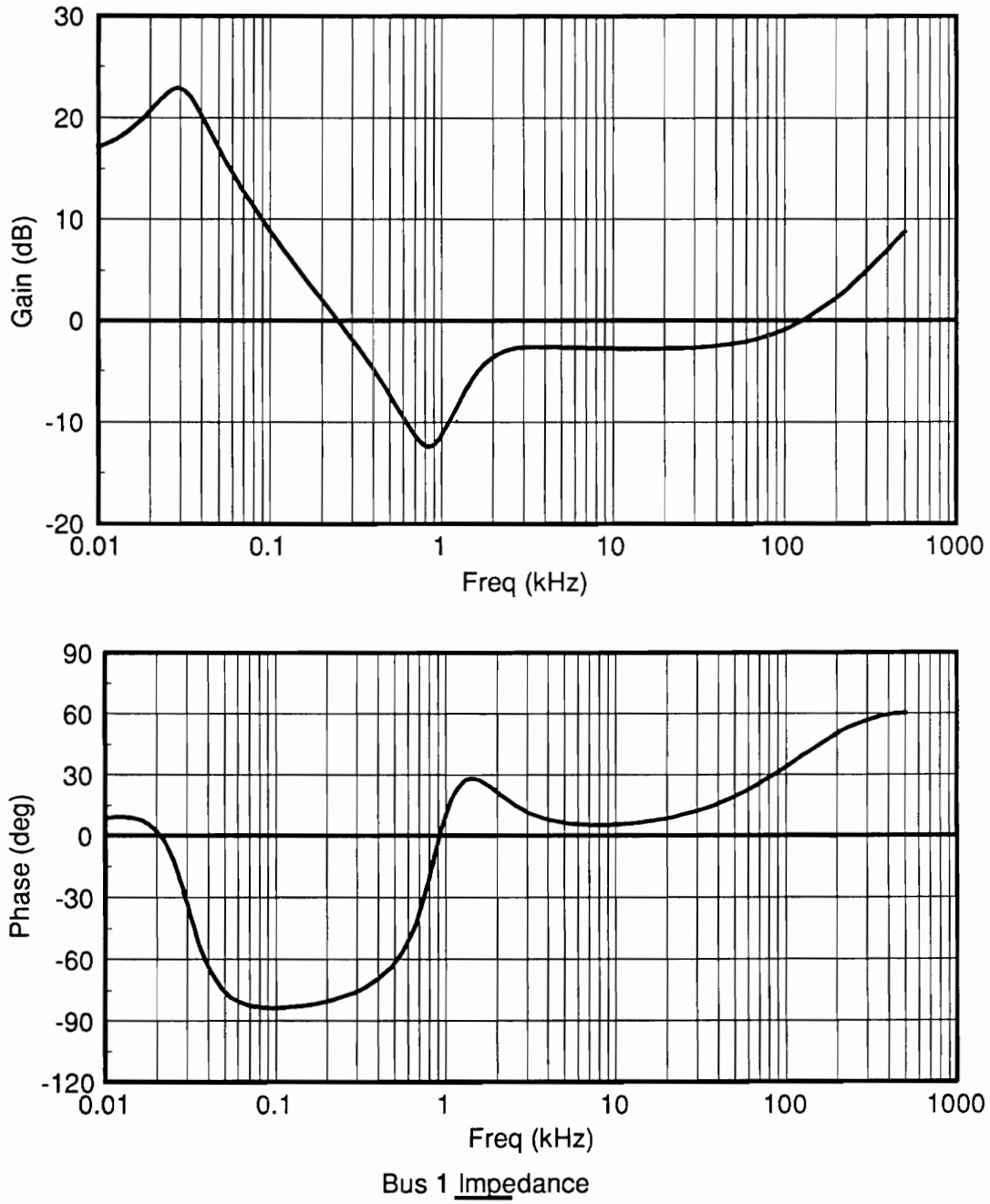

Figure 64. Bus 1 impedance for 5 line conditioners

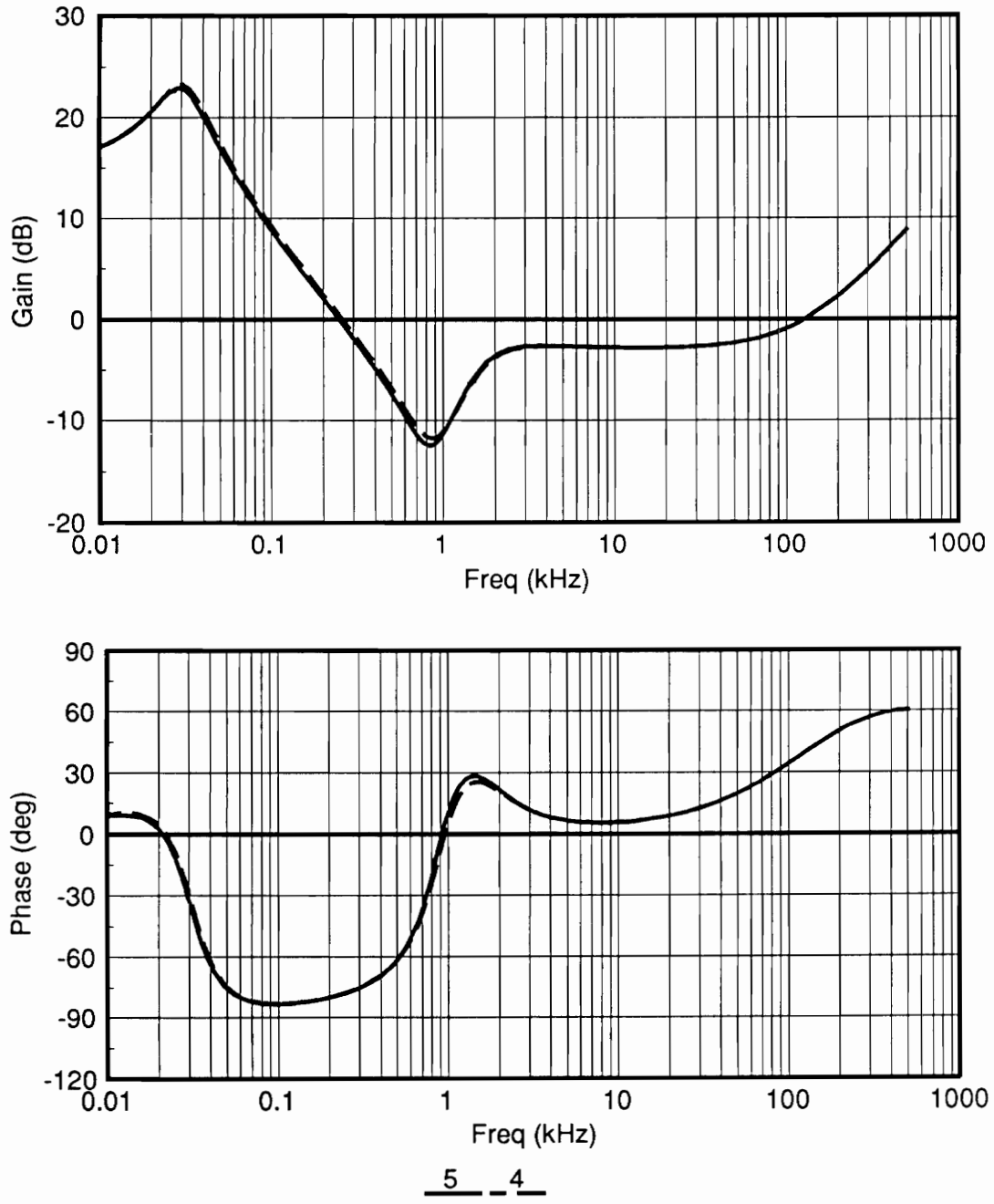

Figure 65. Bus 1 impedance for 4 and 5 line conditioners

It can be seen from Figure 61 that there is a large frequency range of interaction, and we know that the subsystem eigenvalues in this range will change location upon integration. The complex zero of Z_{ib1} at 860Hz is a subsystem eigenvalue, and is expected to shift location upon integration of the subsystems. The two impedances Z_{sb1} and Z_{ib1} intersect at about 2kHz, with a phase margin of about 80°. Therefore, we expect the 860Hz load subsystem eigenvalue to shift to this location, with a slight increase in damping. This is confirmed by examining the eigenvalue listings. Table 5 lists the subsystem eigenvalues for the subsystems defined at bus 1. It can be seen that mode 1 of the load subsystem shifts to mode 3 of the integrated system at 1.6kHz. There is a decrease of Q from 1.5 to 0.8. At the lower frequency of impedance overlap, we would expect the complex source subsystem eigenvalue at 64Hz to shift down to about 30Hz. This is confirmed by examining the mode 1 of the source subsystem shifting to mode 1 of the integrated system shown in Table 4.

To conclude this section, we may verify the lack of interaction between the line conditioner stage and the line input filter/generator source. Figure 67 shows the line conditioner overall loop gain T_1 for the DPS with and without the non-ideal generator source. It is apparent that the presence of the source does not degrade the regulator's loop gain. It can be seen that the generator source causes a very slight disturbance in the phase of T_1 at the lower frequency where Z_{sb1} and Z_{ib1} intersect. Also, a slight change in the phase characteristics of T_1 occurs near 2kHz, which is the upper frequency at which Z_{sb1} intersects with Z_{ib1}. Thus, the effect of the generator source on the loop gain is minimal. For completeness, we would also like to demonstrate that the source has virtually no effect on the load converter stage. Figure 66 shows the 48V bus source impedance for the DPS with and without the non-ideal generator source. The line conditioners act as a buffer and effectively isolates the load converters from the source. This is confirmed since the 48V source impedance is only minimally affected by the generator source. The slight increase in the 48V bus source impedance at very low frequencies is due to the peaking of Z_{sb1}.

Table 5. Eigenvalues for subsystems defined at bus 1

Table 5(a). Bus 1 Source Subsystem Eigenvalues					
Mode	Mult	Real Part	Imaginary Part	Natural Frequency	Damping Ratio
1	1	-335.063	±219.501	400.560	0.836487
2	1	-349.305	0.00E+00	349.305	1.00
3	1	-2.914857E+06	±3.966233E+07	3.976929E+07	7.329E-02
4	1	-5.481615E+06	0.00E+00	5.481615E+06	1.00

Table 5(b). Bus 1 Load Subsystem Eigenvalues					
Mode	Mult	Real Part	Imaginary Part	Natural Frequency	Damping Ratio
1	1	-1809.42	±5092.41	5404.31	0.334810
2	1	-8360.63	0.00E+00	8360.63	1.00
3	4	-9894.48	0.00E+00	9894.48	1.00
7	4	-13008.1	±54748.4	56272.6	0.231163
11	1	-24887.9	±4686.63	25325.3	0.982728
12	1	-44300.7	±55228.5	70800.7	0.625709
13	12	-44634.1	0.00E+00	44634.1	1.00
25	1	-50214.6	0.00E+00	50214.6	1.00
26	1	-100538.	0.00E+00	100538.	1.00
27	4	-133333.	0.00E+00	133333.	1.00
31	12	-155327.	±341199.	374891.	0.414326
43	1	-188761.	±379901.	424212.	0.444968
44	1	-235819.	0.00E+00	235819.	1.00
45	1	-437720.	0.00E+00	437720.	1.00
46	1	-511276.	±498554.	714114.	0.715958
47	4	-654746.	0.00E+00	654746.	1.00
51	12	-1.21951E+06	0.00E+00	1.219512E+06	1.00
63	1	-1.32656E+06	0.00E+00	1.326560E+06	1.00
64	12	-1.43471E+06	0.00E+00	1.434710E+06	1.00
76	1	-3.34404E+07	0.00E+00	3.344046E+07	1.00
77	1	-3.57861E+07	0.00E+00	3.578612E+07	1.00
78	1	-5.28694E+07	0.00E+00	5.286940E+07	1.00
79	1	-1.99941E+08	0.00E+00	1.999412E+08	1.00
80	1	-5.40371E+08	0.00E+00	5.403712E+08	1.00

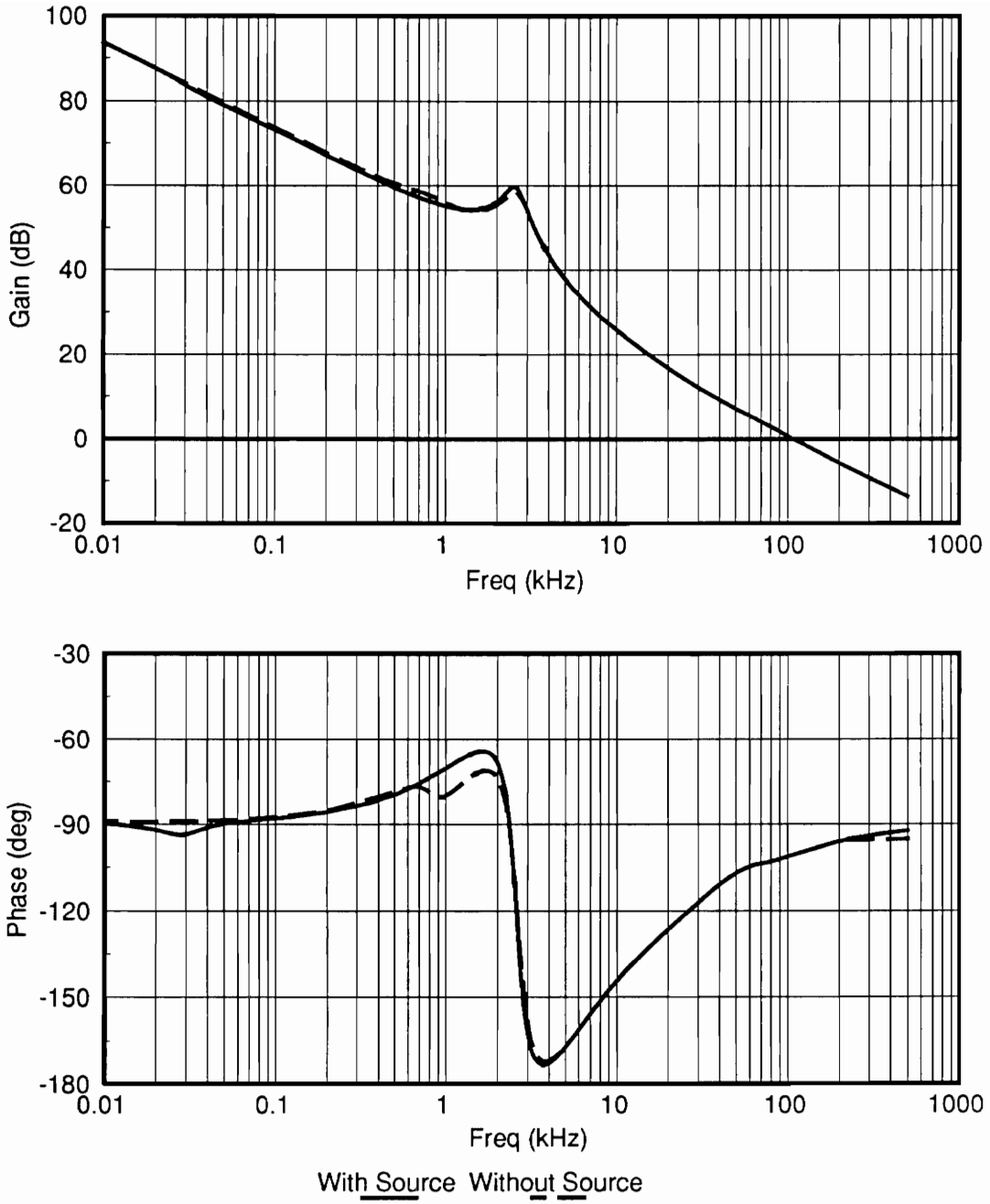

Figure 66. Line conditioner overall loop gain with and without generator source

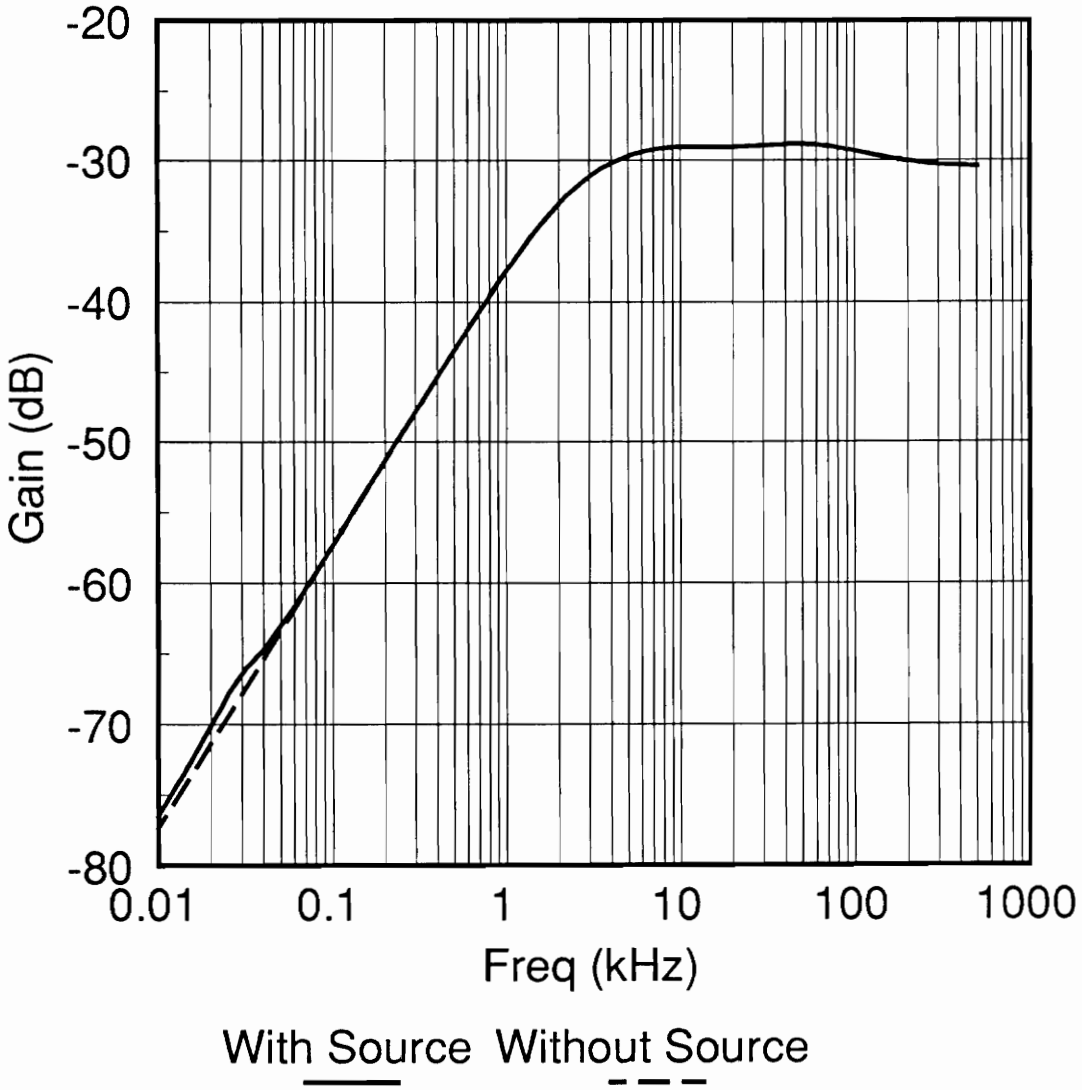

Figure 67. 48V source impedance with and without generator source

4.5 Summary

This chapter addressed the effects of a non-ideal power source on the DPS. As most real world applications of distributed power systems will not see ideal an ideal voltage source, the results of this chapter can be very useful as a guide when performing source interaction analysis.

A small-signal dynamic model of the generator source was used to determine the effect of the source impedance on the system stability and eigenvalue location. The techniques developed in Chapter 2 were applied at two different buses to yield the same results, but from a different location. Stability was determined both from the phase margins and the polar plot of the minor loop gain. The prediction of the eigenvalues due to interaction was performed by examining the bus source and load impedances. The effect of the number of line conditioner modules on the bus 1 and bus 2 impedances was also examined. As expected, the source had no effect on the eigenvalues due to parallel interaction of the line conditioner stages.

Chapter 5

CONCLUSIONS

In this thesis, several important design considerations for distributed power systems were addressed. The size and complexity of the DPS result in various interactions which must be analyzed in order to have a full understanding of the system characteristics. Therefore, methods of analysis were presented and appropriate design guidelines established which will aid the designer dealing with large-scale power systems.

In Chapter 2, the general subsystem interaction analysis was presented. The important results were the development of techniques used for determining stability and eigenvalue location based on the terminal quantities of the subsystems. It was shown that the output impedance of the source subsystem and the input impedance of the load subsystem provide all of the information needed to determine the integrated system stability and eigenvalue location. The minor loop gain T_m was defined, and was used in two methods to determine stability. One method defined the phase margins of the minor loop gain for both the positive and negative slope crossovers to determine stability. A second method method applied the Nyquist criterion to the polar plot of the minor loop gain. Either method will determine the absolute stability of the integrated system. It was also shown that stability could be deter-

mined by examination of the phase characteristics of $1 + T_m$ at the crossover points of T_m. Finally, the shift of subsystem eigenvalues upon system integration was explained qualitatively using a graphical technique.

Chapter 3 of the thesis covered the design of input filters for the DPS. In Section 3.2, the simplified case of input filters for single module current-mode controlled regulators was presented. It was shown how the non-ideal source impedance affects the regulator's loop gain, audiosusceptibility, and output impedance. Of importance here, was the result that the criteria used to assure minimal interaction are the same for both voltage and current-mode controlled regulators. Also, it was shown that under certain conditions, the outer loop gain and the output impedance will not reveal unwanted interactions. However, the overall loop gain should reveal interaction in all cases.

Section 3.3 discussed the general case of input filters for parallel modules. Of most importance here was the identification of a filter model which preserves all of the filter dynamics. It was shown that the single module model does not predict the eigenvalues due to parallel interaction, but can still be used to predict the remaining system eigenvalues and some of the system characteristics such as the loop gain, audiosusceptibility, and output impedance.

Section 3.4 discussed the design and analysis of the line input filter. The filter topology was first chosen to satisfy large-signal considerations. It was shown that simply distributing the second stage capacitance did not eliminate the large ripple current found on the distribution lines. Therefore, both the second stage capacitance and inductance were distributed to each line conditioner module. Section 3.4.2 presented a stability analysis of the filter topology chosen in Section 3.4.1. It was shown that due to parallel interaction, the filter was unstable. Therefore, additional damping was introduced into the second stage which stabilized the eigenvalues due to parallel interaction. Circuit simulation was provided to back up the analysis results. A set of non-iterative design guidelines for the line input filter was given. Finally, the application of the impedance comparison technique developed in Chapter 2 to non-

minimal dimensional subsystems was discussed. It was shown that if either of the subsystems was unobservable/uncontrollable from the interface bus, then the system integration would have no effect on the unobservable/uncontrollable eigenvalues.

Section 3.5 covered the design of the intermediate bus filter. It was shown that the filter not only had to minimize interaction with the load converter stage, but also with the line conditioners. A compromise between low filter output impedance and high filter input impedance is necessary to avoid interaction with both stages of regulators. Design guidelines were provided to meet these requirements.

Chapter 4 presented an analysis of the generator source interaction with the DPS. This provided a good example of when a designer is faced with a non-ideal source which may interact with the system. The source interaction was examined at two different buses. Both buses can provide the necessary information needed to determine stability. The shift of eigenvalue location due to interaction was discussed. Finally, it was shown that the source interaction had no effect on the system eigenvalues which occur due to parallel interaction.

Appendix A

Calulation of Line Input Filter Parameter Values

The line input filter parameter values may be easily found by following the design guidelines in Section 3.4.3.

Step 1

First, we must determine the minimum value for KC_2 to satisfy the voltage ripple specification. The worst-case current drawn by the five line conditioners was found in Section 3.4 to be $34A_{p-p}$ at a duty cycle of 0.5 (180*V* line) and heavy load. Assuming that all of this current passes through KC_2, then we may find the peak-to-peak ripple voltage at the filter output:

$$v_{p-p} = \frac{i_{p-p}}{\omega_s KC_2} \tag{A.1}$$

Where ω_s is the switching frequency. Assuming we allow 1% ripple voltage at 180*V*, then $v_{p-p} = 1.8V$. We can then use Equation (A.1) to find C_2:

$$KC_2 \geq \frac{i_{p-p}}{\omega_s V_{p-p}} = \frac{34A}{2\pi\left(250 \times 10^3 Hz\right)(1.8V)} = 12\mu F \qquad (A.2)$$

Step 2

Next, we choose a value for R_c which also gives the peak filter output impedance. A value of 0.5Ω was chosen to avoid excessive interaction with the single module model power stage.

Step 3

We now choose the value of ω_1 to be 6.28krad/sec. This value will provide good settling time and keep the size of L_1 and C_1 to a minimum. Since we want $Q_1 \simeq 1$, we may find L_1 and C_1 by setting the L_1/R_c and R_cC_1 corner frequencies equal to ω_1.

$$L_1 = \frac{R_c}{\omega_1} = \frac{0.5\Omega}{2\pi\left(1 \times 10^3 Hz\right)} = 80\mu H \qquad (A.3)$$

$$C_1 = \frac{1}{R_c\omega_1} = \frac{1}{2\pi\left(1 \times 10^3 Hz\right)(0.5\Omega)} = 320\mu F \qquad (A.4)$$

Step 4

At frequencies above the second stage corner, we may approximate the filter reverse current gain by Equation (A.5).

$$H_s(s) \simeq \frac{\omega_1\omega_2^2}{s^3} \quad \text{when} \quad s >> \omega_2 \qquad (A.5)$$

Since we know the required attenuation of the filter at $s = \omega_s$, we can solve Equation (A.5) for ω_2. Assuming we need 105dB of attenuation, ω_2 is found as shown below:

$$\omega_2 = \sqrt{\frac{A\omega_s^3}{\omega_1}} = \sqrt{\frac{10^{-105/20}[2\pi(250 \times 10^3 Hz)]^3}{2\pi(1 \times 10^3 Hz)}} = 58.9\text{krad/s} \qquad (A.6)$$

Where $A = H_s(\omega_s)$, which is the required attenuation at the switching frequency.

Step 5

As in step 3, we may find the values of L_2 and C_2 by setting the L_2/KR_c and R_cKC_2 corners to ω_2 for $Q_2 \simeq 1$.

$$L_2 = \frac{KR_c}{\omega_2} = \frac{(5)(0.5\Omega)}{2\pi\left(9.4 \times 10^3 Hz\right)} = 42.5\mu H \qquad (A.7)$$

$$C_2 = \frac{1}{KR_c\omega_2} = \frac{1}{(5)(2\pi)\left(9.4 \times 10^3 Hz\right)(0.5\Omega)} = 6.8\mu F \qquad (A.8)$$

Notice that $KC_2 = 34\mu F$ which satisfies the condition in step 1.

Step 6

Finally, we must select C_d and R_d to satisfy Equation (3.34) and to assure that the roots of Equation (3.33) due to parallel interaction will be well damped in the LHP. The following values were chosen, which provide a quality factor of 2 for Equation (3.33):

$C_d = 22\mu F$

$R_d = 5\Omega$

Section 3.4.4 shows the resulting filter attenuation function and output impedance.

Appendix B

Calulation of Intermediate Bus Filter Parameter Values

The intermediate bus filter parameter values may be easily found by following the design guidelines in Section 3.5.2.

Step 1

First, we must determine the minimum value for KC to satisfy the voltage ripple specification. The worst-case current drawn by the thirteen load converters was found to be $174A_{p-p}$ at heavy load. Assuming that all of this current passes through KC, then we may find the peak-to-peak ripple voltage at the filter output:

$$v_{p-p} = \frac{i_{p-p}}{\omega_s KC} \qquad (B.1)$$

Where ω_s is the load converter switching frequency. Assuming we allow 10% ripple voltage at $48V$, then $v_{p-p} = 4.8V$. We can then use Equation (B.1) to find C:

$$KC \geq \frac{i_{p-p}}{\omega_s V_{p-p}} = \frac{174A}{2\pi\left(500 \times 10^3 Hz\right)(4.8V)} = 11.5\mu F \qquad (B.2)$$

Step 2

Next, we plot the line conditioner stage closed-loop output impedance and the load converter stage open-loop input impedance. These are shown in Figure 46 and Figure 47, respectively.

Step 3

The values of $Z_{i_{min}}(s)$ and $Z_{s_{max}}(s)$ were both chosen as -15dBΩ to provide a good separation of impedances to avoid interaction with both stages of regulators. This gives the value of R_d/K as -15dBΩ or 0.18Ω.

Step 4

At frequencies above the complex *LC* corner, we may approximate the filter reverse current gain by Equation (B.3).

$$H_s(s) \simeq \frac{\omega_o^2}{s^2} \quad \text{when} \quad s >> \omega_o \qquad (B.3)$$

Since we know the required attenuation of the filter at $s = \omega_s$, we can solve Equation (B.3) for ω_o. Assuming we need 35dB of attenuation, ω_o is found as shown below:

$$\omega_o = \sqrt{A\omega_s^2} = \sqrt{10^{-105/20}[2\pi(500 \times 10^3 Hz)]^2} = 418krad/s \text{ or } 66.5kHz \qquad (B.4)$$

Where $A = H_s(\omega_s)$, which is the required attenuation at the switching frequency.

Step 5

We may find the value of L by setting the L/R_d corner to ω_o.

$$L = \frac{R_d}{\omega_o} = \frac{2.5\Omega}{2\pi(66.5 \times 10^3 Hz)} \simeq 6\mu H \qquad (B.5)$$

Step 6

We may find the value of C by setting the R_dC corner to ω_o.

$$C = \frac{1}{R_d\omega_o} = \frac{1}{(2.5\Omega)(66.5 \times 10^3 Hz)} \simeq 1\mu H \qquad (B.6)$$

Notice that $KC = 13\mu F$ which satisfies the condition in step 1.

Step 7

Finally, we must select C_d to be much greater than C. A value of $10\mu F$ was chosen.

Section 3.5.2 shows the resulting filter attenuation function and output impedance.

BIBLIOGRAPHY

1. R.D. Middlebrook, "Input Filter Considerations in Design and Application of Switching Regulators," IEEE Industry Applications Society Annual Meeting, 1976 Record, pp. 366-382.

2. B.H. Cho, "Modeling and Analysis of Spacecraft Power Systems," Ph.D. Dissertation, VPI&SU, Blacksburg, VA, Oct. 1985.

3. Chi-Tsong Chen, *Linear System Theory and Design*, CBS College Publishing, 1984.

4. R.D. Middlebrook, "Design Techniques for Preventing Input Filter Oscillations in Switched-Mode Regulators," Proceedings of Powercon 5, The Fifth National Solid-State Power Conversion Conference, May 1978.

5. Sandra Y. Erich and William M. Polivka, "Input Filter Design for Current-Programmed Regulators," IEEE 1990 APEC Record, pp. 781-791.

6. C. Kohut, "Input Filter Considerations in the Design and Analysis of Switching Regulators Using Current-Mode-Programming," IEEE 1990 APEC Record, NOT PRINTED.

7. Vatche Vorperian, "Simplified Analysis of PWM Converters Using the Model of the PWM Switch: Parts I and II," IEEE Transactions on AES, May, 1990, pp. 490-505.

8. Raymond B. Ridley, Bo H. Cho, and Fred C.Y. Lee, "Analysis and Interpretation of Loop Gains of Multiloop-Controlled Switching Regulators," IEEE Transactions on Power Electronics, October, 1988.

9. Raymond B. Ridley, "Small-signal Analysis of Parallel Power Converters," Masters Thesis, VPI&SU, Blacksburg, VA, June 1986.

10. Lucian R. Lewis II, "Small-signal Analysis and Design of a Distributed Power System," Masters Thesis, VPI&SU, Blacksburg, VA, February 1990.

11. B. Choi, B.H. Cho, R.B. Ridley and F.C. Lee, "Control Strategy for Multi-Module Parallel Converter System," IEEE 1990 PESC Record, June 1990.

12. Erik M. Kvalheim, "Comparison of Input Current Spectral Components for Flyback PWM and Resonant Converters," Masters Thesis, VPI&SU, Blacksburg, VA, Jan. 1991.

13. S. Schulz, J. Liu, B. Cho, and F.C. Lee, "Large-signal Modeling and Simulation of Distributed Power Systems," VPEC Power Electronics Seminar, VPI&SU, Blacksburg, VA, Sept. 1989.

14. S. Schulz, B.H. Cho, and F.C. Lee, "Design Considerations for a Distributed Power System," IEEE 1990 PESC Record, June 1990.

15. R. Lewis, S. Schulz, J. Liu, B. H. Cho, F. C. Lee, "Distributed Power System Analysis - Phase II Final Report," Report to IBM Manassas, VPI&SU, Blacksburg, VA, March 1989.

16. Bruce Carsten, "Distributed Power Systems of the Future Utilizing High Frequency Converters," HFPC Proceedings, April 1987.

Vita

Steven Ernest Schulz was born in Oceanside, NY on October 22, 1966. He received the B.S. degree in electrical engineering (*Summa Cum Laude*) from North Carolina State University in 1988. In August 1988, Steven joined the Virginia Power Electronics Center at Virginia Tech to begin research for his masters degree. In 1989, he was awarded the Bradley Fellowship in Electrical Engineering to continue his research efforts in the area of power electronics. He completed the M.S. program in electrical engineering at Virginia Tech in January 1991.

His research interests include the modelling, analysis, and design of power conversion systems. After graduating, he plans to seek employment in the power electronics industry.